



Interreg



France (Channel Manche) England

ICE REPORT T1.4: A COMMUNITY SPECIFIC ASSESSMENT OF LOCAL ENERGY

13/03/2018



BRETAGNE
DÉVELOPPEMENT
INNOVATION



PLYMOUTH
UNIVERSITY

UEA

marine

Deliverable T1.4: A Community Specific Assessment of Local Energy

Jon Hardwick, Siming Zheng, Helen C.M. Smith, Oscar Fitch-Roy, Jonathan Williams, Peter M. Connor, Senthilarasu Sundaram, Gregorio Iglesias.



About ICE

Supported by Interreg VA France (Channel) England, the Intelligent Community Energy (ICE) project aims to design and implement innovative smart energy solutions for isolated territories in the Channel area. Islands and isolated communities face unique energy challenges. Many islands have no connection to wider electricity distribution systems and are dependent on imported energy supplies, typically fossil fuel driven. The energy systems that isolated communities depend on tend to be less reliable, more expensive and have more associated greenhouse gas (GHG) emissions than mainland grid systems. In response to these problems, the ICE project considers the entire energy cycle, from production to consumption, and integrates new and established technologies in order to deliver innovative energy system solutions. These solutions will be implemented and tested at our unique pilot demonstration sites (Ushant island and the University of East Anglia's campus), to demonstrate their feasibility and to develop a general model for isolated smart energy systems elsewhere. The ICE consortium brings together researcher and business support organisations in France and the UK, and engagement with SMEs will support project rollout and promote European cooperation.



Executive summary

This report builds on the output generated in ICE reports T1.1.1 and T1.1.2 to assess the current generation and demand characteristics for the two target sites: the island of Ushant off Northwest France and the University of East Anglia campus in Norfolk, England. Resource assessments are carried out for three renewable generation technologies: solar PV, wind and tidal stream (Ushant only). Included in the resource quantification are the estimated power that could be exported to the local grid and a comparison with the demand. As all three technologies are dependent on naturally variable resources and the times of generation cannot be controlled, an assessment on the correlation of generation times with consumption times is included. In addition to the raw resource availability a discussion of the technical, environmental and social constraints to deploying these technologies is included. Two other potential forms of renewable generation, biomass and wave power, are discussed briefly.

The report finds that each renewable technology has the potential to provide electricity to the island's grid. The time of day in which generation would occur however is not aligned with the current demand profile and installation of the technologies on their own would result in the need to curtail generation or dump energy. Installing a combination of wind, solar and/or tidal generation would enable the island to reduce the amount of electricity generated from fossil fuels. In order to maximise the amount of low-carbon energy used and make full use of renewable generation:

- An energy storage solution should be installed
- Energy reduction measures should be increased
- Consumption behaviour should be altered so that times of use better correlate to times of generation.

This work along with discussion of storage solutions and behavioural changes all support the development of the low-carbon innovative solution being prepared by the ICE project. The outputs from this report will feed in to the energy storage and network reliability studies being undertaken for ICE report T1.2 and the generalised methodology being developed for ICE reports T2.1 and T3.1.



Contents

Executive summary	3
1 Introduction	11
2 Ushant Island Energy Assessment	13
2.1 Site Overview	13
2.2 Energy Demand Assessment	15
2.2.1 Electricity supply	15
2.2.2 Electricity demand	15
2.2.3 Demand-side management.....	18
2.3 Local Network Conditions	20
2.4 Resource Quantification: Solar	22
2.4.1 Methodology.....	22
2.4.2 Resource Constraints	22
2.4.3 Technical Constraints	25
2.4.4 Environmental, Social and Political Constraints.....	26
2.4.5 Site Identification.....	27
2.4.6 Power Production	30
2.4.6.1 Sports Centre PV Installation	30
2.4.6.2 Planned Projects	31
2.4.6.3 Expansion of solar power across the island	35
2.5 Resource Quantification: Wind.....	37
2.5.1 Methodology.....	37
2.5.2 Resource Constraints	38
2.5.3 Technical Constraints	40
2.5.4 Environmental, Social and Political Constraints.....	41
2.5.5 Site Identification.....	41
2.5.6 Power Production	41
2.6 Resource Quantification: Tidal.....	45
2.6.1 Methodology.....	45
2.6.2 Resource constraints.....	45
2.6.2.1 Bathymetry.....	45
2.6.2.1 Tidal Range.....	48
2.6.2.2 Tidal Currents.....	51
2.6.3 Technical Constraints	52



2.6.4	Environmental, Social and Political Constraints.....	53
2.6.5	Site Identification	56
2.6.6	Power Production	60
2.7	Other low carbon generation technologies	62
2.7.1	Wave	62
2.7.2	Biomass	62
2.7.2.1	PLAXX	63
2.7.2.2	SEAB	64
2.8	Demand side technology	65
2.8.1	Energy Efficiency	65
2.8.2	Alternative Heating: Heat Pumps.....	65
2.9	Scenarios for energy generation.....	66
	Scenario 1: Planned solar installations (5 sites) and one 300kW wind turbine.....	67
	Scenario 2: Extensive solar (20% of rooftops) and one 800kW wind turbine	68
	Scenario 3: Extensive solar (20% of rooftops) and one 2MW wind turbine.....	69
	Scenario 4: Sabella D10 tidal turbine and planned solar (5 sites)	70
	Scenario 5: Sabella D10 tidal turbine and extensive solar installations (20% of rooftops)	71
	Scenario 6: Two Sabella D10 tidal turbines and planned solar installations (5 sites).....	72
	Scenario 7: Sabella D10 tidal turbine, extensive solar installations (20% of rooftops) and an 800kW wind turbine	73
3	University of East Anglia Campus Energy Assessment	75
3.1	Site Overview	75
3.2	Energy Demand Assessment.....	76
3.3	Local Network Conditions	77
3.4	Resource Assessment: Solar	78
3.4.1	Resource Constraints	78
3.4.2	Technical Constraints	81
3.4.3	Environmental, Social and Political Constraints.....	81
3.4.3.1	Site Identification	81
3.4.4	Power Production	82
3.5	Resource Assessment: Wind	83
3.5.1	Methodology.....	83
3.5.2	Resource Constraints	83
3.5.3	Technical Constraints	85



3.5.4	Environmental, social and Political Constraints.....	85
3.5.5	Site Identification.....	85
3.5.6	Power Production	85
3.6	Supply of other generation technologies	86
3.6.1	Biomass	86
3.7	Demand side technology	86
3.8	Scenarios for energy generation.....	86
	Scenario 1: 1MW solar with an 800kW wind turbine	86
	Scenario 2: 2MW solar with a 2MW wind turbine	87
4	Conclusions	89
	References	91
	Appendix 1: PVsyst reports.....	94
	Appendix 2: Tidal harmonic analysis.....	95
	A2.1 Harmonic analysis overview	95
	A2.2 Tidal level.....	95
	A2.3 Tidal current.....	97
	Appendix 3: Tidal resource modelling study.....	99
	A3.1 Hydrodynamic model overview	99
	A3.2 Grids.....	99
	A3.3 Boundary conditions.....	101
	Open boundary conditions	101
	Closed boundary conditions	101
	Fresh water inflow locations and data used	101
	Bottom friction parameterisation.....	102
	Other parameters	102
	A3.4 Initial conditions	102
	A3.5 Calibration and validation.....	102
	Appendix 4: Tidal turbine power production calculations.....	107
	A4.1 Weighted tidal velocities	107
	A3.2 Power density.....	108
	A3.3 Annual electrical power.....	108
	Velocity distribution.....	108
	Electrical power per bin	109
	Mean annual electrical power	110



Annual energy production	112
--------------------------------	-----



Table of Figures

Figure 2.1 Map showing the location of Ushant in France. (Base map source: Open Street map).....	13
Figure 2.2 Aerial photography of Ushant. (Source: IGN)	14
Figure 2.3 Breakdown of types of visitor to Ushant (Îles du Ponant, 2017).	14
Figure 2.4 Time series of electricity demand on Ushant, showing hourly readings (grey) and daily averages (red).	16
Figure 2.5 Seasonal variation of electrical energy demand on Ushant.	17
Figure 2.6 Average electrical demand on Ushant (left axis, green) shown against heating degree days (right axis, purple).	18
Figure 2.7 Average electricity demand on Ushant throughout the day for each month of the year... ..	19
Figure 2.8 Histogram of electrical energy demand on Ushant.	20
Figure 2.9 High Voltage Electrical network on Ushant (Source: Programmation pluriannuelle de l'énergie Volet relatif aux îles du Ponant, EDF).	21
Figure 2.10 Average annual GHI for France, provided by SolarGIS (SolarGIS, 2018).	23
Figure 2.11 Solar radiation by month on Ushant.	24
Figure 2.12 Mean solar radiation throughout the day for each month of the year on Ushant.	25
Figure 2.13 The sports centre building on Ushant showing the lower half of PV installation.	28
Figure 2.14 Computer images of the multipurpose room (left) and youth hostel (right) showing example solar installations,	29
Figure 2.15 Map of Lampaul showing solar rooftop sites. The operating solar PV installation on the sports centre (blue), the planned solar projects (green) and potential rooftop sites (red) are shown. (Base map source: IGN).	30
Figure 2.16 Electricity production from the PV installation on the Ushant sports centre building.	31
Figure 2.17 Predicted electricity production from the proposed solar installations using PVSyst models.	32
Figure 2.18 Comparison of solar generation from planned developments and island electrical demand.	33
Figure 2.19 The average monthly electrical demand (blue) shown against the amount of solar generation from 20% coverage of all available rooftops for scenario 1 (red) and scenario 2 (yellow).	36
Figure 2.20 Comparison of solar generation from extensive solar covering 20% of the island rooftops and island electrical demand.	36
Figure 2.21 Average monthly wind speed at 10m and 100m above sea level.	38
Figure 2.22 Intra-day wind speed at 100m compared with intra-day demand profile.	39
Figure 2.23 Distribution of wind speeds at 100m.	39
Figure 2.24 GIS of Ushant showing areas constrained by roads (yellow) or buildings (blue).	41
Figure 2.25 Manufacturer power curves for three wind turbine models.	42
Figure 2.26 Time series comparing the electrical generation from each wind turbine to the island's demand for 2016. Net surplus/deficit of generation shown in green.	44
Figure 2.27 Sabella D10 tidal turbine in the Brest assembly area (Paboeuf et al., 2016).	45
Figure 2.28 Bathymetric contours, with colour scale showing depth in metres.	47
Figure 2.29 Locations of the tidal measurement stations.	48
Figure 2.30 Annual plot of the tidal height at Ushant and Le Conquet for 2017.	49



Figure 2.31 30-day (Aug 2017) plot of the tidal height above a datum at the sites of Ushant and Le Conquet.....	50
Figure 2.32 50-hour plot of the tidal range at spring tide	51
Figure 2.33 Measured time series of the amplitude and direction (anticlockwise convention from the East) of the current 10m above the seabed at point #1010 in March-April 1993 (Guillou and Thiébot,2016; Guillou and Chapalain, 2017).	52
Figure 2.34 Technical constraints in the waters around Ushant (Intertek, 2015).	52
Figure 2.35 Seabed geology constraints in Ushant region (Intertek, 2015).	53
Figure 2.36 Iroise Marine Nature Park (Agence des aires marines protégées, 2015).	54
Figure 2.37 Environmental constraints in the Ushant region (Intertek, 2015).....	55
Figure 2.38 Socio-economic constraints in the Ushant region (Intertek, 2015).	56
Figure 2.39 Amplitude of tidal current at 10 m above seabed (SHOM, 2018).	57
Figure 2.40 Depth averaged tidal velocities around Ushant at 2-hrly intervals through the tidal cycle.	58
Figure 2.41 Locations of Point A and Point B.....	59
Figure 2.42: Plot of the tidal current at 12.5 m above the seabed at Point A and B, respectively, in August 2017.	59
Figure 2.43 Comparison of estimated power from Sabella D10 turbine and Ushant electrical demand for 2016.....	61
Figure 2.44 The PLAXX process (Source: Green Car Congress, 2016).....	63
Figure 2.45 Scenario 1: Generation compared with demand for 2016.	68
Figure 2.46 Scenario 2: Generation compared with demand for 2016.	69
Figure 2.47 Scenario 3: Generation compared with demand for 2016.	70
Figure 2.48 Scenario 4: Generation compared with demand for 2016.	71
Figure 2.49 Scenario 5: Generation compared with demand for 2016.	72
Figure 2.50 Scenario 6: Generation compared with demand for 2016.	73
Figure 2.51 Scenario 7: Generation compared with demand for 2016.	74
Figure 3.1 Map showing the location of the UEA site in the UK. (Source: Open Street Map)	75
Figure 3.2 Aerial photography of the UEA campus. (Source: Google Maps)	76
Figure 3.3 Sankey diagram showing energy production and use in 2015-16.	77
Figure 3.4 Average annual GHI for the UK, provided by SolarGIS (SolarGIS, 2018).....	79
Figure 3.5 Monthly solar radiation on the UEA campus.....	80
Figure 3.6 Mean solar radiation throughout the day for each month of the year at UEA.	81
Figure 3.7 GIS of the UEA campus showing buildings with existing solar installations (yellow), buildings with the potential for solar installations (blue) and listed buildings (grey).	82
Figure 3.8 Monthly average wind speed.....	83
Figure 3.9 Daily variation in wind speed at the campus.	84
Figure 3.10 Distribution of wind speeds at Norwich Airport (100m).	84
Figure 3.11 Time series of generation for UEA wind turbine examples.	86
Figure 3.12 Scenario 1 generation time series (2016).	87
Figure 3.13 Scenario 2 generation time series (2016).	88



Table of Tables

Table 2.1 Annual energy consumption on Ushant.....	16
Table 2.2 Ushant electrical network details.....	21
Table 2.3 Monthly irradiance values for Ushant, as direct normal irradiance (DNI), global horizontal irradiance (GHI) and global irradiance on a plane inclined at 35°. (G(35)).....	24
Table 2.4 Regulations for solar installations in France (Source: PV Financing (2017), In Sun We Trust (2016)).....	26
Table 2.5 Comparison of the PVsyst model against measured production data for the Ushant solar plant of the sports centre.	31
Table 2.6 Summary of proposed solar projects on municipal buildings.	34
Table 2.7 Hours of generation surplus/deficit.	43
Table 2.8 Seasonal variation in wind generation.....	43
Table 2.9 20 selected tidal constituents at the sites of Ushant and Le Conquet.....	48
Table 2.10 Maximum, minimum and average tidal range for each month of 2017.....	50
Table 2.11 Estimated generation parameters for the Sabella D10 turbine.....	60
Table 2.12 SEAB modular units.	64
Table 2.13 Summary of scenarios	66
Table 2.14 Scenario 1 generation parameters.....	67
Table 2.15 Scenario 2 generation parameters.....	69
Table 2.16 Scenario 3 generation parameters.....	70
Table 2.17 Scenario 4 generation parameters.....	71
Table 2.18 Scenario 5 generation parameters.....	72
Table 2.19 Scenario 6 generation parameters.....	73
Table 2.20 Scenario 7 generation parameters.....	74
Table 3.1 Description of PV installations on the UEA campus.....	78
Table 3.2 Solar irradiance for the UEA campus	80
Table 3.3 Output values for UEA wind generation examples.	85
Table 3.4 Scenario 1 generation parameters.....	87
Table 3.5 Scenario 2 generation parameters.....	87



1 Introduction

This document presents an assessment of the current energy supply and the potential for renewable energy generation for the two isolated communities studied as part of the ICE project: the island of Ushant off Northwest France and the University of East Anglia Campus in Norfolk, UK.

Current energy consumption is discussed with electrical demand data analysed and consumption trends presented. The peak demand values for each site are identified as well as annual, seasonal and daily profiles. These profiles are addressed later in the report in conjunction with the periods of generation from renewable energy technologies.

A quantification of renewable energy resources for different energy generating technologies is undertaken for both sites. The Ushant study quantifies solar, wind and tidal energy resources and the amount of energy that could be utilised is calculated. Biomass and energy from waste technologies are considered with discussion of imported or island-produced materials. The UEA study identifies solar, wind and biomass resources. Where renewable technologies are deemed to be suitable for installation, subject to resource, technical feasibility, environmental and political constraints then suitable sites at the two locations are identified and several scenarios for generation are produced. Scenarios for using a combination of renewable energy technologies to supply the sites are presented along with any storage and backup needs.

An overview of the various renewable energy technologies and methodologies for quantifying the energy resource is provided in the earlier ICE report “T1.1.1: An Overview of Renewable Energy Supply Potential” (Hardwick et al., 2018). That report describes the methodology and constraints for undertaking resource assessments for each renewable technology in a general sense. Guidelines and best practice reports from certification agencies other industry leaders are cited as providing the best methodology for resource assessment. The policy and governance issues for deploying renewable energy technologies on Ushant and at the UEA campus are addressed in the ICE report “T1.1.2: An overview of renewable energy policy and regulatory considerations in Ouessant and the UEA campus” (Fitch-Roy and Connor, 2018).

Renewable energy production is only one aspect of a smart energy system for the isolated communities being researched by the ICE project. In order for the energy produced from solar, wind and marine sources to be of maximum benefit to the Ushant and/or UEA communities there will need to be a number of additional measures in the form of both new physical infrastructure (for example, storage technologies or smart control and monitoring systems) and behavioural changes (for example, incentives to use energy at non-standard times). These measures are discussed in the forthcoming outputs of the ICE project. T1.2 follows on from the findings of this document and discusses the technical reliability and cost issues related to smart grid and storage technologies at the focal sites. T1.3 will further use the outputs of this report in conducting a life-cycle analysis on smart isolated energy networks to allow comparison of the old and new approaches to supply in the context of overall environmental impacts. Findings will feed into the development of a generalised methodological approach for low carbon transition in isolated territories. This methodology, developed by the ICE project team, will bring together knowledge and expertise from the initial studies in the ICE project as well as other academic and industrial research collaborations. A key output of the



ICE project will be a transferable methodology for redesigning energy systems of isolated communities to transition to smart low carbon networks.

A graphical information system (GIS) was produced containing maps of the two sites. The GIS was used to identify constrained areas and possible sites. Data from IGN (the French governments mapping organisation (IGN, 2018)), Google maps (Google, 2018) and Open Street Maps (OpenStreetMap, 2018) include high resolution aerial photography and maps of the Ushant and UEA. From these data features such as roads and rooftops were identified and used in including or excluding sites from consideration for each technology.

This report is split geographically, with the energy assessment and renewable technology resource quantification sections first presented for the Ushant site followed by the comparable sections for the UEA campus site. For each site:

- Section 2.1 (Ushant) and 3.1 (UEA) present high-level overviews of the sites including general parameters about area and population, a description of the types of energy users, the governance and a map of the site.
- Sections 2.2 & 2.3 and 3.2 & 3.3 describe the current energy situation at each site, these sections include an energy demand assessment and details about the local energy network.
- Sections 2.4, 2.5 & 2.6 and 3.4 & 3.5 provide resource assessment for a number of different renewable generation technologies, solar, wind and marine technologies are addressed and the potential for generation quantified. Energy efficiency and demand side technologies are briefly discussed but will be covered in more detail elsewhere in the ICE project.
- Section 2.9 and 3.8 present some example scenarios where a combination of renewable technologies are installed together.
- Section 4 concludes the report.



2 Ushant Island Energy Assessment

2.1 Site Overview

Ushant (Fr: Ouessant) is an island community located off the northwest coast of Brittany in the Iroise Sea, at the southern end of the western entrance to the Channel (Figure 2.1). The island is the largest and most westerly of the Îles du Ponant, with an area of 15.01km². It is largely flat, with the highest elevation at just 61m above mean sea level. The island is a rocky surface covered with many grass fields and there is very little woodland. Around the edge of the island are rocky cliffs interspersed with several sandy beaches, and the surrounding waters contain many small islands and outcrops.



Figure 2.1 Map showing the location of Ushant in France. (Base map source: Open Street map)

The permanent population of the island is approximately 850 people, however, there are large numbers of seasonal visitors and tourists and the population reaches approximately 3000 during the busiest summer months. An aerial photographic map of the island is presented in Figure 2.2. The town of Lampaul is the largest settlement on the island and is the location of the majority of services including shops, hotels, restaurants and other businesses. Domestic properties are spread across the



island with several small hamlets and individual dwellings. The majority of people and cargo are brought to the island by sea via daily ferry services from the mainland and regular freight services. There is also a small passenger air service bringing people from Brest Airport.

Tourism and the associated retail and service sectors are the largest source of income for the island with smaller contributions from the fishing and agriculture sectors. There are also small artisanal industries (e.g. honey, seaweed cosmetics) but no heavy industry.



Figure 2.2 Aerial photograph of Ushant. (Source: IGN)

The island receives approximately 120,000 visitors per year with an average stay of one night. 96% of the visitors are French and 60% are from Brittany. The types of visitors to the island are shown in Figure 2.3. Hiking, camping and bird watching are popular pursuits with visitors on the island. There are just two hotels on the island, with many visitors staying in guesthouses or campsites. (Îles du Ponant, 2017)

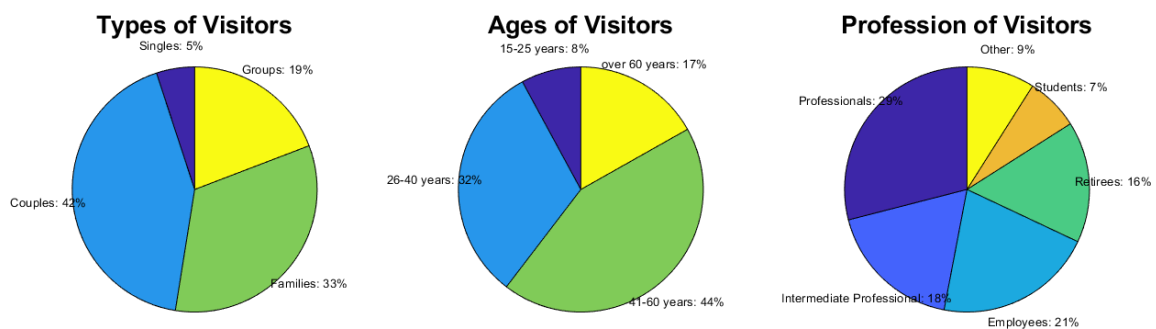


Figure 2.3 Breakdown of types of visitor to Ushant (Îles du Ponant, 2017).



The island is aiming to have 70% of all electricity generation from renewable energy sources by 2020 and 100% by 2030 (Îles du Ponant, 2016). For the island to meet these goals there will need to be a significant amount of new renewable generating capacity installed. This report considers solar PV, tidal stream, wind, and biomass generation technologies as potential contributors to Ushant's energy future. Each of these technologies, discussed in more detail in ICE report T1.1.1, is sufficiently technically mature and can be deployed within the constraints discussed in ICE reports T1.1.1 and T1.1.2. In this section, the raw resource for each technology is quantified using available data from measured sources or numerical modelling and used to calculate the amount of electrical energy that could be provided to the island.

2.2 Energy Demand Assessment

2.2.1 Electricity supply

French legislation ensures that consumers have access to the same electricity tariffs anywhere in France. Hence consumers in overseas departments (e.g. Réunion, Saint Pierre and Miquelon) or on French islands (e.g. Ushant, Molène) pay the same rates for electricity as consumers in mainland France. The extra costs of providing power to consumers in remote communities is effectively socialised across all French energy consumers by a levy on electricity bills (Fitch-Roy & Connor, 2018). The cost of other fuels is not subsidised and is therefore considerably more expensive on Ushant than on the mainland. Due to the subsidised costs of electricity and the logistical difficulty and high cost of receiving other fuel types, electricity is the main source of energy on the island for domestic and commercial use (Sogreah, 2009).

The island's electrical demand is met by supply from five diesel generators located at the generating plant close to Lampaul. There is one 500kW unit and four 1.2MW units and they are actively controlled to match the electricity demand on the island grid. The island is an electrically isolated system; there is no interconnector cable from Ushant to the mainland or to other inhabited islands. A 1MW, 0.5 MWh Lithium-Ion battery was installed in 2017, which is used to improve the efficiency of the generators by providing stored energy to assist in meeting short term spikes in demand and reducing the need to start another generator. A 45kW_p solar PV system was also installed on the sports hall rooftop in Lampaul in 2017.

2.2.2 Electricity demand

Electrical demand data are provided by EDF and are publicly available through a web portal (EDF, 2016). The EDF Island Energy Systems Department is responsible for generation and supply of electricity on Ushant. They are the sole energy producer and customer supplier. The data provide hourly demand readings from January 2011 – December 2016. The annual energy consumption is presented in Table 2.1, and time series of hourly demand and daily averages in Figure 2.4.



Table 2.1 Annual energy consumption on Ushant.

Year	Value [MWh]
2011	6145.09
2012	6614.44
2013	7011.73
2014	6370.53
2015	6467.82
2016	6807.08
Total (2011-2016)	39416.7

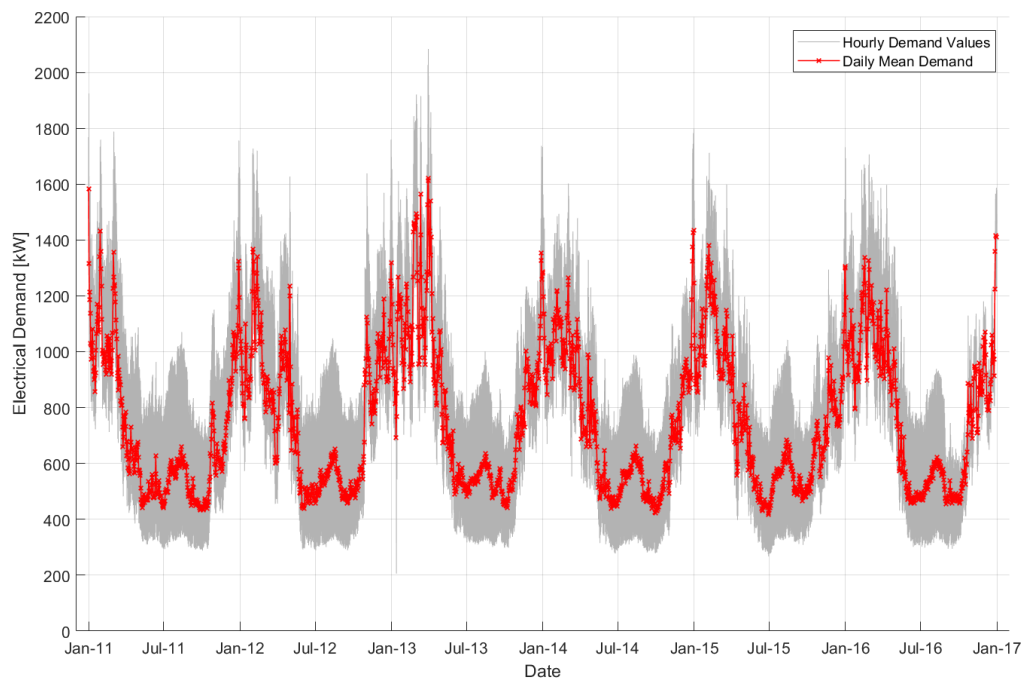


Figure 2.4 Time series of electricity demand on Ushant, showing hourly readings (grey) and daily averages (red).

The peak energy demand recorded throughout the six years of available data is 2.08MW, in March 2013. This is the only occasion where demand of over 2MW was measured, with the peak demand in other years measuring between 1.7 and 1.9MW. The current generation facility has the capacity to deliver 5.3MW of power, or more if the battery unit were used to supplement a short-term spike; the highest peak demand is therefore only 39% of current generation capacity.



There is significant seasonal variation in the electrical demand on the island. Electricity consumption is much higher during the winter as the majority of buildings on the islands rely on electrical heating (Sogreah, 2009). As the island has a significant tourist population there is also an increase in electrical demand during holiday periods (EDF, 2016). There is a marked increase in demand throughout July and August compared with the rest of the summer, however consumption is still much lower than during the winter months. Every year there is a large spike in demand over the Christmas and New Year holiday period, where the larger holiday population coincides with the need for electrical heating. The seasonal variation of the energy demand calculated from the EDF data is shown in Figure 2.5.

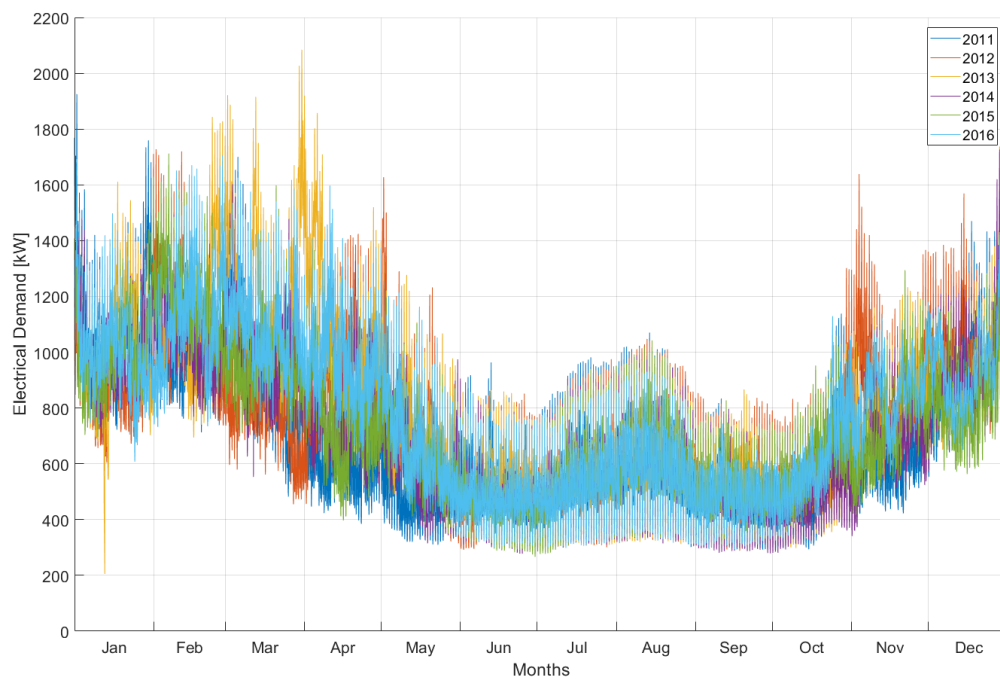


Figure 2.5 Seasonal variation of electrical energy demand on Ushant.

The link between electrical demand and heating is further emphasised in Figure 2.6 where the average daily demand is compared with the heating degree days (HDD). HDD are defined as the number of degrees that the daily average temperature is below the reference value of 15.5°C in the EU. This is the value at which buildings are considered to require heating, and the measure is an indicator of how much heating is required (European Environment Agency, 2016). It can be seen that particularly cold days with high HDD values coincide with spikes in electrical energy demand, especially where these fall within holiday periods.



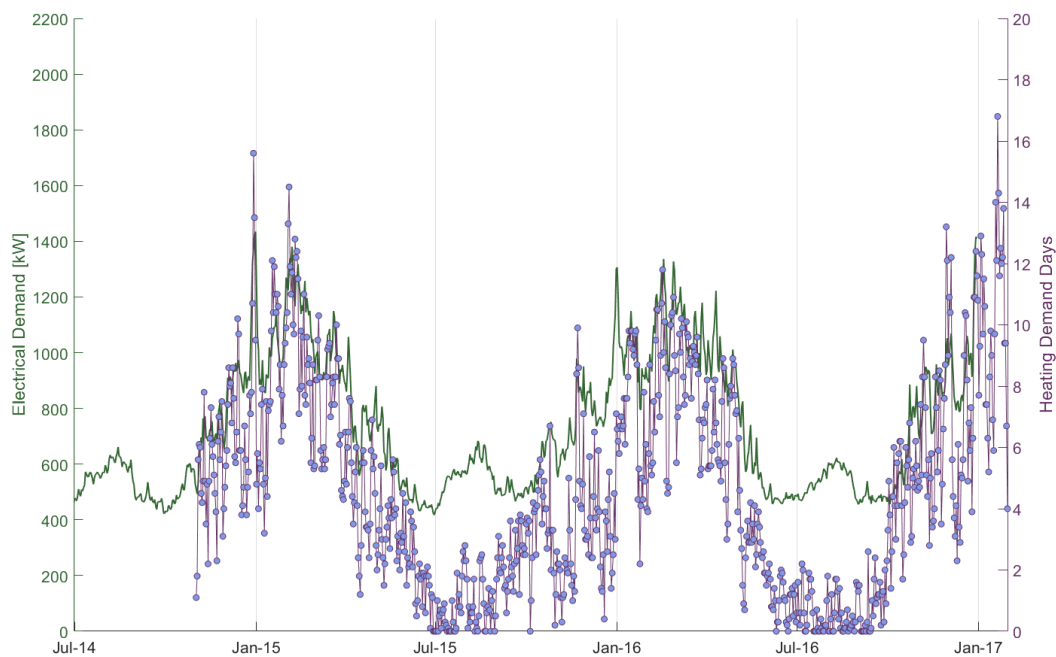


Figure 2.6 Average electrical demand on Ushant (left axis, green) shown against heating degree days (right axis, purple).

Electricity use throughout the day is shown in Figure 2.7 for each month of the year. The profile throughout the day follows a similar trend for each month of the year with a larger baseload throughout the winter to account for the demand for electrical heating. It shows that the highest demand is in the late evening between 22:00 - 23:00. Because most electricity use is in domestic buildings, the daily profiles closely follow the typical routine of residents and holiday makers: energy is used in the mornings before people leave for the day and when they are at home in the evenings. Less electricity is needed during the day when people are out of the house and the least of all is used at night.

Despite the peak electrical demand of over 2MW, more than 80% of the time demand is less than 1MW and 98% of the time less than 1.4MW. A histogram of the electrical demand is shown in Figure 2.8 describing the periods of demand for the island's electrical consumption.

2.2.3 Demand-side management

The island administration and SDEF (the domain network operator for the region) have been working to improve energy efficiency on the island and a number of measures have been implemented to reduce energy consumption. Some of the energy saving measures already implemented are:

- Distribution of low energy LED light bulbs to replace older less efficient lighting. 5,748 bulbs have been distributed on Ushant, saving an estimated 264MWh every year.
- Renovation of street lighting throughout the island with energy efficient LEDs. 119 LEDs have been installed, saving an estimated 19.8MWh per year.
- A scheme to enable islanders to exchange older high energy refrigerators with new and efficient models. 138 devices have been exchanged, saving an estimated 34.5MWh per year.



It has been suggested by the island administration that a reduction in electricity consumption of 19% has already been realised (Palluel, personal communication, November 2017). If further energy efficiency measures are undertaken and/or changes to consumer behaviour introduced then the following results could be achieved:

- A further decrease of overall energy consumption
- A less pronounced daily evening demand peak.
- A daily demand profile more closely matching the generation profiles from renewable technologies such as solar, wind and tidal.

One of the key challenges to achieving 100% renewable generation will be finding a solution to aligning the electrical generation periods of renewable technologies with the times of peak demand. Most of the renewable technologies discussed in this report have very variable times of generation that do not match the times of peak consumption. In order to overcome these difficulties, the energy system will require one or more of:

1. Sufficient reserve generation from on-demand sources (e.g. biomass generator) to cover peak loads.
2. Sufficient energy storage installed to enable energy to be delivered at non-generating times.
3. Further energy efficiency measures implemented and changes in the behaviour of consumers to spread load in order to better correlate with times of generation.

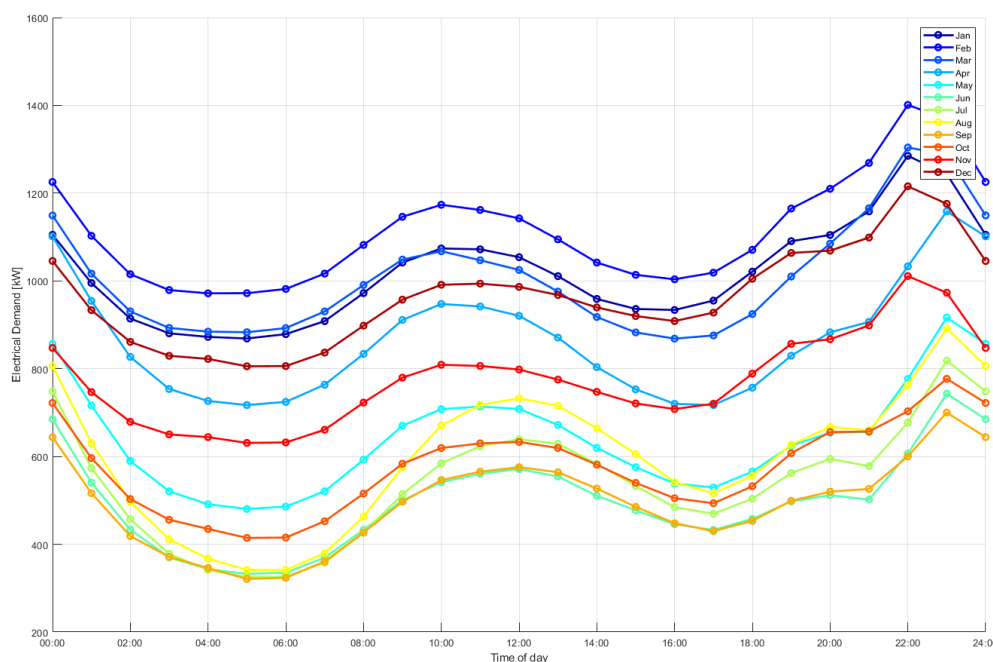


Figure 2.7 Average electricity demand on Ushant throughout the day for each month of the year.



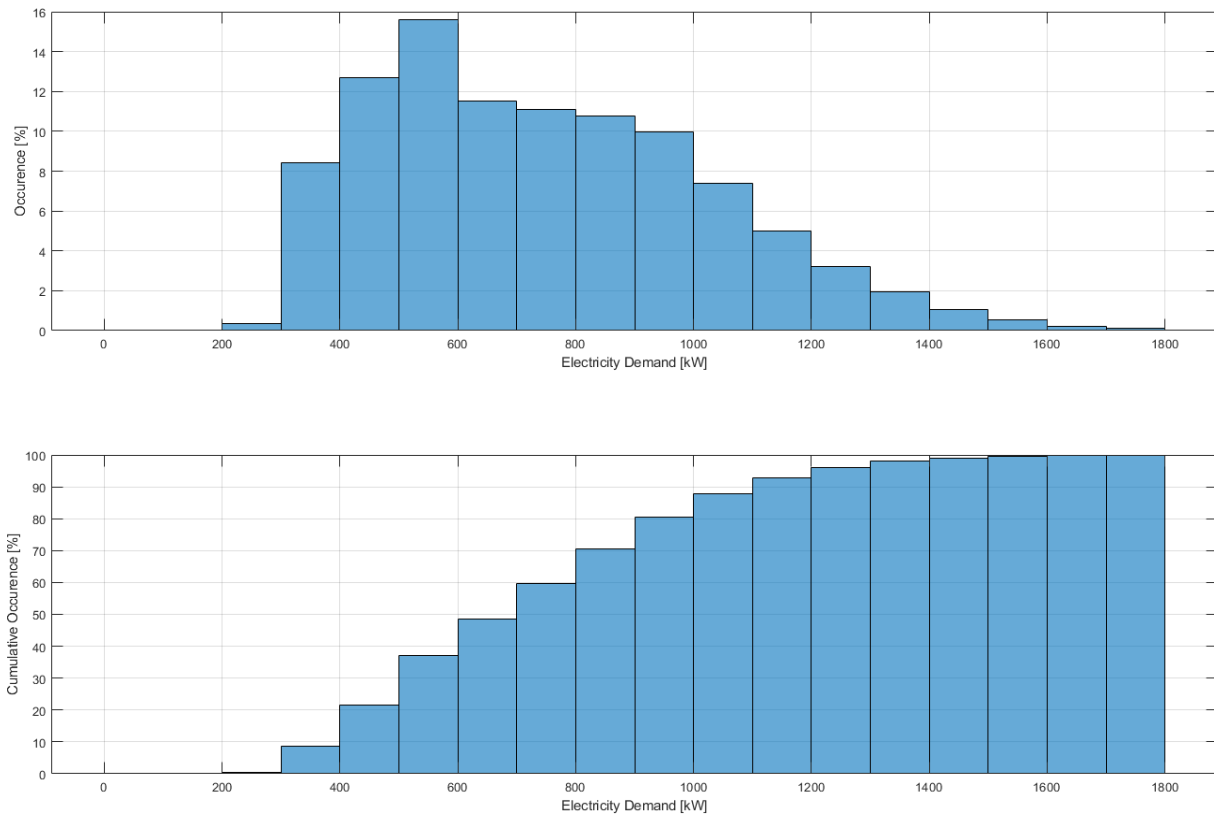


Figure 2.8 Histogram of electrical energy demand on Ushant.

2.3 Local Network Conditions

The Ushant electrical grid consists of two main networks: a high voltage network (HV) and low voltage network/distributed network (LV). The total length of the HV network is approximately 28.4 km and all the cables are underground. There are 34 nodes/connections on the HV network for load distribution. These nodes connect the HV network with the LV network via transformers for distribution to domestic and commercial premises. The LV network consists of a combination of types of lines: overhead cables (6.8km), twisted cable (2.5km) and underground lines (33.3km). There is a weak section in the LV network, which is approximately 4km long. The total length of the LV network is 42.7km. The network is illustrated in Figure 2.9, and the data summarised in Table 2.2.





Figure 2.9 High Voltage Electrical network on Ushant (Source: Programmation pluriannuelle de l'énergie Volet relatif aux îles du Ponant, EDF).

Table 2.2 Ushant electrical network details.

LV lines					HV lines		Number of transformer nodes
Overhead	Twisted	Underground	including weak Sections	LV TOTAL	Underground	LV TOTAL	
6.833km	2.532 km	33.353 km	4.026 km	42.718 km	28. 455 km	28.455km	34



2.4 Resource Quantification: Solar

Solar photovoltaic generation is an established technology that could be installed in many locations across the island. In addition to the PV plant installed in 2017 on the sports centre building there are several other projects in development, managed by the local network operator SDEF (Gallo, 2018 personal email communication). In addition to the planned solar projects there are over 1000 other rooftops identified from GIS mapping which have suitable orientation and area to support solar panels.

2.4.1 Methodology

Modelled and measured solar radiation data were used to calculate the amount of electrical energy which can be produced from various solar installations on Ushant. ICE report 'T1.1.1: An Overview of Renewable Energy Supply Potential' (Hardwick et. al., 2018) provides details on the methodology for undertaking a general solar resource assessment. In this study, data specific to Ushant are considered and several example projects presented.

Data from the Photovoltaic Graphical Information System (PVGIS) were used to estimate the expected amount of solar radiation that will be received on Ushant, with seasonal and intraday profiles studied. PVGIS provides average monthly and hourly data values across Europe by interpolating irradiation collected from meteo-stations and satellite data collected from the Climate Monitoring Satellite Application Facility (CMSAF). PVGIS has been validated in several academic studies and used in the initial assessment of many solar projects (Huld, et. al. 2012).

Several specific PV installations are considered in section 2.4.5. For these projects, the power production calculations were undertaken using the PVsyst software package. PVsyst is an industry-leading software package for designing solar installations. In addition to the data from PVGIS, PVsyst accesses a large database of monthly measured irradiance values from Meteonorm, and hourly data are constructed synthetically from the monthly averages and used to provide detailed profiles of power production (Mermoud & Wittmer, 2014). In addition to irradiance data, PVsyst also considers temperature, precipitation and other meteorological parameters.

Approximately six months of power production values from the existing solar installation on the island sports centre have been analysed and compared with the PVsyst model of the installation. While this is a very small sample it does show that actual power production matches closely with the predictions from the PVsyst model.

In order to estimate the electrical potential of solar PV on Ushant, a rough model was constructed to estimate the power production from a large expansion of rooftop solar around the island. This study utilised a number of PVsyst examples and was scaled up to cover a large number of rooftops. A control rooftop array was designed in PVsyst and the power production calculated. The model was run several times with the control rooftop orientated in different directions. The power production values were then combined and scaled up to represent 20% of island rooftops. Further details of the modelled calculations are shown in section 2.4.6.3.

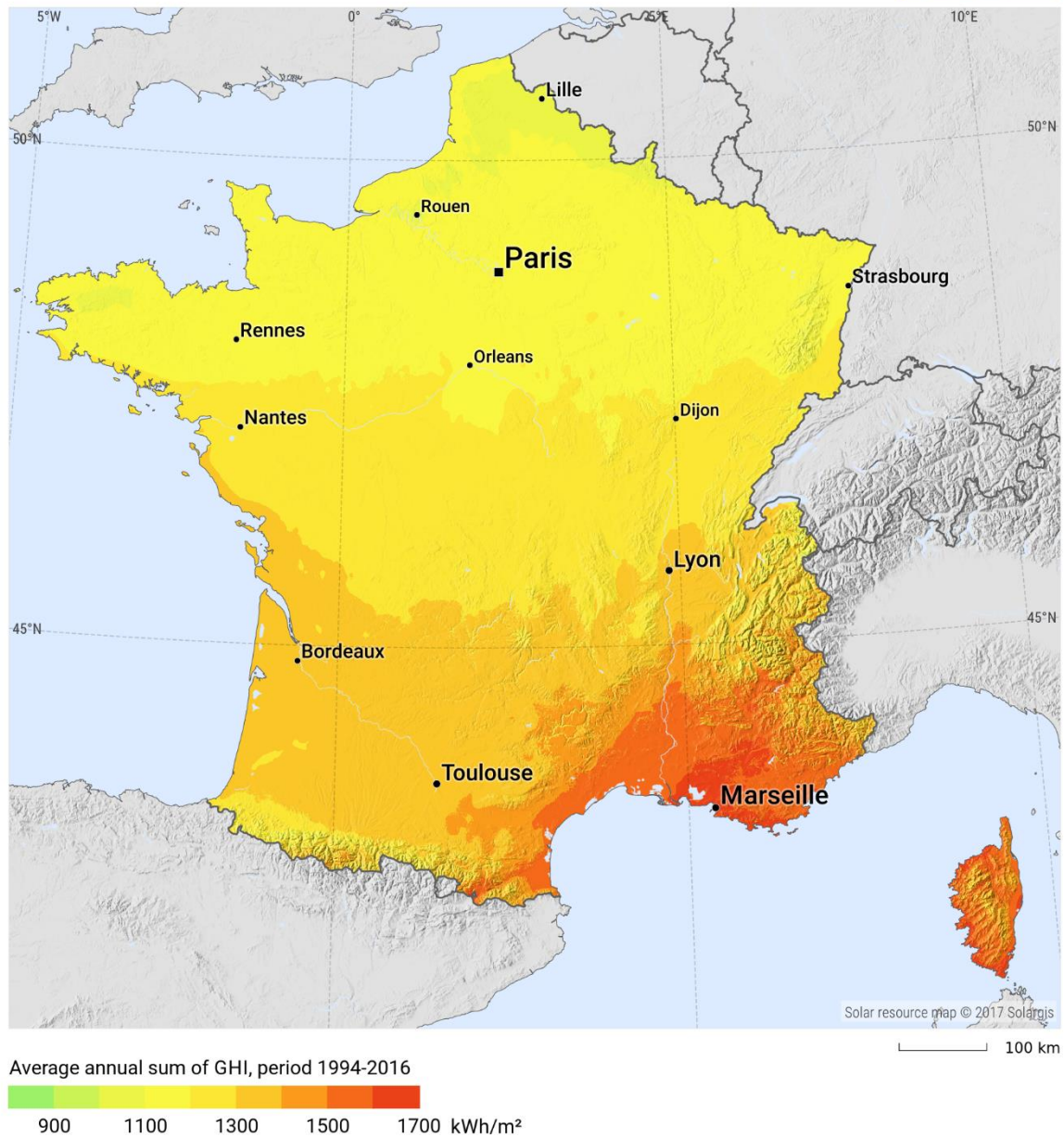
2.4.2 Resource Constraints

Data from the PVGIS-CMSAF solar radiation model suggests that Ushant can expect to receive 1256 kWh/m²/year of direct normal irradiation (DNI) and 1295 kWh/m²/year of global horizontal irradiation (GHI) (Figure 2.10). As the island is 48° north of the Equator there will be significant seasonal variation



in both length of the days and intensity of the radiation. Table 2.3 and Figure 2.11 show the expected radiation per month, and it can be seen that approximately 75% of the DNI occurs in the months April to September. The optimum angle of inclination for fixed panels is 36° at the latitude of the island (Huld et. al. 2012). The mean variation in irradiance over each 24-hour period per month is shown in Figure 2.12, illustrating the variation due to the number of daylight hours.

GLOBAL HORIZONTAL IRRADIATION FRANCE

SOLARGIS


This map is licensed by Solargis under the Creative Commons Attribution license (CC BY-SA 4.0). You are encouraged to use content of the map to benefit yourself and others in creative ways. For more information, please visit <http://solargis.com/download>.

Figure 2.10 Average annual GHI for France, provided by SolarGIS (SolarGIS, 2018).



Table 2.3 Monthly irradiance values for Ushant, as direct normal irradiance (DNI), global horizontal irradiance (GHI) and global irradiance on a plane inclined at 35°. (G(35)).

Month	DNI [kWh/m ²]	GHI [kWh/m ²]	G(35) [kWh/m ²]
Jan	33.83	30.33	47.74
Feb	50.67	49.3	71.47
Mar	95.83	97.18	132.68
Apr	152	149.33	170.1
May	160.83	183.33	182.9
Jun	161.5	186.5	179.4
Jul	167.67	188.83	181.35
Aug	147.5	158.5	169.88
Sep	122	117.5	154.2
Oct	81.33	73.52	104.47
Nov	42.33	36.75	57.9
Dec	30.5	24.12	43.4
Total	1246	1295.2	1495.5

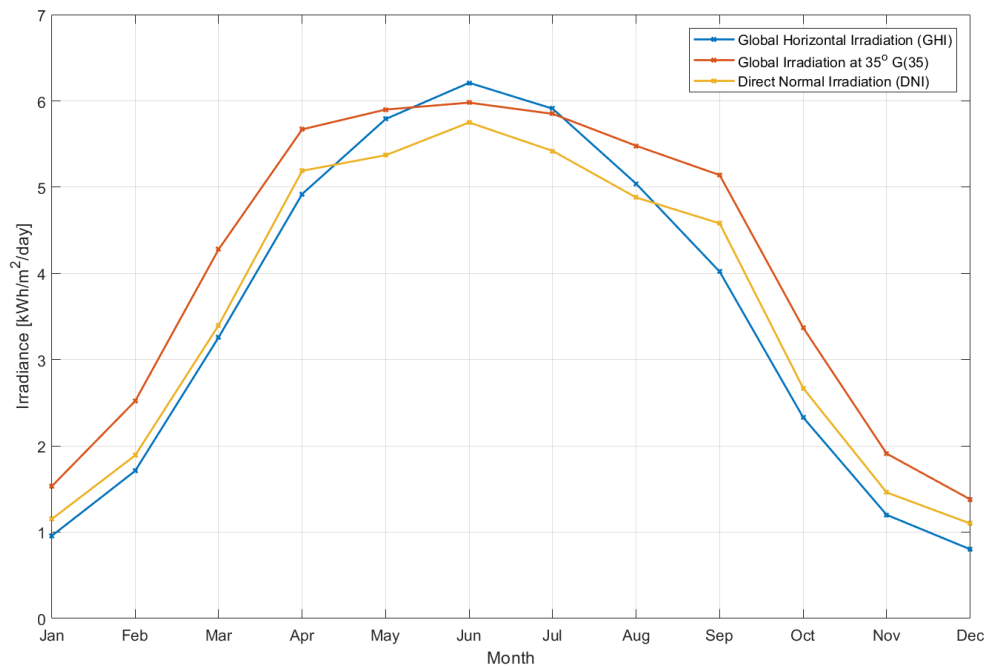


Figure 2.11 Solar radiation by month on Ushant.



The resource is sufficient to provide a large quantity of electricity to the island during the summer months. However, the demand for energy is greatest during the winter months when solar will be limited in the amount of energy which can be produced; for example, there is five times more solar radiation in July than in December, yet the consumption is only half as much. The daily demand profile in winter will not fit well with solar generation, the largest usage peaks in winter occur after dark when there is no generation.

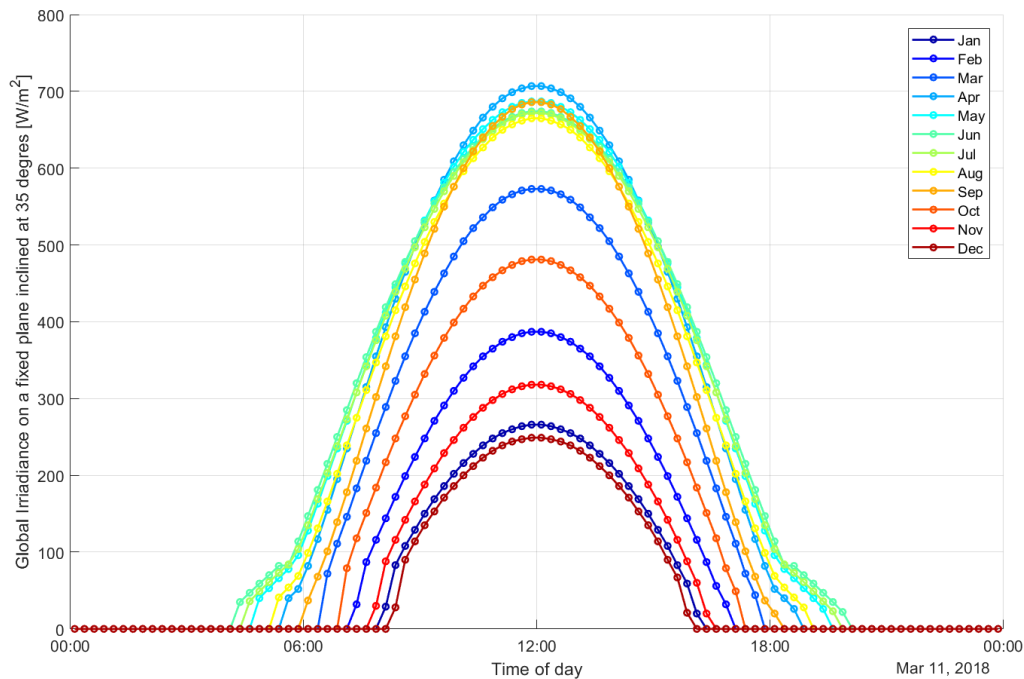


Figure 2.12 Mean solar radiation throughout the day for each month of the year on Ushant.

The majority of roofs on the island are pitched at 35° which is very close to the optimum angle of 36° providing excellent conditions for rooftop solar.

2.4.3 Technical Constraints

Rooftop solar panels can be installed on most buildings and are most effective on south facing pitched roofs. Flat roofed buildings can also accommodate panels on fixed or gimbaled frames. Many of the buildings on Ushant are over 100 years old so it will be important to ensure that a proper structural assessment of the rooftop is undertaken by qualified personnel before any installations go ahead.

The size of a PV installation may be limited by the size of the electrical supply infrastructure; in France, this is typically 6, 9 or 12kW for domestic properties (Fournisseurs Electricite, 2018). Properties will not be able to export more power than the maximum rated value of their grid connection. For commercial buildings and larger domestic properties there may be a higher rated three-phase electrical connection. This will usually allow for installation of a larger PV array, and in this case a three-phase inverter (or three single-phase inverters) should be installed to ensure that the exported power is correctly balanced across the phases.

The equipment for installation of rooftop panels is not particularly large or complex. Solar installation companies are widespread throughout the region and while there are none located on the island the



equipment and personnel can travel to Ushant on the ferry without any special transportation requirements.

Independent solar farms may be installed away from existing grid connections, however, in this case a connection to the network will also need to be constructed. The installation route and methodology should be taken into account when planning a project. Proximity to existing infrastructure will be a key factor in deciding where to site a project.

2.4.4 Environmental, Social and Political Constraints

Rooftop solar installations in France are generally not required to obtain planning permission unless there are particular restrictions due to conservation or special historic significance. We are not aware of any significant impediments of this type on Ushant.

Development of ground-mounted solar PV is legally possible on Ushant. The regulations for development in France are summarised in Table 2.4. Any projects on private land outside a conservation area, Natural Park or other protected space, of less than 3kWp and with a maximum height of less than 1.8m, are exempt from the planning process. Installations smaller than 250kWp (whether ground or roof-mounted) generally require only a declaration of works, made to the town hall in exchange for a statement of non-opposition (arrête de non-opposition), issued by the office of the Mayor. In an area of protected architectural heritage (such as urban areas of Ushant), the office of the public architect may impose conditions, such as the colour and appearance of the panels.

Table 2.4 Regulations for solar installations in France (Source: PV Financing (2017), In Sun We Trust (2016)).

Size	Characteristics	Administrative procedures
Power less than 3kW _p	Height less than 1.80m	Exempt
Power less than 3kW _p	In current or planned protected area such as national or regional natural park	Declaration of works
Power less than 3kW _p	Height > 1.8m	Declaration of works
Power between 3 and 250kW _p		Declaration of works
Power between 3 and 250kW _p	In current or planned protected area such as national or regional natural park	Not permitted
Power greater than 250kW _p		Building permit Impact assessment Public enquiry



For installations larger than 250kW, however, an impact assessment and public enquiry are required. Coastal and landscape protection legislation, the use of land for livestock grazing and Ushant's status as part of the Regional Natural Park of Armorique mean that sites are somewhat limited and local resistance to such developments can be expected. For this reason, small ground-mounted or rooftop options should be explored and exploited to the greatest extent possible before considering commercial-scale ground mounted PV, despite the possible cost and performance benefits of these systems.

One of the primary challenges for building and operating non-domestic renewable electricity generation project on Ushant is reported to be the complexity and cost of obtaining a connection to the island's electricity network. The data provision required by the network owner (Enedis) can be lengthy and, following the network's own study of the required network upgrades, the cost of works can appear high, challenging the viability of some projects. The cost-of-works calculation process undertaken by Enedis is not available to this study at this time. Developers in non-connected or isolated areas of France such as Ushant may face the additional cost of connecting the generation equipment to devices designed to remotely manage output to protect grid stability at times of high solar generation and low demand. The institutional set-up is described in ICE project report 1.1.2 (Fitch-Roy & Connor, 2018).

The sequencing of the connection process is also challenging for developers. For example, in early 2018 a requirement was introduced for developers to provide solar-panel certification documents before applying for a connection to the network. This effectively means that the generation hardware specification must be determined (through tender, if the procurer is a public agency) before the connection application can be prepared, rather than developers working on both of these items in parallel. The reason for not allowing a connection within a certain specification envelope is assumed to be associated with the delicate nature of the local network, although the decision-making process is unclear to this study at this time.

2.4.5 Site Identification

In September 2017 a 45KW_p solar plant installed on the roof of Ushant's sports centre building (shown in Figure 2.13). The project comprised two blocks of panels fixed to the building roof: one set of 88 panels on the lower section of roof pitched at 37° and one set of 110 panels on the upper section of roof pitched at 17° from the horizontal. The panels installed are each 275W, 1st generation mono-silicon solar cells manufactured by BenQ Solar. The panels are connected to the island's electrical grid through two SMA Sunny Tripower inverters (one 20kW and one 25kW). The components and parameters of the projects were input into a PVsyst model and an analysis of this project was run. It was calculated that the installation would provide an expected 58.1MWh of electricity to the island grid each year. A description of this model and analysis of the first months of operation are presented in Section 2.4.6.1.





Figure 2.13 The sports centre building on Ushant showing the lower half of PV installation.

Further solar PV projects have been proposed for Ushant and four sites are currently being considered for development of rooftop solar panels by SDEF. Models were developed on PVsyst to assess the potential of these sites, and components similar to the ones used in the sports centre project were selected and applied to the exact rooftop specifications of the selected buildings. Results of the model indicate that if these four sites are developed then there could be a further 162 MWh per year of electrical energy supplied to the island grid. It should be noted that the models undertaken for this study do not necessarily correspond to the exact specifications of the projects planned by SDEF. The sites investigated are as follows:

- **Salle Ployvalente (multipurpose room)** – This is a multipurpose hall available for meetings and other activities to the residents of the island. The main part of the building has a pitched roof orientated towards the southeast (-16° from south). There is an L-shaped section of the building meaning that the not all of the length of the building can be developed for PV. An image of the building is shown in Figure 2.14. The available area is calculated from the GIS to be approximately 216m^2 , providing ample space for a PV installation. A system was designed using the same panels and similar inverters to the sports centre project. The modelled 13.2kW_p installation was analysed on PVsyst.
- **Auberge de Jeunesse (youth hostel)** – The youth hostel is located just outside the main settlement of Lampaul. The main axis of the building has a pitched rooftop orientated at -30° degrees east of south-facing and the rooftop is comprised of several different sections with higher and lower sections visible, shown in Figure 2.14. For the current study only the largest unobstructed section of the main rooftop is used in the model. It may be possible to utilize other sections of the roof for a larger installation in future studies. An 8.8kW_p system was designed on PVsyst and the outputs analysed.
- **Mairie (town hall)** – The town hall is a building with offices for the mayor and local government staff as well as a meeting room for the public. It has a suitable pitched roof orientated at -32° from south which would be suitable for a solar installation. A system was designed on PVsyst with a capacity of 9.0kW_p .



- **Service Technique (technical service buildings)** – This is a compound with three long buildings and several smaller shed-type structures. The three large buildings have long pitched roofs that are orientated -22° east of south and would be suitable for a PV installation. Three different schemes were modelled for these buildings. Plan 1 is the smallest installation: a 22kW_p system was designed on PVsyst, with panels placed only on the southern building. A second model for the site, plan 2, proposed installing panels comprising 82.5kW_p of capacity on the southern and middle buildings. Finally, plan 3 devised covering all buildings with panels, with a capacity of 113kW_p .

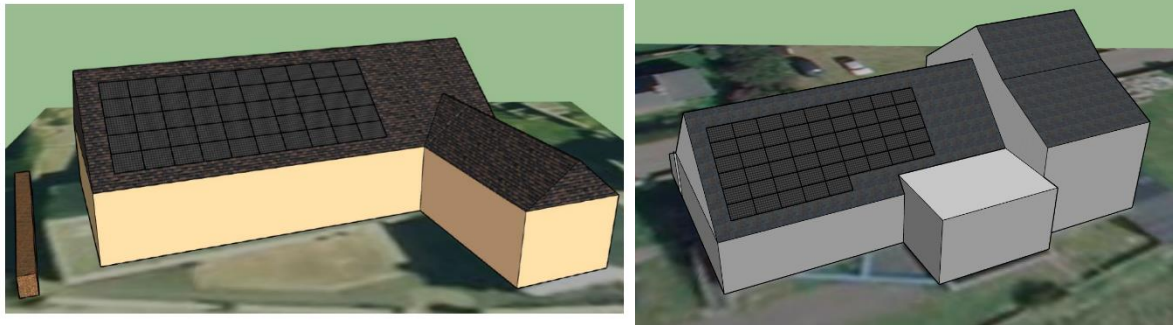


Figure 2.14 Computer images of the multipurpose room (left) and youth hostel (right) showing example solar installations,

In addition to the sites currently being investigated for development by SDEF, further theoretical projects were investigated: Firstly, a large 1MW_p ground-mounted solar installation, and secondly, an expansion of rooftop solar to 20% of all buildings on the island.

Ground-mounted solar farm – An option for significantly expanding solar generation on the island would be to develop a large solar installation at a single location. A ground-mounted solar farm could be developed to have a larger capacity than any individual rooftop and would benefit from cost savings by installing a large number of panels at a single site. Using PVsyst, a solar farm was designed with an installed peak capacity of 1.1MW . The site would cover at least 2 hectares and would require a suitable location to be made available. A full public enquiry and impact assessment would be required before a plant of this size could be realised.

Expansion to other rooftops - In addition to the public buildings there are over 1000 other rooftops identified on the GIS map of the island which have suitable space and orientation to make solar PV possible. If these sites are exploited then a large amount of the island's summer demand can be met. An example of these rooftops is shown for the main town of Lampaul in Figure 2.15.





Figure 2.15 Map of Lampaul showing solar rooftop sites. The operating solar PV installation on the sports centre (blue), the planned solar projects (green) and potential rooftop sites (red) are shown. (Base map source: IGN)

2.4.6 Power Production

2.4.6.1 Sports Centre PV Installation

The PV installation on the sports centre roof commenced full operation on 2nd October 2017. In the period from its installation until 10th April 2018 it provided 21.83 MWh of electricity to the island grid. Figure 2.16 shows the total electricity production for each day within this period. As this period covers only six months in the autumn and winter it does not allow a complete assessment of the system. It does, however, show good agreement with the predicted output from the PVsyst model of the system. Table 2.5 shows the electricity production totals for the available months compared with the expected production predicted by the PVsyst model. The PVsyst model undertakes calculations using radiation values for each month based on averages over many years. Direct comparison with individual months cannot therefore be used to validate the model. What can be ascertained, however, from the close agreement is that the PV installation is producing values within a small percentage of the model predictions (the model is under predicting by 9.3% in the six month period). Once the project has been in operation for a longer period then further comparisons can be made and a complete assessment of the facility's performance undertaken.



Table 2.5 Comparison of the PVsyst model against measured production data for the Ushant solar plant of the sports centre.

Month	PVsyst Model Predicted Production [kWh]	Actual Measured Output [kWh]	Model Percentage Error [%]
October (2 nd Oct onwards)	3535	3375	4.7
November	2473	2650	-6.7
December	1610	1401	14.1
January	1816	2080	-12.7
February	2882	4293	-32.9
March	4773	5033	-5.2
Six Month Total	17089	18832	-9.3

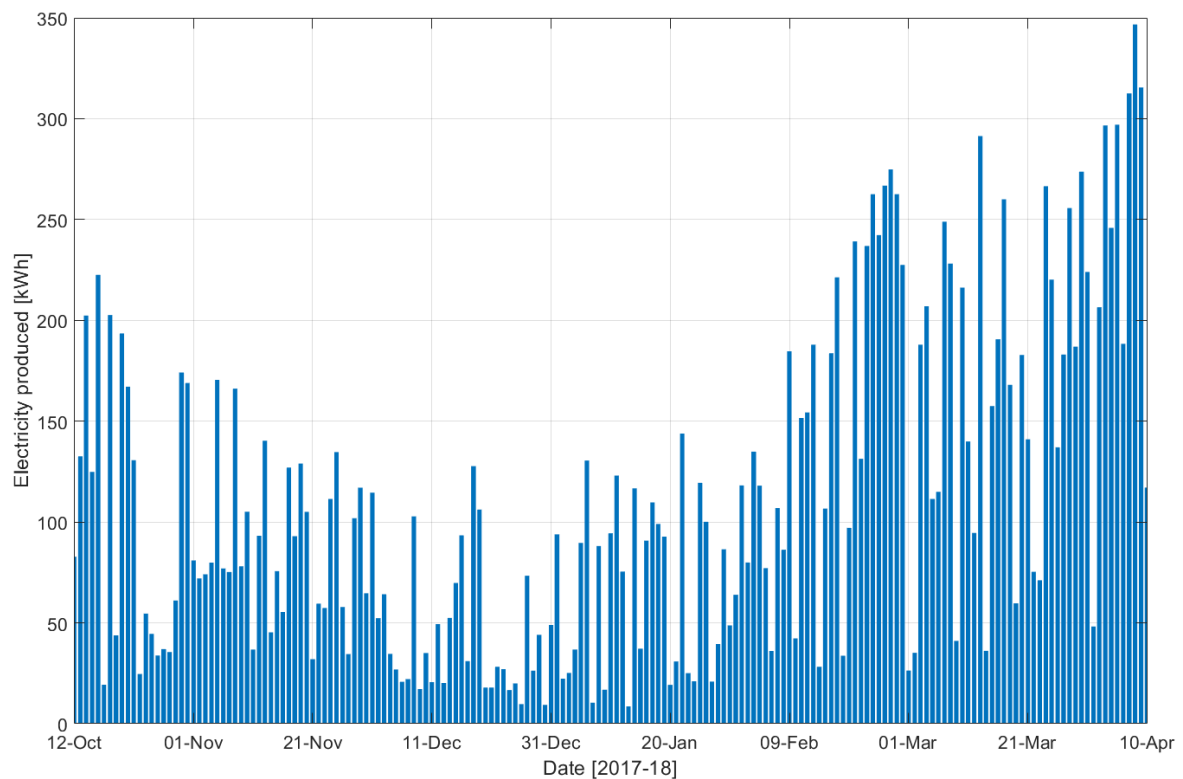


Figure 2.16 Electricity production from the PV installation on the Ushant sports centre building.

2.4.6.2 Planned Projects

Salle Ployvalente: An array was designed using PVsyst with 13.2kWp installed capacity, incorporating 48 275W panels covering an area of 77m². The model suggests that this installation could provide 14.38MWh of electricity to the grid each year.



Auberge de Jeunesse: An array was designed with 8.8kWp of installed capacity, incorporating 32 275W panels and covering an area of 52m². The PVsyst model suggests that this installation could provide 8.51MWh of electricity to the grid each year.

Mairie: An array was designed with 9.0kWp of installed capacity, incorporating 36 panels and covering an area of 58m². The PVsyst model suggests that this installation could provide 9.73MWh of electricity to the grid each year.

Service Technique: Three possible projects were modelled in PVsyst:

- Plan 1 involves installation of panels on just the most southerly building, incorporating 80 panels covering 129m² of the rooftop and providing 22kWp of installed capacity. The PVsyst model predicts this will provide 21.58MWh of electrical power generation.
- Plan 2 is a larger installation which covers both of the large buildings with PV panels and uses 300 panels in total, covering 483m². This gives an installed capacity of 82.5kWp and would provide 76.3MWh of electricity per year.
- Plan 3 involves covering all three buildings with solar panels, incorporating 410 panels covering 662m² of rooftop area. This gives an installed capacity of 113kWp and would provide 94MWh of electricity per year.

The full PVsyst reports for these projects are located in [Appendix 1](#), and the results summarised in [Error! Reference source not found.](#)

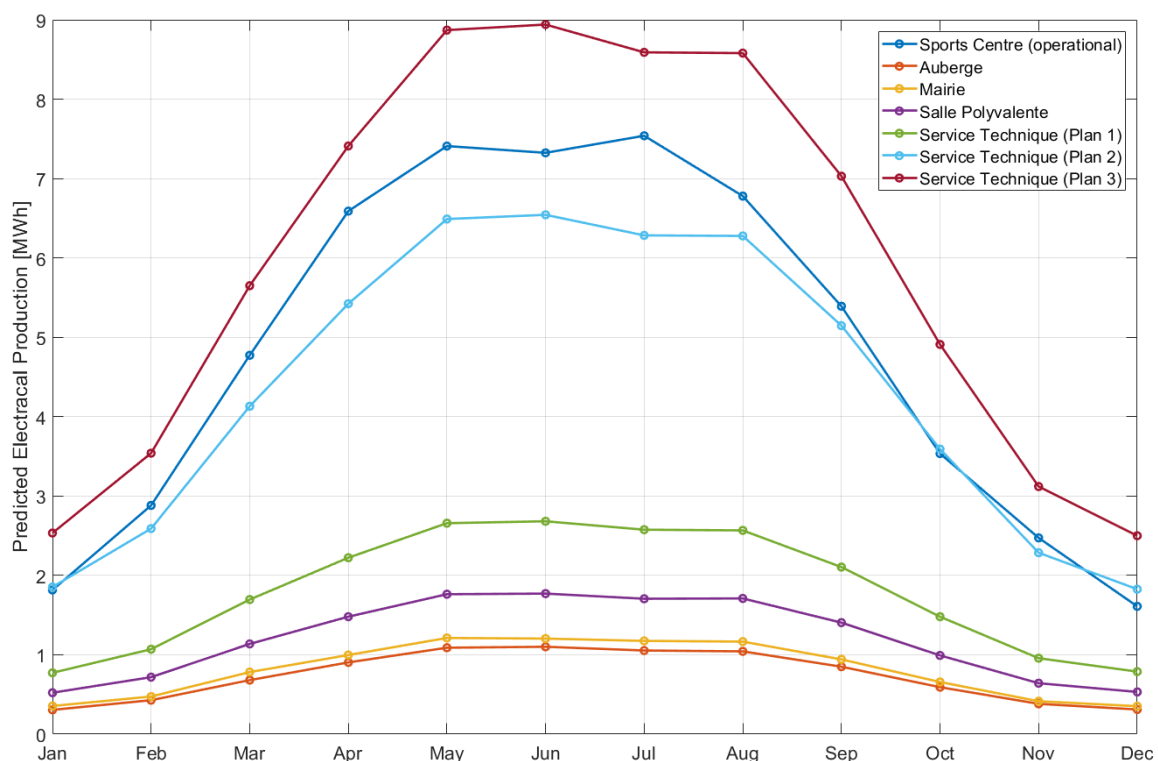


Figure 2.17 Predicted electricity production from the proposed solar installations using PVsyst models.

Figure 2.17 shows the predicted monthly power production from the planned installations using the PVsyst models. If all were implemented, with plan 3 on the technical service buildings, there could be



a total of 162.64MWh of electrical power per year supplied to the grid from these solar projects. The estimated generation for a typical year from these projects is compared with the islands electrical demand for 2016 and shown in Figure 2.18. Only a small proportion of the demand would be fulfilled and the majority of generation would need to come from other sources.

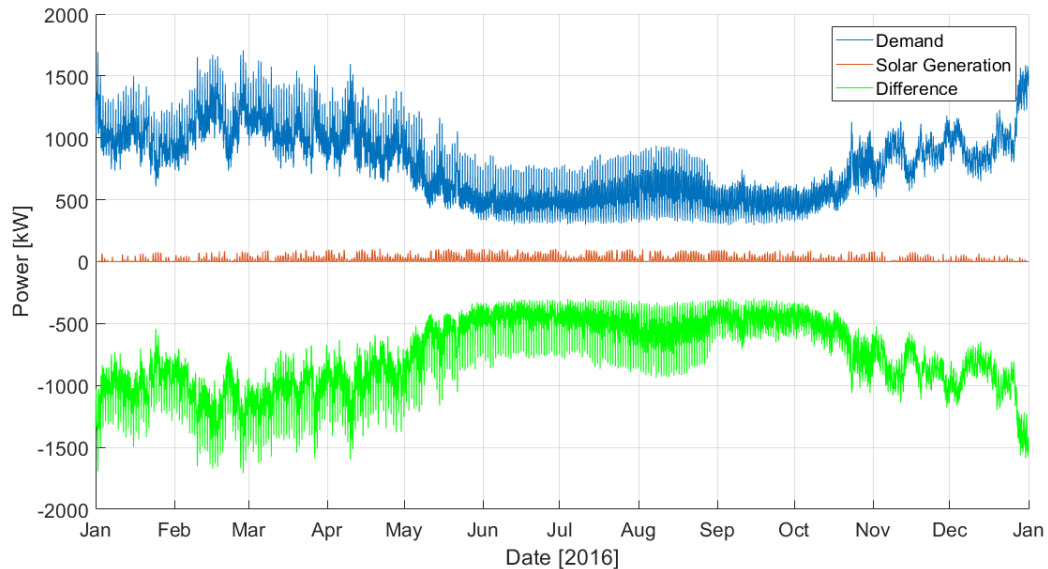







Figure 2.18 Comparison of solar generation from planned developments and island electrical demand.

Ground-mounted solar farm: If an 1100kW_p solar farm was deployed on the island then the PVsyst model suggests that it would supply 1166MWh of electricity to the island, approximately 25% of the island's annual load. As with the other solar projects this power would be generated mostly in the summer months and all during daylight hours. The hours in the middle of the day have a lower demand than the evenings and demand in the summer is lower than the winter, therefore there are many occasions where the entire electrical demand of the island would be outstripped by generation from a large solar farm. A large amount of storage and a shift in demand behaviour of consumers would be required to make use of this extra electricity at times when it would be needed.



Table 2.6 Summary of proposed solar projects on municipal buildings.

Site	Aerial Photo	Location	Rooftop Area (estimated from GIS)	Rooftop Orientation [degrees from South]	Capacity of modelled installation [kW _p]	Electrical energy exported to grid [kWh/yr]
Sports Centre (operational)		48.458757 N; 5.100076 W	1122m ²	-17	45.0	58100
Multipurpose Room		48.458038 N; 5.100368 W	216 m ²	-16	13.2	14380
Youth Hostel		48.459103 N; 5.096837 W	210 m ²	-30	8.8	8510
Town Hall		48.455346 N; 5.097461 W	182 m ²	-32	9.0	9730
Technical Service Building (plan 1)		48.45926 N; 5.089362 W	(341 + 379 + 332) = 1052 m ²	-22	22	21580
Technical Service Building (plan 2)					82.5	76300
Technical Service Building (plan 3)					113.0	94000



2.4.6.3 Expansion of solar power across the island

GIS maps were used to identify all potentially suitable rooftops on the island. A total of 1178 rooftops were identified, covering an area of 110,000m². Theoretically, this provides sufficient roof space for over 18MW_p of installed solar capacity. Not all rooftops will be suitable however, and many building owners will be unable or unwilling to install panels. If even a small proportion of these rooftops were utilised then a significant proportion of the island's electricity demand could be satisfied during the summer months. Information about the incentives and mechanisms for installation of domestic solar in France are detailed in Ice deliverable 1.1.2 (Fitch-Roy and Connor, 2018).

In an example scenario, a model was devised to estimate the electrical production if approximately 20% of the island's roof space had solar PV panels installed. Historically, most domestic dwellings on Ushant follow the design of a traditional Breton house, new buildings have to follow landscaping planning regulations and are therefore mostly of that same style, with a consistent roof pitch of 35°. This was therefore used as the pitch angle for all roofs in the model. A sample 3kW system was designed and analysed on PVsyst. The model was run several times varying the angle of azimuth each time. The results of the model were then scaled up to estimate the results from many installations around the island. Two different methodologies were applied:

- Method 1: An assumption was made that the rooftops receiving solar installations are randomly distributed from the available roofs on the island, and the angle of azimuth of the roofs was assumed to be evenly distributed in range of orientations from -90° to +90° around south facing.
- Method 2: An assumption was made that the owners of south facing buildings would be more likely to install solar panels than non-south facing buildings, therefore a higher proportion of the buildings with orientations closer to south were considered for development and a lower number of rooftops with orientations close to east or west.

If these scenarios were implemented then a total of 3744MWh (scenario 1) or 3889MWh (scenario 2) could be supplied to the grid, i.e. 57% or 59% of the island's total demand. Figure 2.19 shows the monthly electricity generation that could be achieved from solar PV under scenarios 1 and 2, with 20% of suitable rooftops on Ushant being used. In these example scenarios, the amount of energy generated would be close to the total demand in the summer months (May – September), however, it would only have a small impact in the winter months when generation would need to be met by other sources. The hourly comparison between a typical years' generation and the island's electrical demand for 2016 can be seen in Figure 2.20. There are many periods where generation is greater than the island demand; when this is the case there will need to be means for the energy to be used elsewhere, for example through storage technologies, or dumped. Solar energy is only produced during daylight hours so if it were to be used to cover a large proportion of the island's consumption,



changes to the times of consumption in addition to an energy storage solution would be required. This is discussed in the ICE report T1.1.2.

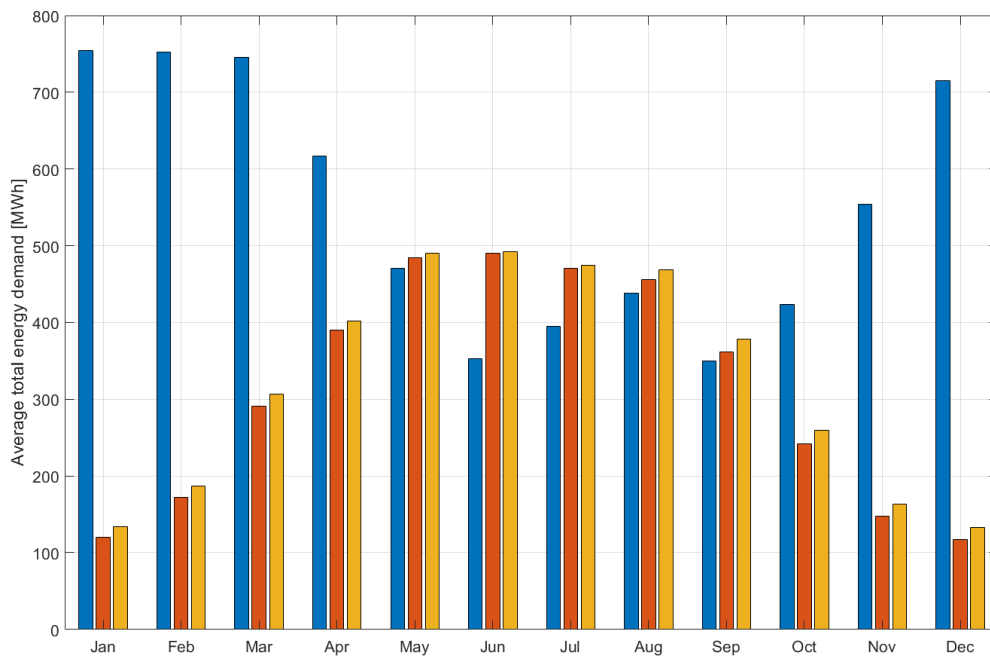


Figure 2.19 The average monthly electrical demand (blue) shown against the amount of solar generation from 20% coverage of all available rooftops for scenario 1 (red) and scenario 2 (yellow).

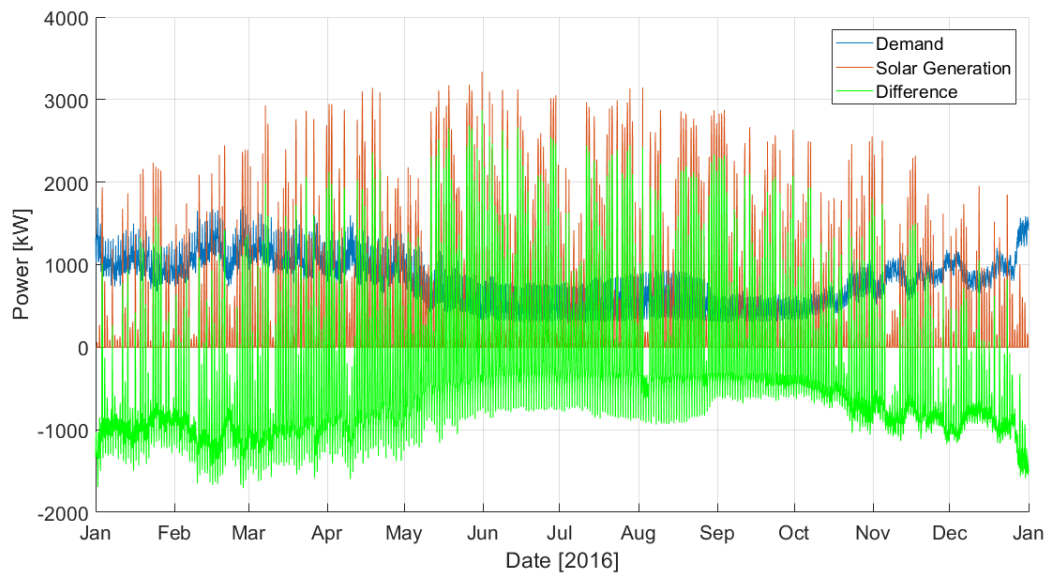


Figure 2.20 Comparison of solar generation from extensive solar covering 20% of the island rooftops and island electrical demand.



2.5 Resource Quantification: Wind

Wind energy is a well-established technology, and installations from single devices producing a few kW to farms of several hundred MW are generating electricity world-wide. Onshore wind does not have a happy history on Ushant however. In the 1980s, attempts to exploit the island's enviable wind resource were disrupted by technical problems (Pleijel, 2015; CORDIS, 1984), although improved technological understanding throughout the sector means that it is unlikely that the problems would recur with a modern wind energy installation. As an advanced and cost-effective technology, there is strong potential for wind energy to be part of the energy mix on Ushant, however, local opposition and planning constraints may prevent development.

2.5.1 Methodology

For this report, modelled wind speed data are used to estimate the resource available to be exploited by one or more wind turbines on Ushant.

The Global Wind Atlas (GWA) (DTU, 2017) provides average wind speed and power values for sites across the world. The data are modelled initially on a coarse scale grid using a re-analysis model, then the data are refined with a mesoscale model and accurate topography. Validation is undertaken at many sites where measured data are available. The GWA outputs values at 50m, 100m and 200m above sea level.

Measured wind speed data from almost thirty thousand observation stations around the world are available from the NOAA (National Oceanic and Atmospheric Administration, a US government agency), with the airfield on Ushant having records dating back to 1936. For the 10 years from 2007-2017, hourly wind speed and directional data were recorded from the airfield. The record for this period is 98.5% complete. As this data is recorded at surface level it has been scaled up to 100m (and to the nacelle heights for example installations) for wind speed and power calculations using a log profile.

A further source of wind speed data is the ECMWF Interim ERA-Reanalysis model (Dee, et al, 2011). This is a global atmospheric re-analysis model providing a number of surface and atmospheric parameters. Data from ECMWF forecast models are combined with available observations and used to produce a coherent record of the evolution of the global atmosphere. Among the parameters produced are global data values for wind speed over the period 1989 – 2015 in the form of six-hourly average wind speeds at 10m above sea level (Berrisford, et. al., 2011). For this study 26 years of data were extracted from the model and the seasonal and daily variation analysed. With the acquisition of the measured NOAA data the ECMWF model was not used in the calculations of wind speed or power, nonetheless it remains an available dataset for future calculations.

For this study, power production from a wind turbine was calculated by applying the NOAA data to the power curve for a selected turbine. It was then possible to match the times of each wind speed to the generation curve of the turbine and the output power shown.

The resource data are coarse and there is no spatial variation across the island. Sites constrained for technical, social or political reasons are shown as being unavailable but a specific site is not identified within the scope of this report.



2.5.2 Resource Constraints

Located on the Atlantic shoreline, Ushant has a considerable wind resource, with an average 717W/m^2 of wind power at 100m above sea-level (Global Wind Atlas, 2017).

Over the 10 years from 2007-2017 the NOAA measured data show an average wind speed for the island of 7.7ms^{-1} and a maximum sustained speed of 32.4ms^{-1} . As wind turbines are tall structures with a hub height of between 50 – 200m it is necessary to scale the wind speed to represent the values at a higher level. Wind speed at 100m is typically used as a starting point for a wind resource assessment (Brower, 2012). Wind profiles follow a logarithmic relationship related to the roughness length of the surface (z_0). This is a length scaling parameter for the log profile and is different depending on the constitution of the surface, for example, urban areas and forests will have relatively high roughness lengths (1-2m) whereas calm water or flat deserts would have relatively small values (0.0001-0.005m). For Ushant, if a surface roughness of $z_0 = 0.03$ is assumed (representing conditions expected from farmland with few buildings) then an average wind speed at 100m of 10.69ms^{-1} and a maximum of 45.2ms^{-1} can be derived from the NOAA data (NOAA, 2018). Average monthly values scaled to 10m and 100m are shown in Figure 2.21. The available data are constrained to hourly averages of wind speed, therefore maximum gust speeds are not available; these data should be examined if they become available in the future. The wind speed shows seasonal variation, with higher values on average throughout the winter months, coinciding with the island's increased electrical demand.

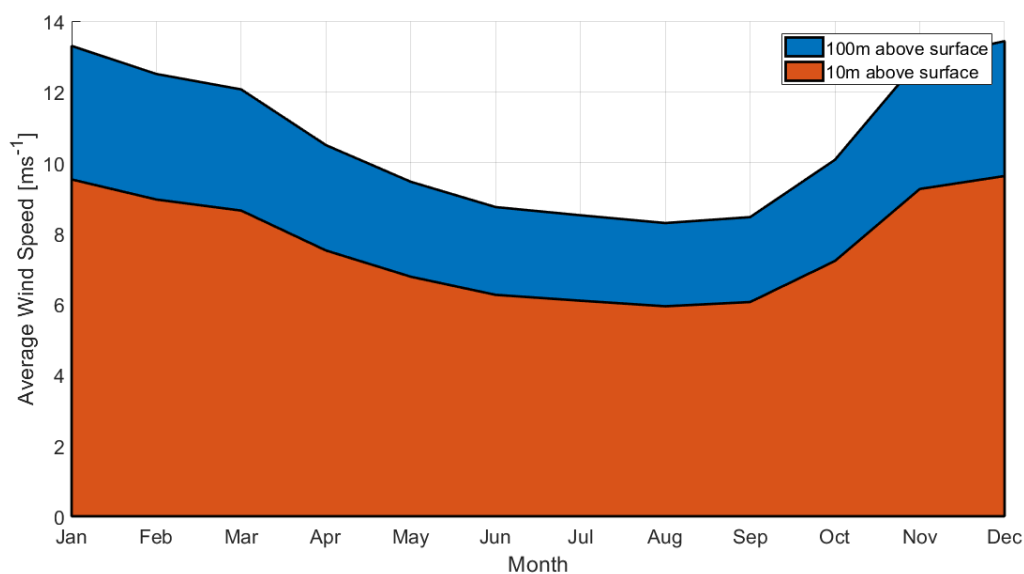


Figure 2.21 Average monthly wind speed at 10m and 100m above sea level.



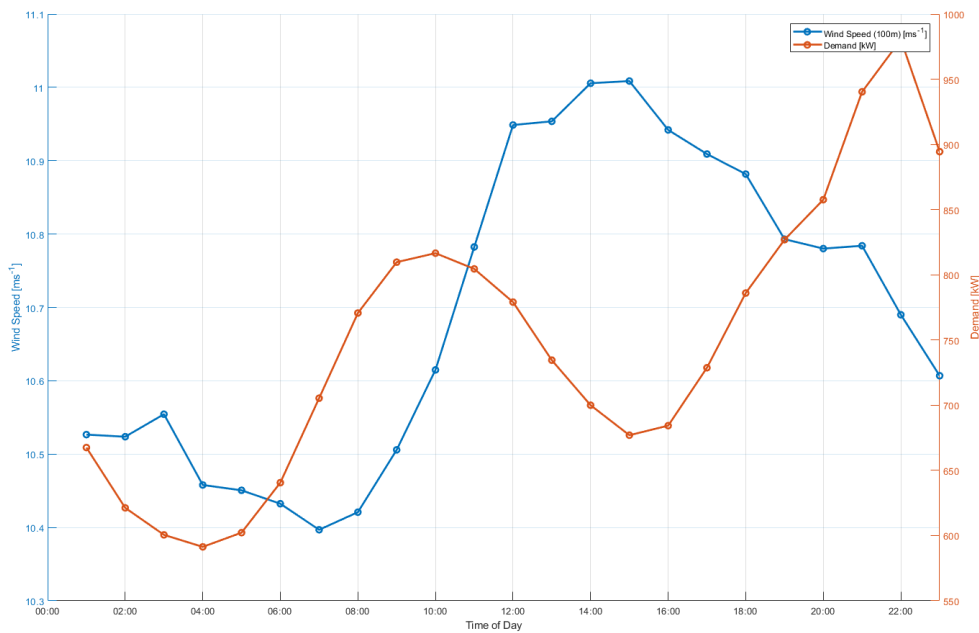


Figure 2.22 Intra-day wind speed at 100m compared with intra-day demand profile.

There is also a pattern to the intra-day variation in the wind speeds, with wind speeds highest on average in the afternoon and lowest in the early morning. Figure 2.22 compares the intra-day profiles of the average wind speed with the electrical demand; there is some correlation in the shape of the profiles but the maximum peaks of wind speed and demand do not coincide. Figure 2.22 is only a representation of the average profiles and individual days will show different data. A full distribution of wind speeds collected for 10 years (2006-2016) is shown in Figure 2.23.

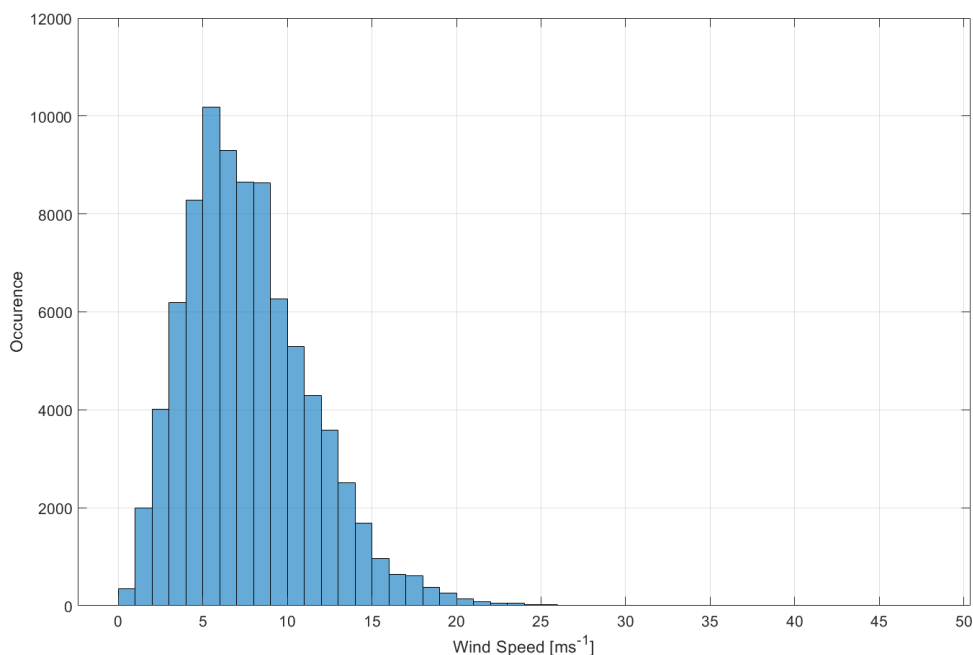


Figure 2.23 Distribution of wind speeds at 100m.



2.5.3 Technical Constraints

Successful installation of one or more wind turbines on the island will require a site with access for large construction vehicles, suitable geological terrain and a suitable cable route to the island's electrical grid. The turbines will need to be shipped to the island along with any bespoke construction equipment, therefore shipping and port requirements need to be considered in the planning.

The site of any wind turbines(s) will need to be connected to the island electrical network, and the route and distance of any high voltage and low voltage cabling will contribute to the cost and complexity of the installation. The high voltage network is shown in Figure 2.9 (in Section 2.3). It will be necessary to ensure that the cables and components are of sufficient capacity to export the maximum power from the turbine(s).

The island is mostly rock covered with a thin layer of soil and vegetation. Several installation techniques are available depending on the soil and rock conditions. Where there is bedrock close to the surface drilled piles or gravity bases can be used (Ashlock and Schaefer, 2011). The terrain is predominantly clear, with pasture or rocky surface, which makes it unlikely that any problems will be encountered locating a site with suitable terrain. The small areas of woodland, marsh or watercourses will be discounted from site selection.

Wind turbines should be located a safe distance from roads and buildings, for example, a minimum horizontal distance between turbines and roads is recommended by the UK Highways Agency of the maximum height of the turbine (from base to the highest point of the blades) plus 50m (Department of Transport, 2013). This is discussed in ICE report T1.1.1 (Hardwick et. al, 2018). Figure 2.24 shows the regions constrained by proximity to residential buildings and roads, analysed in GIS. The low density of roads and buildings on Ushant mean that there are available sites outside these buffer zones that can be seen on the GIS map. There is also a radar tower located on the north of the island; discussions with the relevant authorities should be undertaken to ensure that any turbines will be acceptable.





Figure 2.24 GIS of Ushant showing areas constrained by roads (yellow) or buildings (blue).

2.5.4 Environmental, Social and Political Constraints

A poor opinion of wind technology has persisted within the community since the failed project in the 1980s. Planning law also makes installation very challenging, given the island's geographical constraints and unique natural environment. While it may be legally feasible to build new onshore wind, local and NGO opposition to development is likely to mean that there are little or no real prospects in the immediate future. Nevertheless, the potential for wind energy is substantial and there is at least one live project to install a wind turbine, although a meteorological mast, planned as part of a resource measurement campaign was declined permission to build in 2018.

2.5.5 Site Identification

The island is very flat and there are no features that would affect the resource significantly at the hub height of a wind turbine. Available modelled wind data for the island are not of sufficiently high resolution to show variation across the island. The selection of suitable sites will therefore be best dictated by technical, environmental and social factors.

As the island's population density is low there are many choices of locations which fall the required distance from any properties; excluding sites a minimum of 500m from residences will minimise disruption from noise and shadows. However, locating a socially acceptable site will involve discussions between the energy companies, the island administration and the island residents.

2.5.6 Power Production

If wind turbines were installed on Ushant then a significant proportion of the island's electrical needs could be fulfilled. Examples are presented for three commercially available and commonly deployed wind turbines of differing sizes:



- An Enercon E33-300 – A 300kW rated turbine with a rotor diameter of 33m, deployed on a tower 35-47m high
- An Enercon E53-800 – An 800kW rated turbine with a rotor diameter of 53m, installed at a hub height of 60-73m
- A Vestas V90/2MW turbine - A 2MW turbine with a diameter of 90m, installed between 80-105m about the ground.

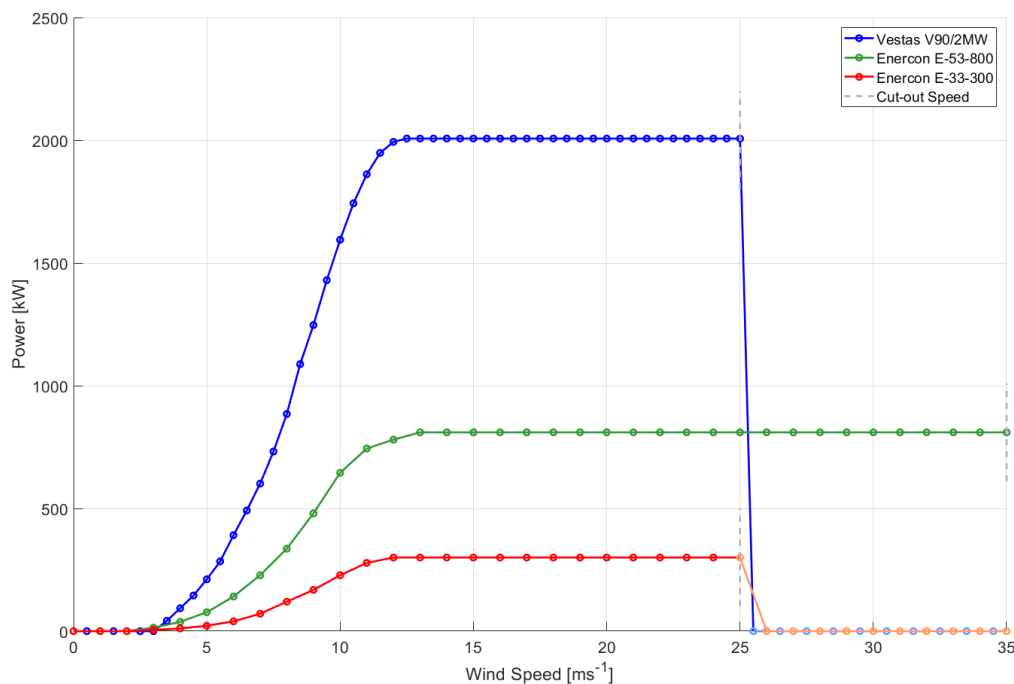


Figure 2.25 Manufacturer power curves for three wind turbine models.

The examples presented in this report are each for a single installed wind turbine. The calculations assume that a turbine is installed on ground 10m above sea level and use wind speed data from the NOAA database recorded from the Ushant airfield (described above in 2.5.1). The turbine nacelles are assumed to be installed in at the mid-point of the recommend hub-height ranges. Figure 2.25 shows the power curves for the selected turbines and indicates the cut-out wind speed where the turbines shut down for protection. A time series of wind speed measurements was collated from the NOAA data for the year 2016 and these data were compared to the island's electrical energy demand. The total amount of electrical energy that could have been generated in 2016 is 10.8GWh for the V90/2MW turbine, 4.4GWh for the E53-800 turbine and 1.5GWh for the E33-300 turbine. The electrical demand for the island for 2016 was 6.8GWh. While it appears that a single wind turbine can fulfil all the island's electrical needs it is important to investigate whether the timing of generation matches the demand requirements. The difference between generation and demand was analysed for each hour of 2016. Times when generation exceeded demand are noted as being generation surplus, when demand exceeded generation as generation deficit. The results are shown in Table 2.7.



Table 2.7 Hours of generation surplus/deficit.

Turbine	Generation surplus [hours]	Generation deficit [hours]
Vestas V90/2MW	6060	2723
Enercon E53-800	1726	7057
Enercon E33-300	1	8782

There is a large seasonal disparity in the electrical demand with 60% of electrical use occurring in the winter months (October – March). The seasonality of wind generation was examined to see whether the faster wind speeds in the winter months transferred to higher electrical generation. The wind generation is distributed in almost the same seasonal proportions to the electrical demand, shown in Table 2.8.

Table 2.8 Seasonal variation in wind generation.

Turbine	Summer Generation	Winter Generation	Proportion
Vestas V90/2MW	4.6GWh	6.2GWh	42.5% / 57.5%
Enercon E53-800	1.7GWh	2.6GWh	41.0% / 59.0%
Enercon E33-300	0.6GWh	0.9GWh	41.3% / 58.7%
Demand	2.7GWh	4.1GWh	39.3% / 60.7%

During periods of generation surplus the entire island's electrical requirements are being fulfilled by the single example wind turbine. Where the turbine is generating significantly more power than the islands demand then the turbine output can be curtailed. During periods of generation deficit other sources of generation will be required to supply the rest of the demand.

The comparison between generation from the turbines and the island demand is presented in Figure 2.26; the surplus/deficit is shown in green with positive values representing a surplus and negative a deficit.

Scenarios examining combinations of renewable technologies are presented in section 2.9.



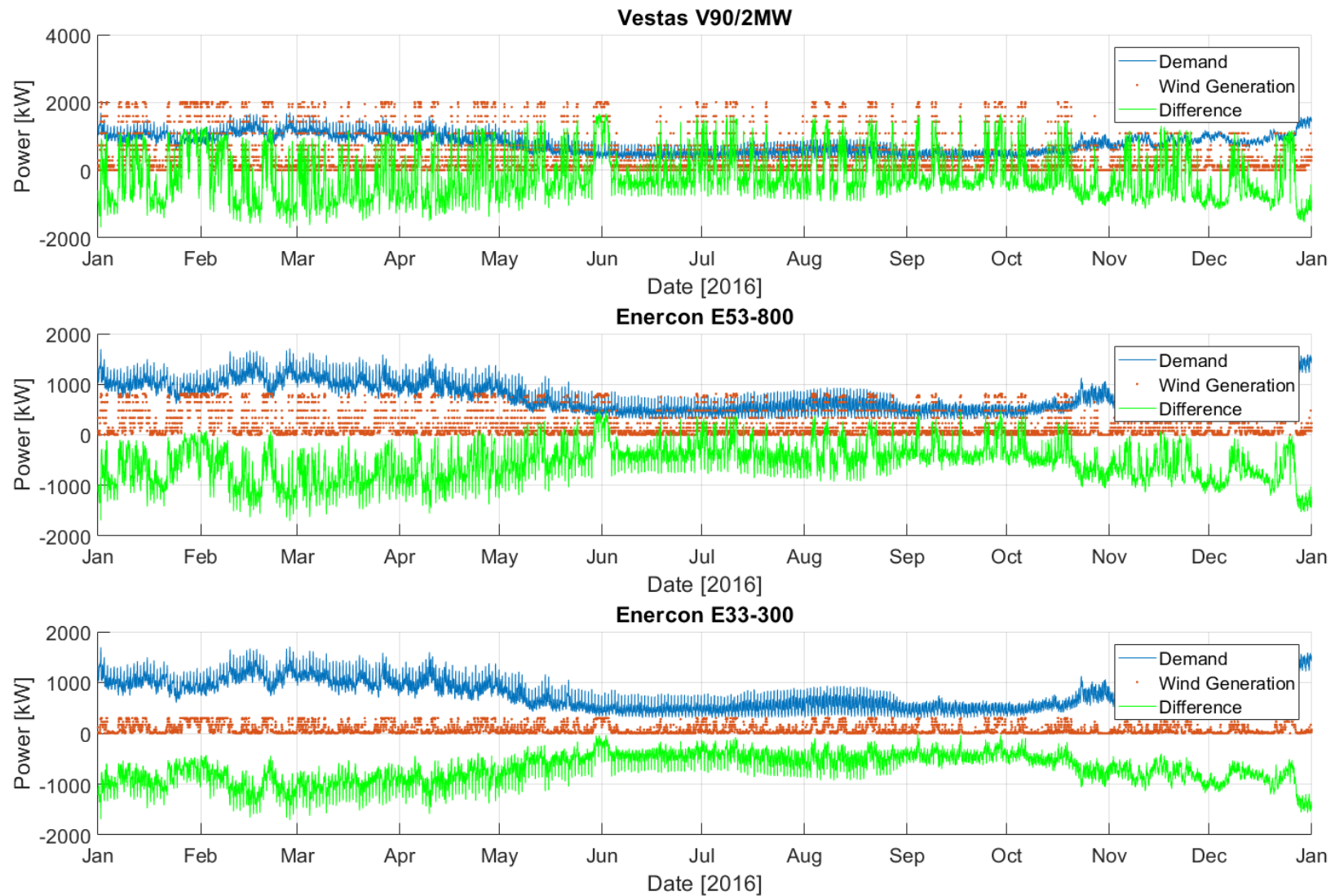


Figure 2.26 Time series comparing the electrical generation from each wind turbine to the island's demand for 2016. Net surplus/deficit of generation shown in green.



2.6 Resource Quantification: Tidal

Tides are caused by constantly changing gravitational forces due to the relative motion between the Earth, Moon and Sun. Tidal streams are the currents caused by the displacement of water due to the rise and fall of the sea surface from the tidal forcing. Recent developments in turbine technology allow the extraction of kinetic energy from tidal flows. Tidal stream resources are generally largest in areas where a good tidal range exists, and where the speed of the currents is amplified by the funnelling effect of the local coastline and seabed, for example, in narrow straits and inlets, around headlands, and in channels between islands. Although the tidal current is highly sensitive to the specific location, the tidal cycle can be predicted with high accuracy over very long periods due to knowledge of the astronomical forces which drive the tides, and therefore the power output of a tidal plant at a given location can also be accurately predicted.

2.6.1 Methodology

The objective of this study is to assess the tidal dynamics around Ushant, identify appropriate sites for tidal energy conversion, and evaluate potential power production. In particular, power production associated with the existing Sabella D10 tidal turbine is assessed. Sabella D10 is a 10 m diameter tidal turbine (Figure 2.27), deployed in the Fromveur Passage off the south-eastern coast of Ushant on 25th June 2015. It was connected to the grid on 5th November 2015, making it is the first French tidal turbine producing electricity and connected to the electrical network (Paboeuf et al., 2016).



Figure 2.27 Sabella D10 tidal turbine in the Brest assembly area (Paboeuf et al., 2016).

2.6.2 Resource constraints

2.6.2.1 Bathymetry

Bathymetry data around Ushant are available at a resolution of 0.001° ($\sim 111\text{m}$) decreasing with distance from the island to a resolution of $0.125'$ ($\sim 230\text{m}$). These form part of a bathymetric DEM (digital elevation model) of the Atlantic seaboard, developed in the HOMONIM project (SHOM, 2018),



which includes part of the North Sea, the Channel and the Bay of Biscay. It also extends beyond the continental shelf to approximately 4800 m depth offshore.

Figure 2.28 shows the bathymetry of the region at three scales. It can be seen that the area outlined in red in the third image would be a suitably homogenous area for tidal stream turbine installation.



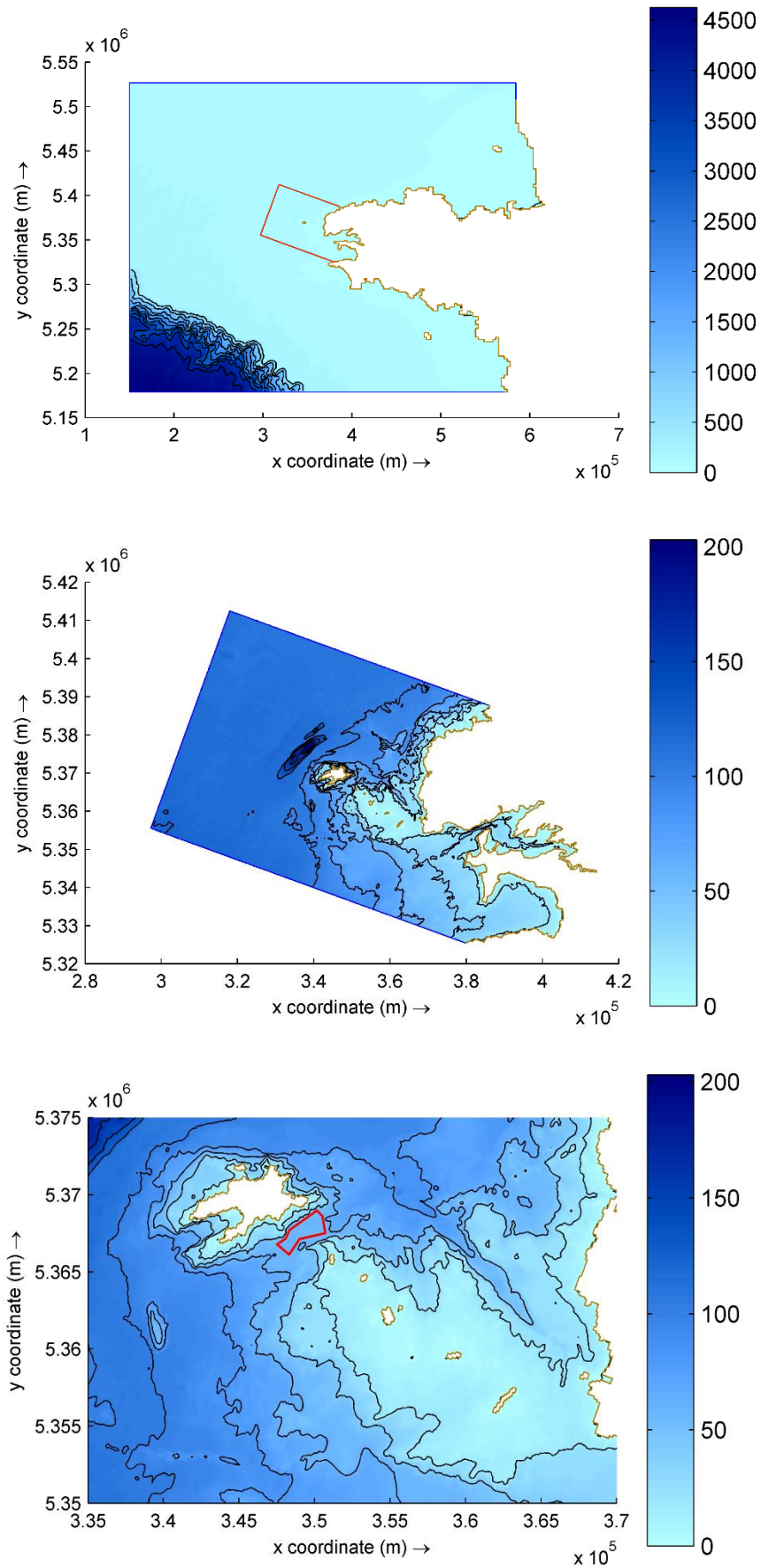


Figure 2.28 Bathymetric contours, with colour scale showing depth in metres.



2.6.2.1 Tidal Range

The two closest tidal measurement stations to the region of interest are Ushant and Le Conquet (as plotted in Figure 2.29). The tidal range at these two sites can be obtained by using tidal constituents. The key parameters of amplitude and phase for 20 selected tidal constituents for Ushant and Le Conquet are given in Table 2.9.

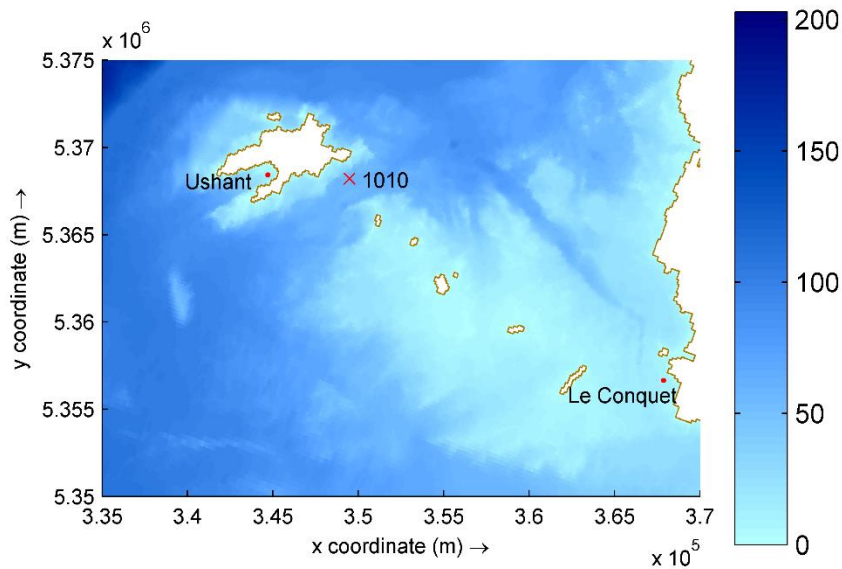


Figure 2.29 Locations of the tidal measurement stations.

Table 2.9 20 selected tidal constituents at the sites of Ushant and Le Conquet.

Constituent name	Ushant		Le Conquet	
	Amplitude (m)	Phase (deg)	Amplitude (m)	Phase (deg)
M2	2.065	110.5159	2.02	112.2159
S2	0.828	149.6	0.735	151.3
N2	0.416	88.8603	0.409	91.9603
K2	0.209	146.4179	0.208	148.3179
NU2	0.09	78.9874	0.086	92.9874
MU2	0.07	103.6318	0.076	95.6318
M4	0.01	129.2318	0.075	141.2318
L2	0.064	88.4715	0.074	95.7715
O1	0.059	323.657	0.071	327.757
K1	0.069	77.8589	0.066	74.5589
MS4	0.02	245.5159	0.057	192.8159
2N2	0.055	71.2046	0.054	84.9046
MM	0.09	254.6556	0.045	239.1556
SSA	0.086	303.0179	0.033	232.5179
MSM	0.027	8.8285	0.03	285.0285
MF	0.041	191.902	0.026	185.302
Q1	0.013	274.6013	0.021	291.1013
P1	0.022	77.8411	0.02	56.2411
OP2	0.018	22.398	0.019	44.398
MSF	0.052	217.7841	0.015	216.8841



Plots of the tidal height at Ushant and Le Conquet for 2017 are presented in Figure 2.30

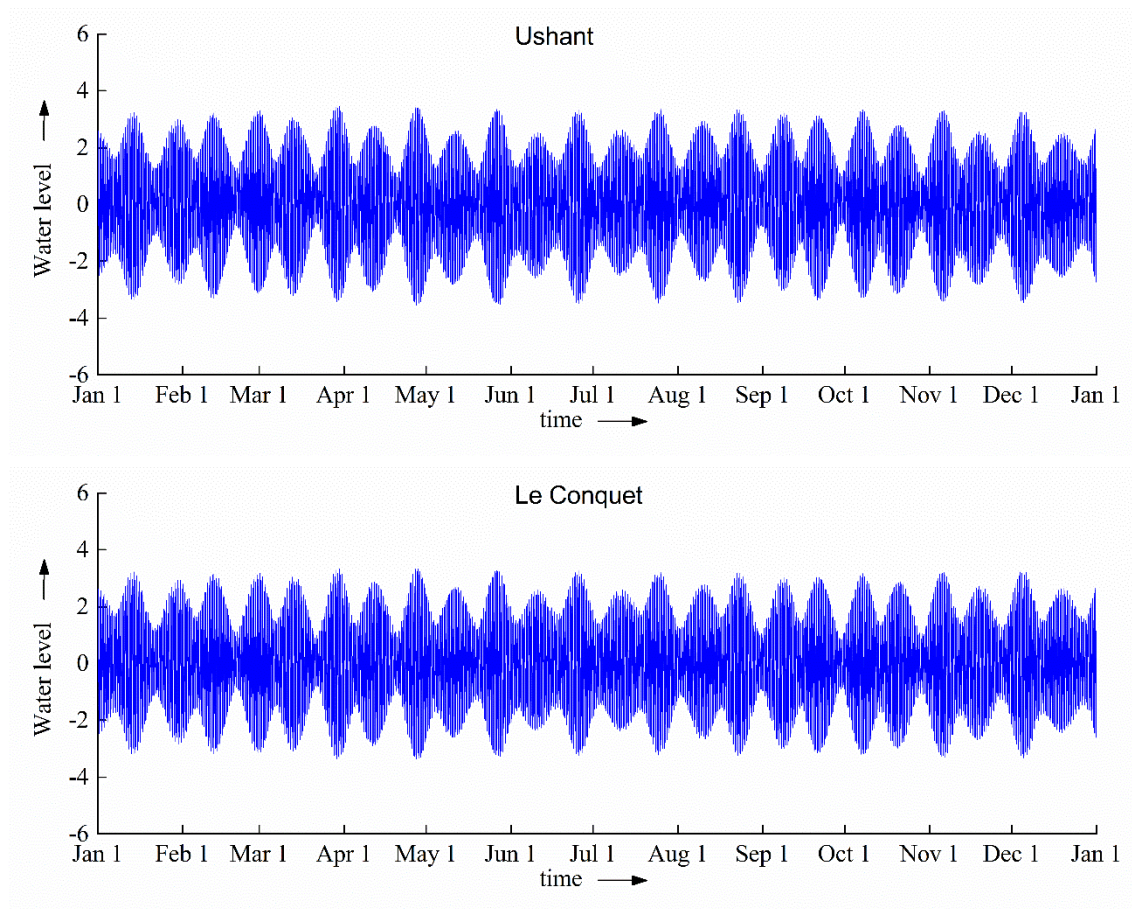


Figure 2.30 Annual plot of the tidal height at Ushant and Le Conquet for 2017.

The tidal range is the difference between the height of high and low water on each tide. The maximum, minimum and average tidal range for each month at these two sites are presented in Table 2.10, from which August 2017 has been determined as representative of the average month for 2017.



Table 2.10 Maximum, minimum and average tidal range for each month of 2017.

Month	Tidal range at Ushant (m)			Tidal range at Le Conquet (m)		
	maximum	minimum	average	maximum	minimum	average
January	6.641	2.289	4.465	6.435	2.200	4.318
February	6.547	1.935	4.241	6.368	1.809	4.089
March	6.905	1.751	4.328	6.705	1.718	4.212
April	6.979	1.732	4.356	6.722	1.817	4.270
May	6.904	2.134	4.519	6.588	2.316	4.452
Jun	6.845	2.793	4.819	6.508	2.992	4.750
July	6.863	2.646	4.755	6.479	2.655	4.567
August	6.795	1.898	4.347	6.439	2.337	4.388
September	6.500	1.632	4.066	6.213	1.665	3.939
October	6.631	1.677	4.154	6.354	1.705	4.030
November	6.708	2.128	4.418	6.492	2.164	4.328
December	6.775	2.677	4.726	6.606	2.717	4.662

Figure 2.31 provides a 30-day plot of the tidal height above and below mean water level at the sites of Ushant and Le Conquet for August 2017, the month identified as representative. The spring and neap cycles can be clearly identified.

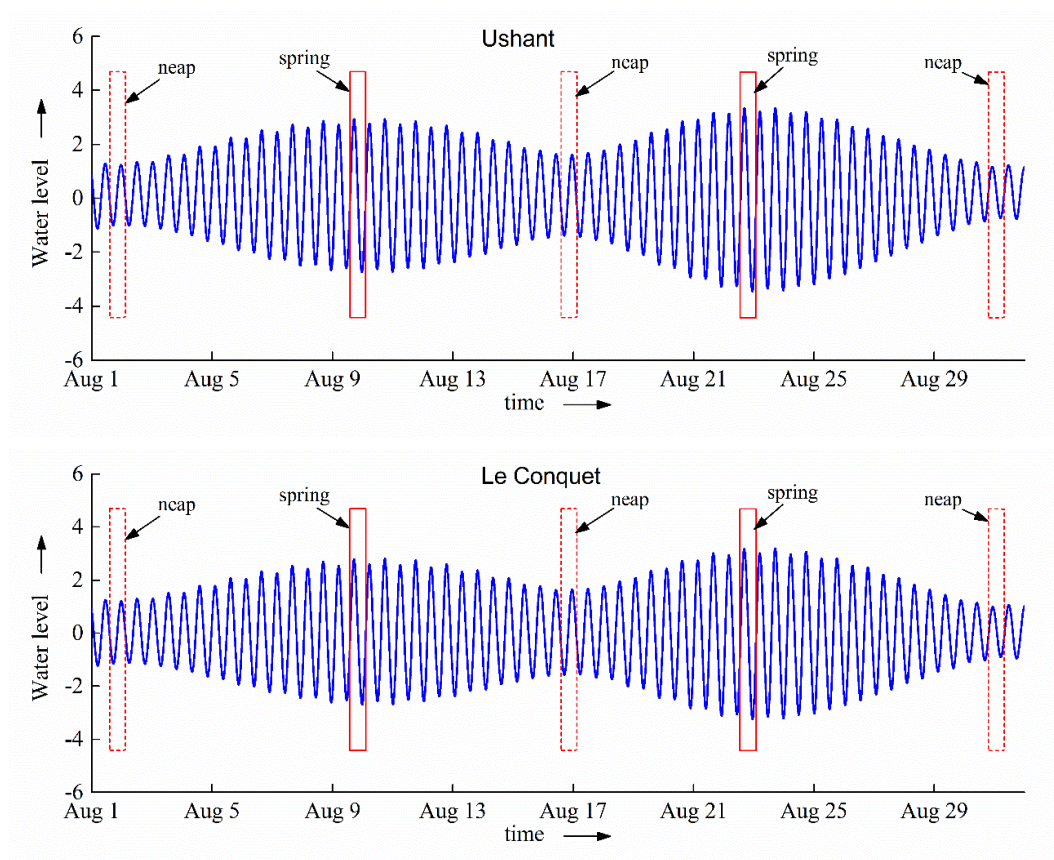


Figure 2.31 30-day (Aug 2017) plot of the tidal height above a datum at the sites of Ushant and Le Conquet.



Figure 2.32 plots the tidal height over a 50-hour period at both sites during spring tides, when the tidal range is at its maximum.

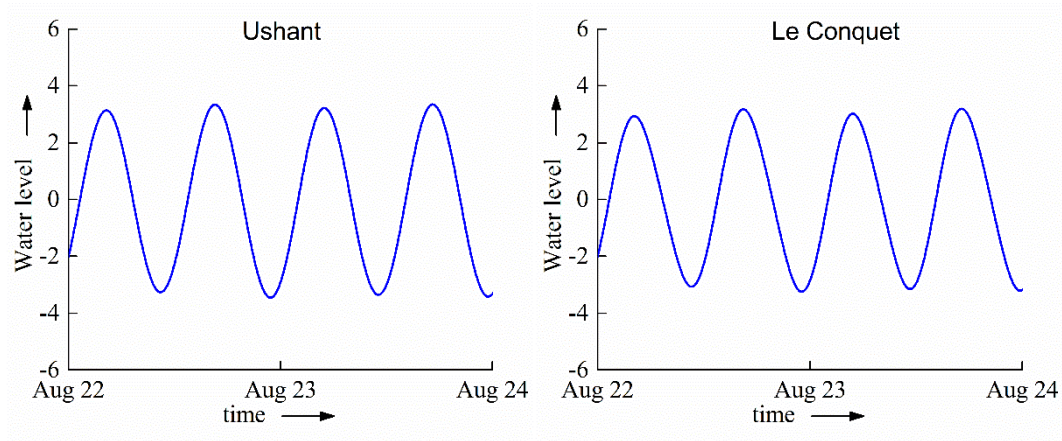


Figure 2.32 50-hour plot of the tidal range at spring tide

Both Ushant and Le Conquet experience two high and two low tides of approximately equal size every lunar day, thus the region has a semi-diurnal tidal cycle.

2.6.2.2 Tidal Currents

Observations of current amplitude and direction 10 m above the seabed at point '1010' (5.056° W, 48.449° N, shown in Figure 2.29), are shown in Figure 2.33, taken from figures presented in Guillou and Thiébot (2016) and Guillou and Chapalain (2017). The data were recorded using a 600 kHz RDI ADCP (acoustic Doppler current profiler) deployed by the French Navy SHOM (Service Hydrographique et Océanographique de la Marine). The measurement period corresponds to the neap-spring tidal condition from 19th March to 2nd April 1993. Whereas ADCP data are available in 2 m bins distributed throughout the water column at the measurement point, comparisons between observations and predictions are performed 10 m above the bed as this corresponds to the operating height of the planned horizontal axis turbines in the Fromveur Passage.

A full tidal harmonic analysis, based on the ADCP measurements, is presented in Appendix 2.

The set-up of a Delft3D hydrodynamic model to simulate the tidal regime around Ushant is presented in Appendix 3.



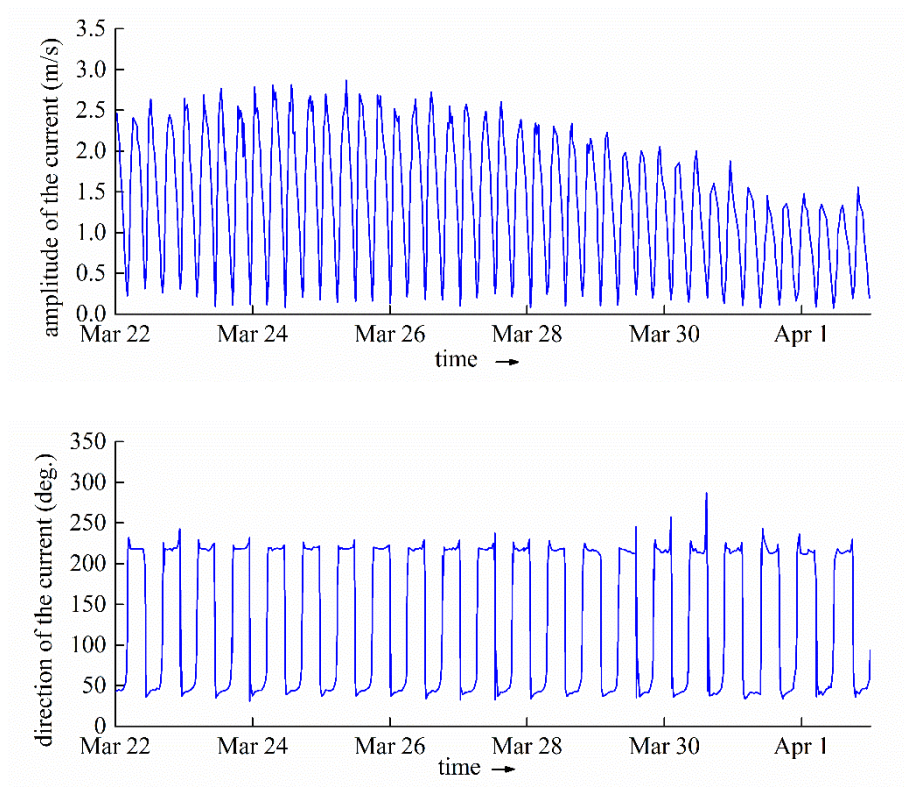


Figure 2.33 Measured time series of the amplitude and direction (anticlockwise convention from the East) of the current 10m above the seabed at point #1010 in March-April 1993 (Guillou and Thiébot, 2016; Guillou and Chapalain, 2017).

2.6.3 Technical Constraints

Cables, piles, wrecks and other technical constraints are illustrated in Figure 2.344. It can be seen that there is one active subsea cable to the west of Ushant, and piles are mostly deployed around the port of Brest. Attention should also be paid to the location of wrecks.

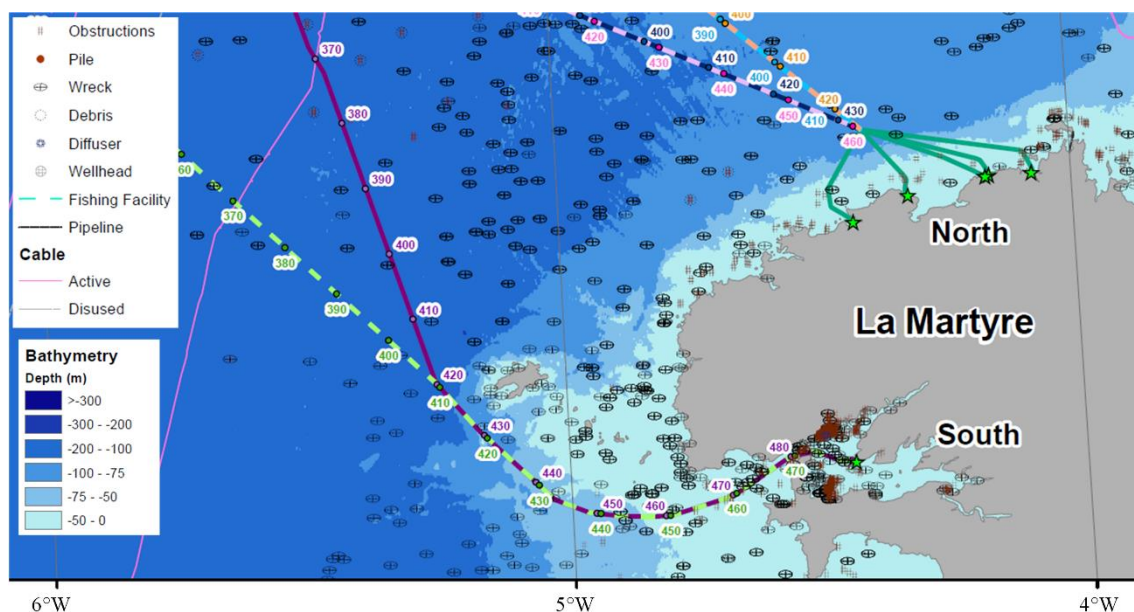


Figure 2.34 Technical constraints in the waters around Ushant (Intertek, 2015).



The offshore services provider Bourbon completed the installation of a subsea electrical cable for Sabella's D10 tidal energy project off Ushant in 2015, with 30 tons of 68 mm diameter cable buried over a 2 km distance, at water depths from 0 to 60 m, in the Fromveur Passage (Subsea World News, 2015).

The impact of tidal energy production on the grid is potentially significant for the existing generators. Therefore, it was agreed with the grid operator to limit the export of power from the Sabella D10 turbine into the grid. The upper limit can vary from 50 kW to 250 kW depending on the grid load on Ushant (Paboeuf et al., 2016).

In addition to man-made constraints, the seabed conditions and geology in the region are important in identifying sites for tidal power extraction. An ideal installation site for tidal stream energy converters should be sufficiently smooth and level for installation, avoiding sediment deposition. The geology of the region is presented in Figure 2.355, showing a predominantly rocky seabed around the island.

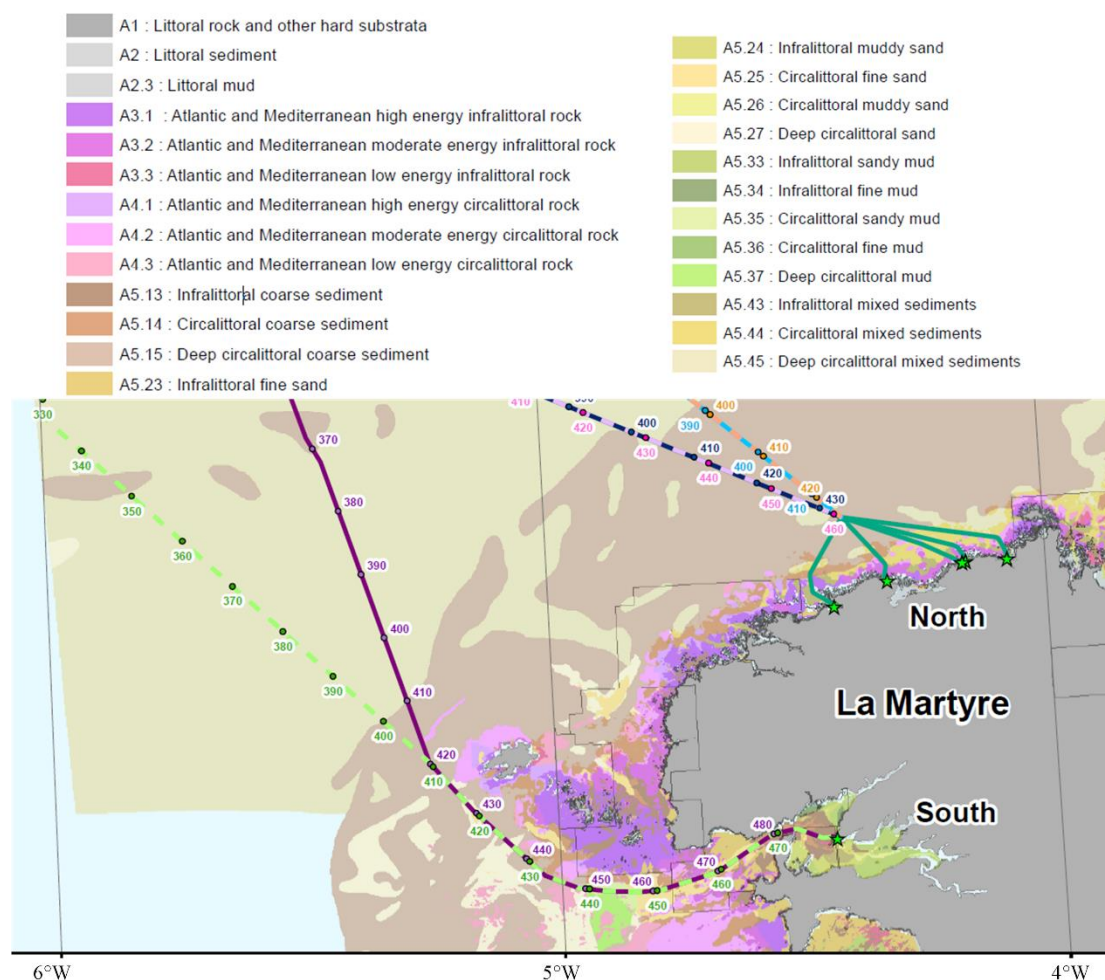


Figure 2.35 Seabed geology constraints in Ushant region (Intertek, 2015).

2.6.4 Environmental, Social and Political Constraints

Ushant is situated within the Parc Naturel Marin d'Iroise (Iroise Marine Nature Park), located off the west coast of Brittany (Figure 2.366). The aim of the Iroise marine park is to improve understanding of the marine environment, to protect both the wildlife and cultural heritage, and to sustainably



develop marine activities such as sustainable fisheries and seaweed farming. The Iroise marine park is not opposed to the Sabella tidal installation, primarily due to a wide-reaching communication and consultation strategy among public bodies, sea users, island residents and the general public (Le Marin, 2013).

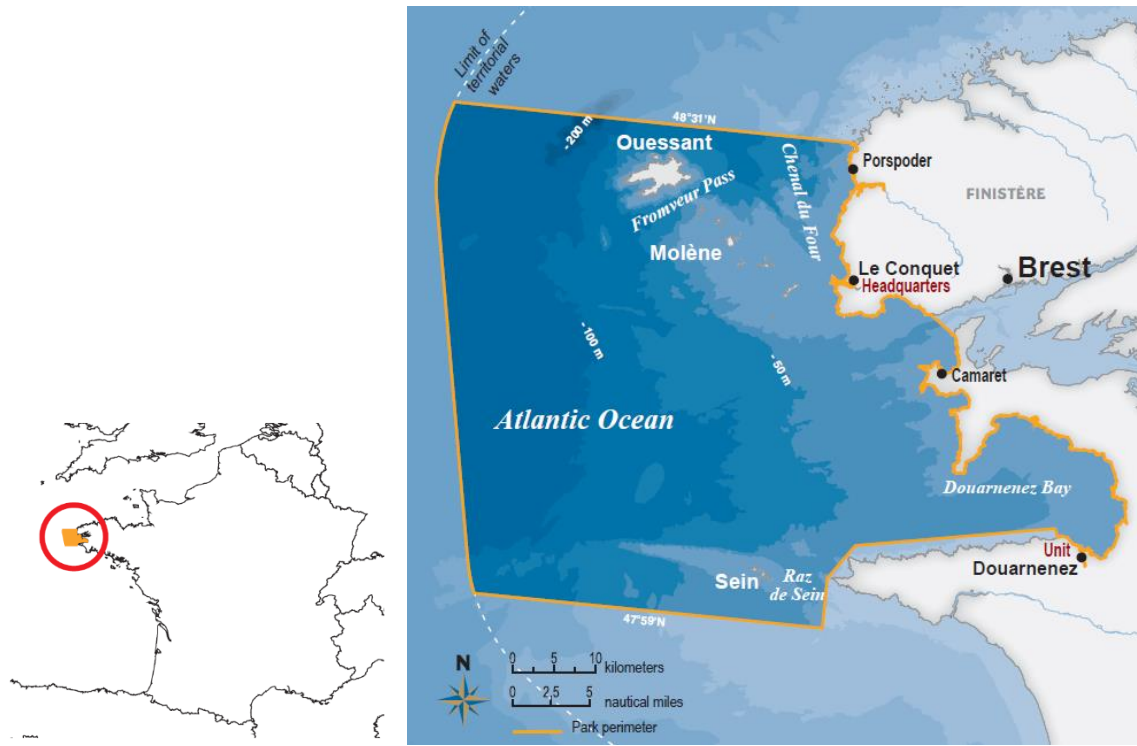


Figure 2.36 Iroise Marine Nature Park (Agence des aires marines protégées, 2015).

In addition to its status as a marine nature park, the region is also a Marine Protected Area under the Oslo-Paris convention. Parts are also listed under the European Habitats and Birds directives and as a UNESCO biosphere reserve (IUCN, 2017). There is an additional protected site, Ouessant-Molène, which is an important area for birds and protected marine species including seals, dolphins, sea otters and basking sharks (Intertek, 2015). The environmental constraints are presented in Figure 2.377.



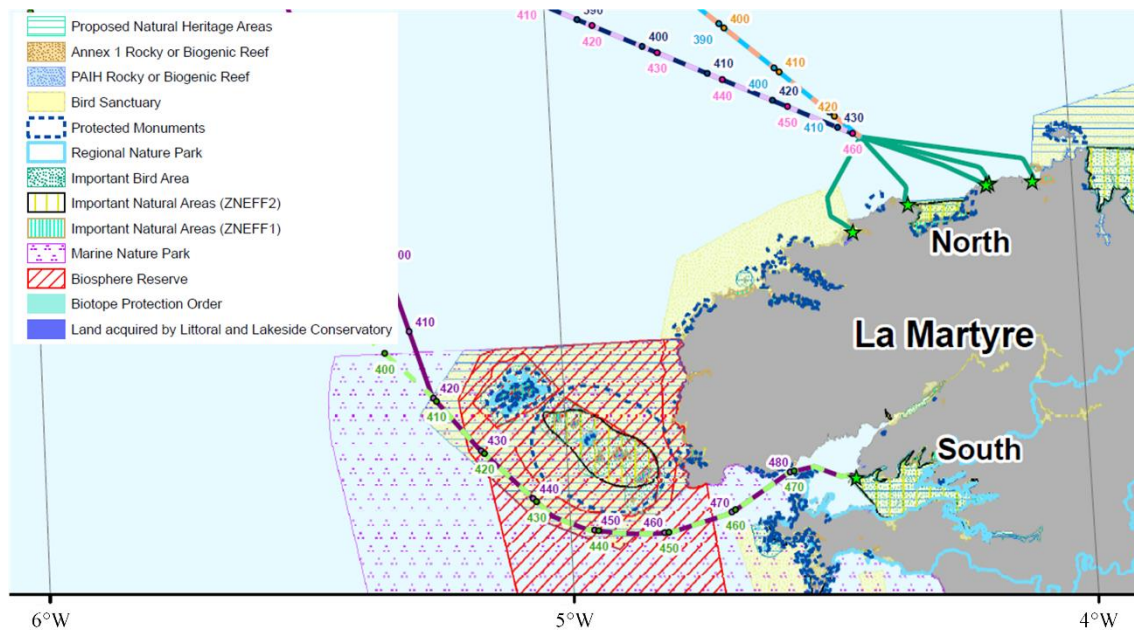


Figure 2.37 Environmental constraints in the Ushant region (Intertek, 2015).

Authority to permit marine renewable energy development in France currently rests with both local and central government. An environmental permit must be issued by the French State and permission to occupy the seabed obtained from the local prefecture. Obtaining an environmental permit requires performance of an environmental impact assessment (EIA), in line with EU requirements if sites are designated as Natura 2000 sites under the Habitats and Birds directives, as the site for the Ushant turbine is, and a protected species assessment. This process requires public consultation. A second permit to occupy the public marine domain is required from the Prefect of the Département (in the case of Ushant, Finistère) considering issues of maritime safety and impacts on economic activity. The public consultation for this permit may be run in conjunction with that for the environmental permit.

There are plans to streamline this process through the issue of a flexible ‘permit envelope’ which can be gained by developers earlier in the development process in order to reduce the risk of designing projects which are unable to gain the required permits. France is also required by the EU Marine Spatial Planning Directive 2014 (European Commission, 2014) to complete a plan identifying and designating sites for ocean energy projects by 2021.

Permits may be limited in time for demonstration projects such as the Sabella D10 device deployed off Ushant. However, the popularity of tidal energy among the local community and limited resistance from local fishers mean that a future permit is likely to be granted.

A map of socio-economic constraints in the region around Ushant is presented in Figure 2.388. In the Fromveur Passage, there are no specific constraints relating to marine traffic. This is due to the large tidal current, which could be very dangerous for shipping. On the north-east side of the island, there are multiple constraints including inshore traffic zones, dumping grounds, traffic separation schemes and dredger transit routes. This could present challenges to offshore deployment in this region.



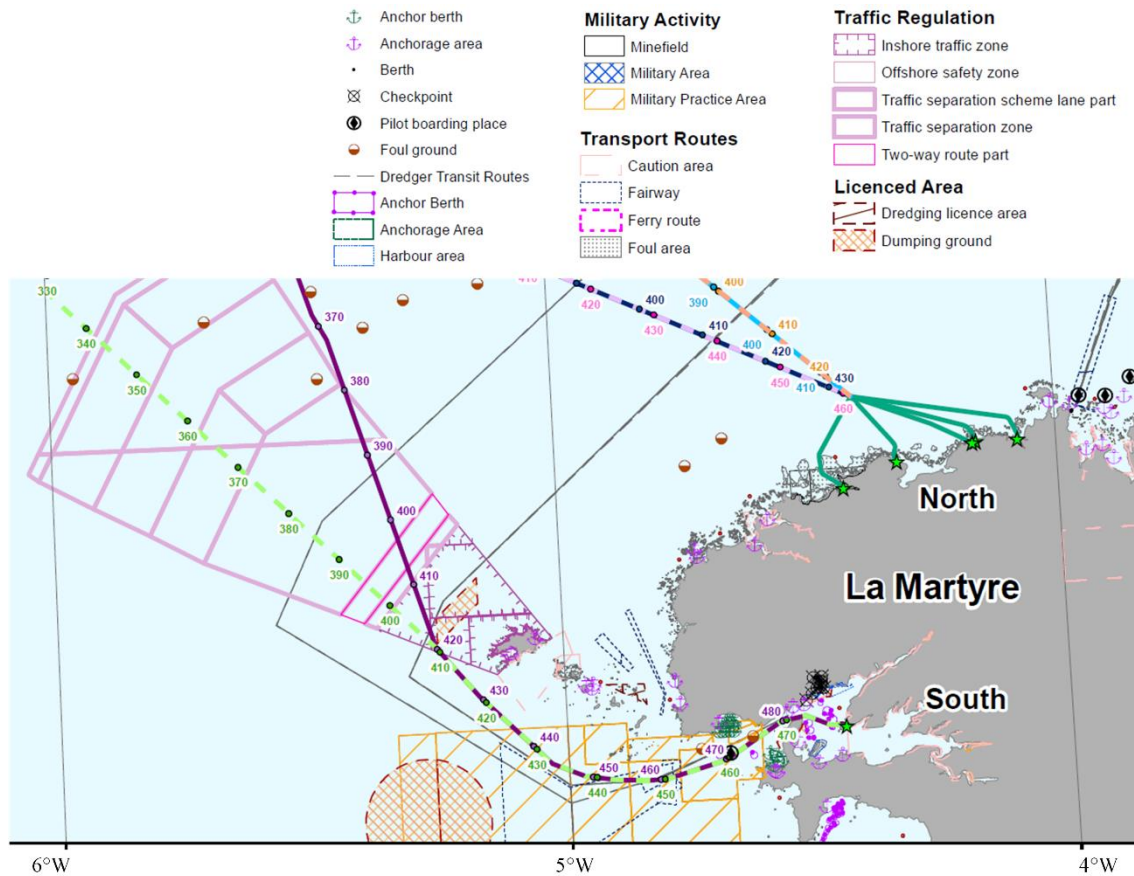


Figure 2.38 Socio-economic constraints in the Ushant region (Intertek, 2015).

2.6.5 Site Identification

The spatial variation of the maximum current 10 m above the seabed around Ushant is shown in Figure 2.399 (SHOM, 2018). This shows three regions, marked as region I, II (the Fromveur Passage) and III, with stronger tidal currents than the rest of the region, and therefore more suitable for potential tidal energy conversion.



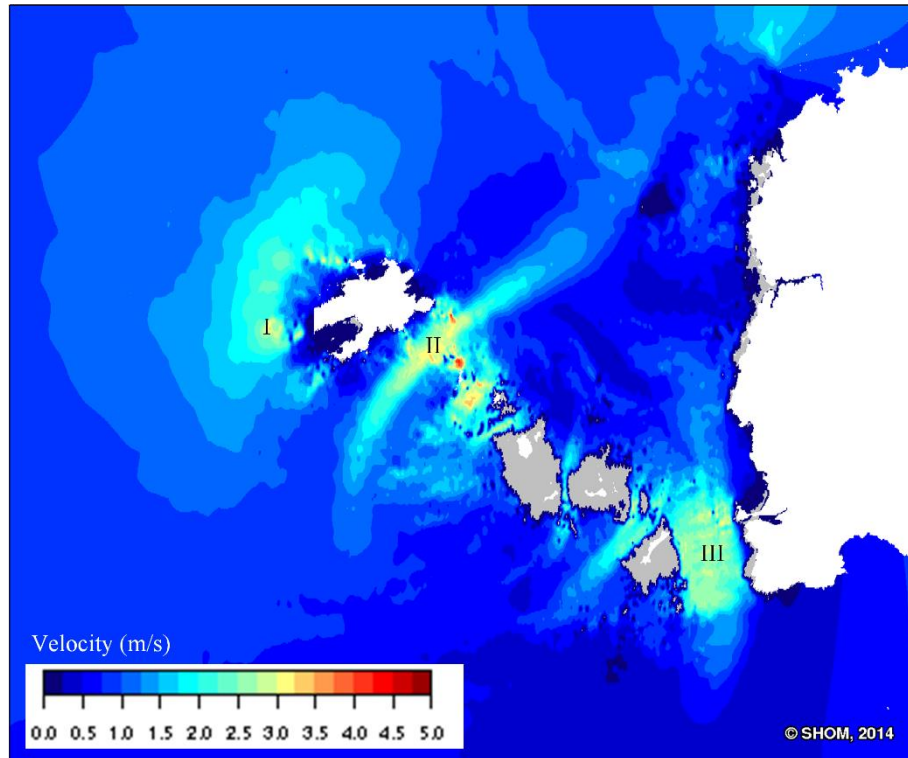


Figure 2.39 Amplitude of tidal current at 10 m above seabed (SHOM, 2018).

For tidal energy converters that are not able to adjust their orientation with the direction of the flow, such as the Sabella D10, the variance in flow directionality across the tidal cycle must also be considered. Figure 2.4040 presents output from the hydrodynamic modelling study (see Appendix 3). Depth-averaged currents are shown at two-hourly time-steps through a tidal cycle, i.e. 00:00:00-10:00:00, on 23rd August 2017. Note that at 00:00:00 and 02:00:00, the current velocities in region I are low, however, these increase as the tidal cycle progresses, reaching 3-3.5 ms^{-1} at 04:00:00 with the direction coming from south-east. The directionality then begins to change, until at 08:00:00 and 10:00:00, the currents in region I are from the north-east, are almost perpendicular to those at 04:00:00 and 06:00:00. This makes the site unsuitable for deployment of tidal turbines that are not able to align themselves with the flow. As a comparison, the currents exhibit approximately bi-linear directionality along a single axis in regions II and III, making these sites better options for tidal energy conversion.



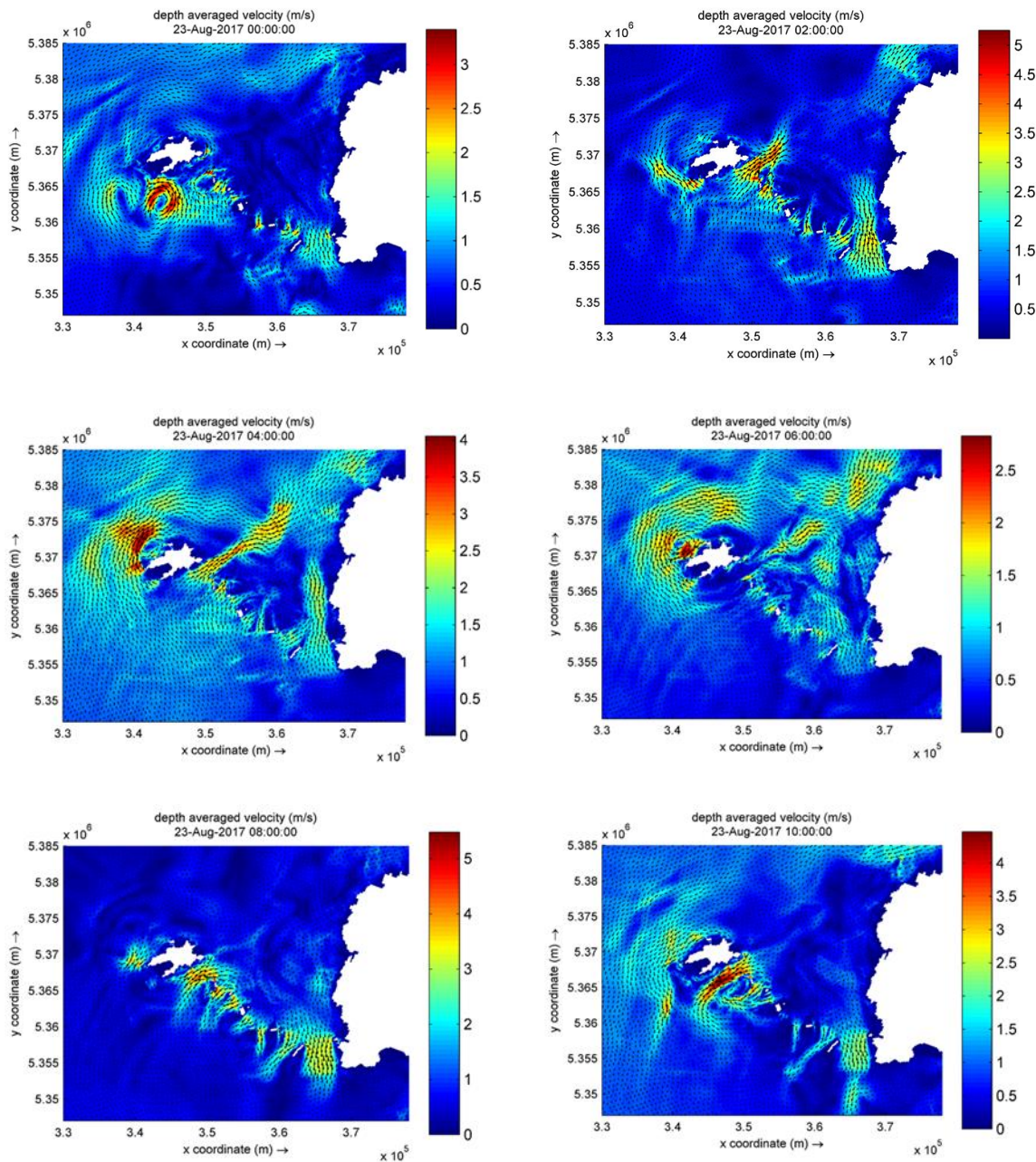


Figure 2.40 Depth averaged tidal velocities around Ushant at 2-hrly intervals through the tidal cycle.

When considering the constraints previously discussed, both regions II and III are located in the marine nature park and biosphere reserve. Region II has the advantage of being closer to Ushant, and permits have already been granted for the deployment of the Sabella D10. Therefore, region II is considered to have the greatest potential for converting tidal power to supply electricity for Ushant.

Two points in region II, denoted as A and B (Figure 2.411), are selected as potential locations for tidal turbine deployment, with A being the site of the Sabella D10. The coordinates of A and B are 48.44759° N, 5.034197° W and 48.44237° N, 5.04152° W, respectively.



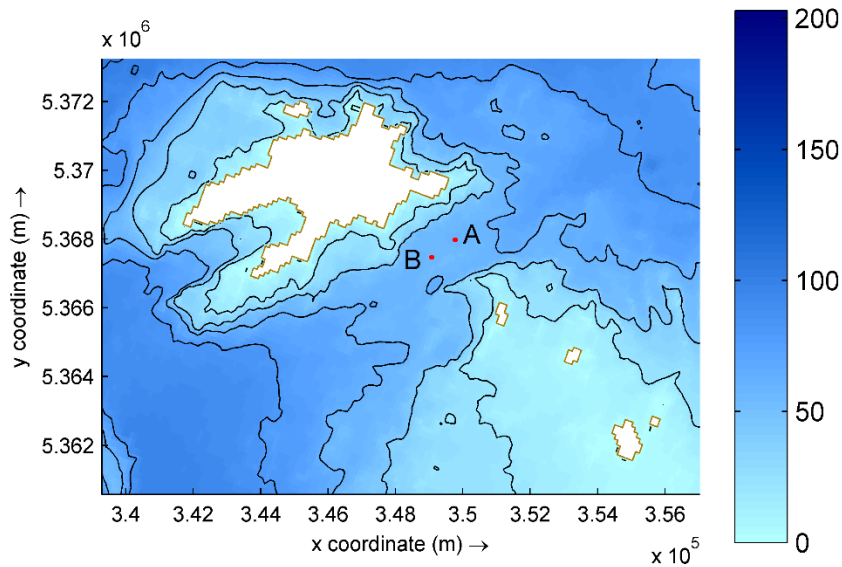


Figure 2.41 Locations of Point A and Point B.

The hub of the Sabella D10 is 12.5m above the seabed, therefore for accurate power production calculations, the flow must be assessed at this depth. Figure 2.42 presents the tidal currents in August 2017 at 12.5m above the seabed at Point A and B respectively, calculated from the numerical model described in Appendix 3 using the depth profile equation.

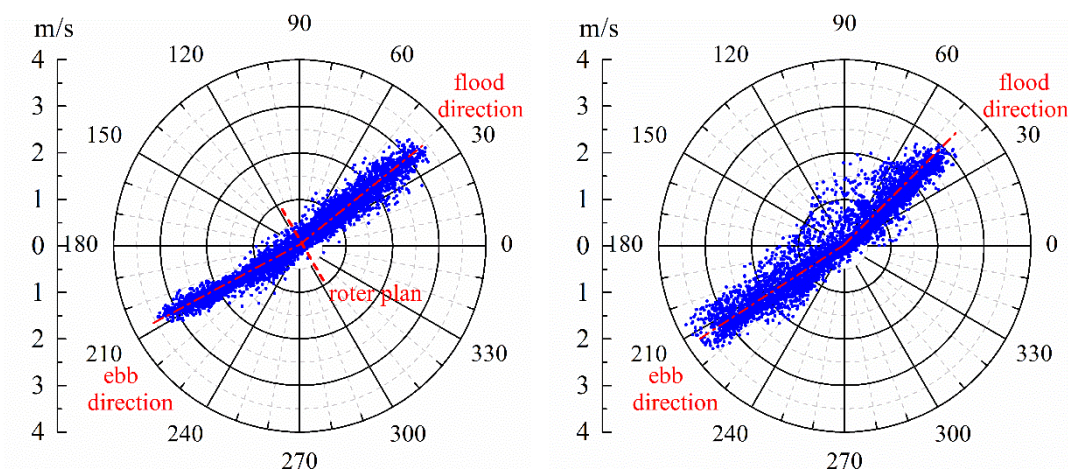


Figure 2.42: Plot of the tidal current at 12.5 m above the seabed at Point A and B, respectively, in August 2017.

The tidal currents flowing north-east are described as flood currents while those flowing south-west are the ebb currents. The maximum velocities of the flood current and ebb current at Point A are both approximately 3.5ms^{-1} , while at Point B they are 3.0ms^{-1} and 3.7ms^{-1} respectively.

Compared with Point B, the currents at Point A are more concentrated around the linear flood and ebb axis and are a more suitable resource for tidal turbines as Sabella D10 which cannot change their orientation. Therefore, it can be concluded that Point A is the more appropriate location for the installation of the Sabella D10. The remainder of this study focuses on tidal current power production at Point A.



2.6.6 Power Production

In order to compare generation from the Sabella D10 turbine to the Ushant demand profile, twelve months of power production were estimated for the year 2016 using the current speeds derived from the harmonic analysis (see Appendix 2). Limitations with time and computing power meant that the Delft3D hydrodynamic model output is only available for August 2017 and there are currently no demand data currently available for that period.

The estimated total amount of electrical energy, using the methodology presented in Appendix 4, that could have been generated in 2016 is 1GWh. The electrical demand for the island for 2016 was 6.8GWh. A Sabella D10 turbine could therefore provide approximately 15% of the island's electrical requirements. It is important to investigate whether the timing of generation matches the demand requirements. The difference between generation and demand was analysed for each hour of 2016. Times when generation exceeded demand were noted as being generation surplus, and when demand exceeded generation it was noted as generation deficit. The results are shown in Table 2.11.

Table 2.11 Estimated generation parameters for the Sabella D10 turbine.

Sabella D10	2016 Power Production Estimations		
	Annual	Summer	Winter
Energy Generation [MWh]	1000.52	509.24	491.29
Surplus (+ve) / Deficit (-ve) [MWh]	-5806.62	-2167.36	-3639.25
Number of hours surplus	153 / 8784	127 / 4392	26 / 4392
Number of hours deficit	8630 / 8784	4265 / 4392	4365 / 4392
Peak surplus [kW]	441.19	441.19	326.49
Peak deficit [kW]	1692.12	1409.15	1692.12

During periods of generation surplus the entire island's electrical requirements are being fulfilled by the Sabella turbine. Where the turbine is generating more power than the island's demand then the



turbine output can be used to charge energy storage systems or dumped. During periods of generation deficit other sources of generation will be required to supply the rest of the demand.

The comparison between generation from the turbine and the island demand is presented in Figure 2.43; the surplus/deficit is shown in green with positive values representing a surplus and negative a deficit.

Scenarios examining combinations of renewable technologies are presented in section 2.9.

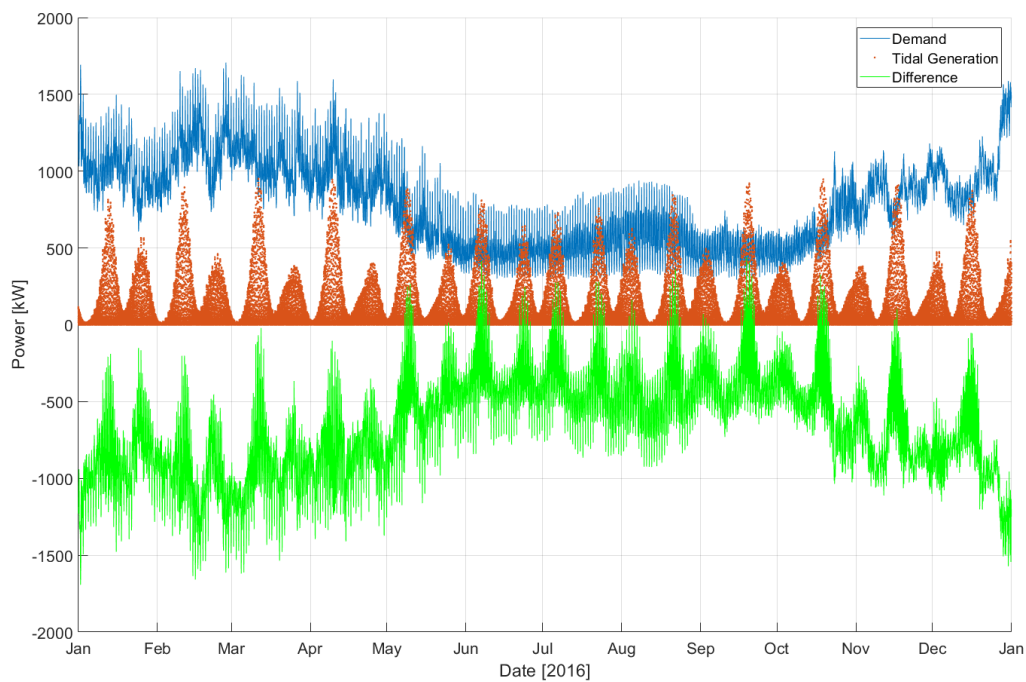


Figure 2.43 Comparison of estimated power from Sabella D10 turbine and Ushant electrical demand for 2016.



2.7 Other low carbon generation technologies

2.7.1 Wave

Ocean waves are a huge, largely untapped, energy resource. Waves are formed when winds blow over the surface of the sea and energy is transferred. The size of the waves generated will depend upon the wind speed, its duration, and the distance of water over which it blows (the fetch). In the nearshore region, waves will also be affected by water depths and currents. The wave motion transports kinetic energy, which can be harnessed by wave energy devices.

The advancement of a large number of designs and concepts is being pursued and investigated by developers to harness the power of waves, but many are at the R&D stage, with only a small number of devices having been tested at large scale and deployed offshore. Despite considerable research and development, the concepts for converting wave motion, i.e. a slow, high-force, reciprocating motion, to one useful for generating electricity, show no sign of converging to a preferred solution. Questions arise over which conversion concept to use, how best to optimise its performance, and how to control such a system (Drew et al., 2009). Compared to wind turbines and tidal turbines, wave energy systems have a much lower maturity level (Tawil et al., 2018), thus they are not considered as part of the energy solution for Ushant at present.

2.7.2 Biomass

In ICE report “T1.1.1 An overview of renewable energy supply potential” (Hardwick et al., 2018), three biomass scenarios were developed:

- Local Direct Scenario - Direct conversion of locally-generated waste or biomass into electrical energy;
- Local Indirect Scenario - Conversion of locally-generated waste or biomass into intermediate fuels that can displace conventional fuels, including fuels used for electricity generation;
- Regional Indirect Scenario - Conversion of regionally-generated waste or biomass into intermediate fuels that can be transported and used for local electricity generation or other uses.

Although the regional indirect scenario is technically feasible, recent work on glycerine-fuelled power generation units has indicated that the economics are rather unattractive at least in the near-term. For ICE, it has therefore been decided to focus attention on the other two biomass scenarios.

As indicated in ICE report T1.1.1, the potential for biomass and waste conversion into useful energy streams is best identified by looking at:

1. Process technologies that can accept a specific range of feedstocks;
2. Availability of these feedstocks from the local biomass/waste arisings.

This avoids wasting a lot of effort quantifying waste streams which cannot realistically be converted into useful energy streams. The two technologies highlighted in T1.1.1 would give a processing capability for:

- Mixed plastic waste, typically packaging waste from commercial and domestic sites;
- Generic organic waste and biomass, ranging from slurry and other farm waste, and commercial food waste through to compostable domestic waste.



It is likely that both of these waste types would be available on Ushant.

In terms of processing capacity, productivity and cost-effectiveness, the two technologies are presented below.

2.7.2.1 PLAXX

The PLAXX technology has been implemented in a modular format that fits into five standard containers for ease of shipping. This scale of unit has a waste processing capacity of 7,000 T/year and can produce diesel-equivalent fuel at a conversion efficiency of 30-40% (depending on feedstock and precise mix of fuel output required). The average cost of such a unit is around \$3M, which equates to a pay-back period of around 2.5 years, assuming the waste is available at zero cost and assuming typical conventional fuel prices. A more detailed financial analysis could be performed, looking at actual delivered fuel prices on Ushant which PLAXX would displace, to give a more precise payback period.

The current process configuration is shown in Figure 2.44.

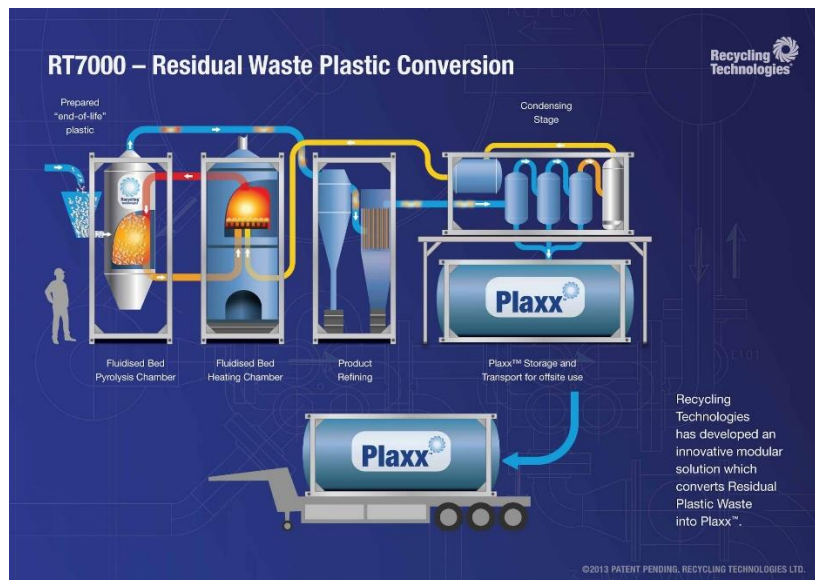


Figure 2.44 The PLAXX process (Source: Green Car Congress, 2016).

The condensing stage of the process is presently being modified into a distillation stage in order to allow better control over the fuels produced. A 700 T/year pilot unit with this new distillation stage is undergoing trials. With a conversion efficiency of 35%, this pilot unit would produce 245 T/year of fuel, split between diesel and lighter fuel fractions, having an average energy content of 43 GJ/T. Thus one 700T unit could produce output energy of 10,500 GJ/year in the form of petro-diesel fuels. This is equivalent to 3,000 MWh/year.

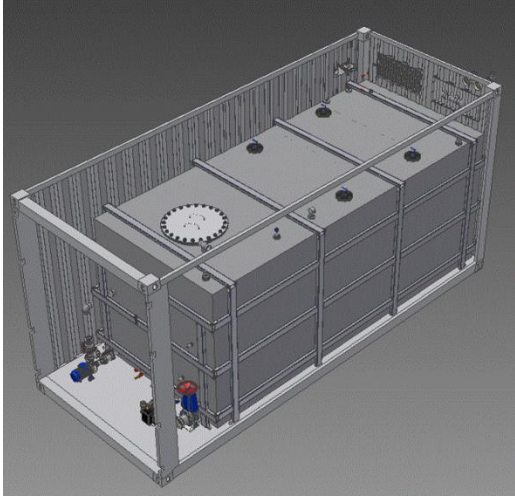


WRAP estimates that average plastic waste arisings (mainly packaging) are about 34kg/person (DEFRA, 2018), so a population of around 10,000 people would be needed to produce 700T of feedstock per year. The island of Ushant is too small to reach this level, so even the smaller pilot PLAXX unit would need to draw on arisings from beyond the island itself.



2.7.2.2 SEAB

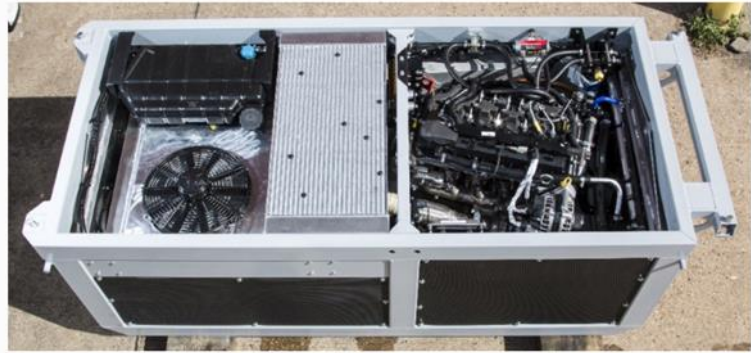
SEAB produces a range of modular units that can meet the processing requirements for different feedstocks and different output requirements. These are outlined in Table 2.12.

Table 2.12 SEAB modular units.

<p>Muckbuster:</p> <p>Digester unit for organic slurry waste (including sewage), producing biogas and fertiliser outputs.</p>	
<p>Flexibuster:</p> <p>Variable feed digester for organic mixed waste (including food), producing biogas and fertiliser outputs.</p>	 <ul style="list-style-type: none"> 1 Waste is loaded, chopped and mixed 2 Pasteurisation 3 Digestion 4 Gas Production (sent to gas storage and power unit – not shown) 5 Digestate and mulch offload
<p>De-waterer:</p> <p>Removing water from organic slurries before digestion.</p>	

Gas engine & generator:

Burns the biogas to produce electricity and heat.



These units are all designed into standard containers that can be integrated into a complete system, and easily deployed. A trial system was installed at a Best Western hotel in Southampton. This digested all the food waste produced by the hotel kitchens and feeds power back into the local grid. It also supplies 100% organic fertiliser to a local horticulture firm, displacing consumption of fossil-fuel based fertilisers.

Another case study has been performed on a down-sized installation at a supermarket in Portugal. This digests 600 kg/day of food waste, generating 10kW of electrical energy and producing both liquid and solid (bagged) fertiliser products for sale.

2.8 Demand side technology

In addition to developing new sources of renewable energy generation, the island of Ushant has implemented several energy use reduction schemes with further schemes planned.

2.8.1 Energy Efficiency

Energy efficiency measures implemented on the island include schemes to replace old light bulbs and refrigerators with LEDs and new efficient models. Further energy efficiency measures could be introduced to decrease the island's electricity peak demand as well as the total consumption. Better insulation of houses would reduce the amount of electricity required for heating and help in lowering the large energy peaks seen in winter. Energy efficiency also represents a method which can reduce islander's energy bills, something that renewable energy installations on the island will not achieve given the current nature of billing on the island. Energy Efficiency programmes may thus engender greater buy-in from the consumer.

2.8.2 Alternative Heating: Heat Pumps

Heat pumps use electrical energy to facilitate heat transfer from a lower temperature source (air, ground or water outside the building) to a higher temperature sink (the space inside the building). Compared with electrical radiators and other space heaters which use resistance to convert electrical energy into heat, heat-pumps can transfer the thermal energy more efficiently. The coefficient of performance (COP) is the amount of thermal energy provided for each unit of electrical energy, for example a radiator with a COP of 1.0 will deliver 1J of thermal energy for every 1J of electricity. As heat pumps enable heat transfer from surroundings, COPs value greater than 1.0 are obtainable; COP values of 3 – 5 are possible in the right conditions (Goth, 2015).



Air source heat pumps: These work by removing heat energy from cooler outdoor air and delivering it indoors into warmer air, i.e. effectively an air conditioning unit operating in reverse. The energy required to deliver heat inside is less than the energy required to create the same temperature increase from an electrical resistance heater. The exact performance coefficient will depend on the outside temperature; the cooler the outside air, the more work the heat pump needs to do and the lower the COP. Air source heat pumps can be installed virtually anywhere and are typically attached to the side of a building in much the same way as a traditional air conditioner.

Ground source heat pumps: These take heat from the ground around a property and use it to heat space. Ground source heat pumps can either be shallow pumps, where the cycle is diverted through pipes buried a shallow distance under soil and the temperature of the soil is used as the source, or deep pumps, where a bore hole is drilled and the cycle is routed down several metres. Since underground temperatures are typically higher than the surface, in cold winters the COP is typically higher. The soil / rock properties are important when looking to install ground source heat pumps, and a study could be performed to determine whether the technology is suitable for Ushant.

Water source heat pumps: These use the heat energy of a nearby water source (river, lake or coast) from which to extract heat and deliver it inside.

Heat pumps can be installed on single buildings as an alternative (or in addition to) electrical radiators, or larger systems can be shared between buildings as part of a district heating system. For example, in Drammen, Norway, a water source heat pump provides heating for 65,000 people using water from the local fjord. (Matt et al., 2013. BBC, 2015).

2.9 Scenarios for energy generation

Seven theoretical scenarios have been developed to assess how the contribution from a combination of solar, wind and tidal renewable generation technologies would compare with the island's electrical demand requirements. The scenarios all involve a combination of the resource assessments described in sections 2.4, 2.5 and 2.6. In order to meet the island's goals of 70% renewable generation by 2020 and 100% by 2030, there will be a mixture of renewable energy generation, demand side energy reduction schemes and/or energy storage systems installed. The scenarios presented here are compared with the energy demand profiles for 2016.

Table 2.13 Summary of scenarios

Scenario	Description
1	Planned solar installations (5 sites) and one 300kW wind turbine
2	Extensive solar (20% of all rooftops) and one 800kW wind turbine
3	Extensive solar and one 2MW wind turbine
4	Sabella D10 tidal turbine and planned solar installations.
5	Sabella D10 tidal turbine and extensive solar.
6	Two Sabella D10 turbines and planned solar installations.



7	Sabella D10 tidal turbine, extensive solar and an 800kW wind turbine.
---	---

The scenarios are designed to provide information on the power production from a mixture of renewable generation technologies. There is no consideration given to the technical, environmental or socio-political constraints in their design. It is likely that some of these scenarios would not be possible on Ushant without changes to the electrical infrastructure, planning regulations or if they proved to be unacceptable to its citizens. If the relevant parties make the decision to proceed with an energy solution similar to these scenarios then those considerations will need to be addressed.

A common finding in these scenarios is that even when the technologies are producing sufficient renewable energy to supply 100% of the island's requirements, the times of generation and use are rarely concurrent. The ICE project is producing a general methodology for planning for a smart energy transition to inform isolated communities (described in ICE project deliverable report T2.1) which will outline further measures, alongside the need for new generation technologies, to better utilise the energy and to enable smart low carbon solutions.

Scenario 1: Planned solar installations (5 sites) and one 300kW wind turbine

The first scenario assesses the electricity generated from the five planned solar installations on municipal buildings and a single Enercon E33-300 300kW wind turbine. Measured hourly solar data was not available for specific years so the solar calculations are based the hourly time series for a 'typical' year using PVsyst. The wind turbine power calculations use the measured NOAA wind speed data scaled up to the hub height for 2016. The solar installation is estimated to provide 162.64MWh of electricity per year and the wind turbine would have provided 1511.2MWh in 2016, giving a total supply of 1673.84MWh to the island's grid. This is 24.5% of the demand for 2016. A time series comparison between the power generated and the island's demand is shown in Figure 2.45. In only one hour throughout 2016 does this scenario manage to supply 100% of the island's electricity, therefore there would need to be alternative generation operating continually throughout the year to ensure that supply is uninterrupted. As there is (almost) no surplus generation there would not be any need to dump energy or curtail devices and the energy from both the solar and wind turbines could be utilised at all times. The generation data are summarised in Table 2.14.

If this scenario were to be implemented on Ushant then there would be a reduction in the amount of energy required to be produced from the diesel generators of approximately 25%. As there are occasions where both the solar and wind technologies are producing zero output (when there is no wind or sunlight) there would still need to be sufficient backup generation to supply the entire peak load.

Table 2.14 Scenario 1 generation parameters.

Scenario 1	Annual (2016)	Summer (Apr – Sep)	Winter (Jan – Mar, Oct – Dec)
Generation [MWh]	1673.84	727.82	945.36
Demand [MWh]	6807.08	2676.61	4130.47



Surplus (+ve) / Deficit (-ve) [MWh]	-5133.90	-1948.79	-3185.11
Number of hours surplus	1 / 8784	1 / 4392	0 / 4392
Number of hours deficit	8783 / 8784	4391 / 4392	4392 / 4392
Largest peak surplus [kW]	5.83	5.83	n/a
Largest peak deficit [kW]	1692.33	1473.67	1692.33
Usable energy generated (discounting surplus generation) [MWh]	1673.17	727.81	945.36

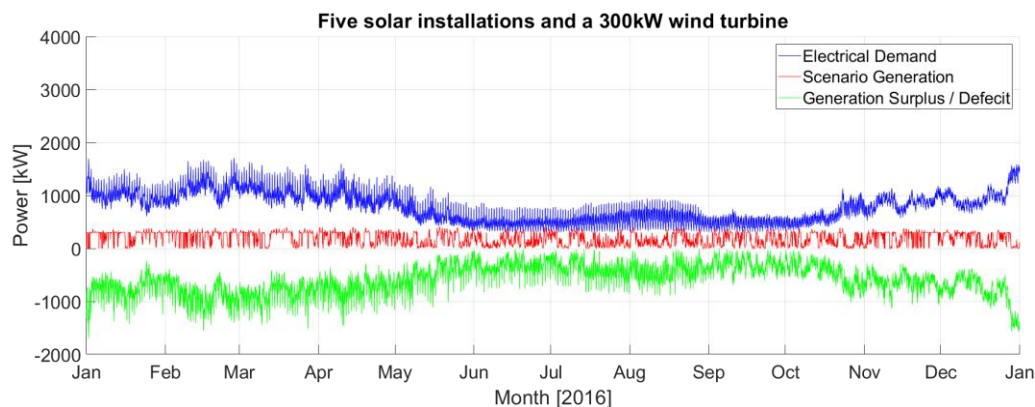


Figure 2.45 Scenario 1: Generation compared with demand for 2016.

Scenario 2: Extensive solar (20% of rooftops) and one 800kW wind turbine

In scenario 2, solar energy generated from an extensive array of rooftop solar panels, calculated using methodology 2 (described in section 2.4.6) is combined with the generation from an Enercon E53-800 800kW wind turbine. The solar power calculations are estimated using data for a typical year and the wind turbine generation is calculated using the NOAA measured wind speeds for 2016, scaled to the height of the turbine. The solar installations are estimated to provide 3888.93MWh to the grid per annum; there is a large seasonal disparity in the generation with 70% of the solar generation coming in the summer months. The wind turbine would have produced 4365.34MWh in 2016. The wind generation sees significant seasonal variation due to strong winter winds, meaning that only 41% of wind generation occurs in the summer, counter-balancing the solar power. The generation parameters are summarised in Table 2.15.

In this scenario there is more electrical energy produced than consumed by the island. Production from the wind turbine can be easily curtailed, however, there will need to be a dump for the excess solar energy. One solution would be to install further battery storage on Ushant which can be charged when there is excess energy and discharged when more energy is needed, typically in the evenings when demand is higher but there is no solar power being produced.



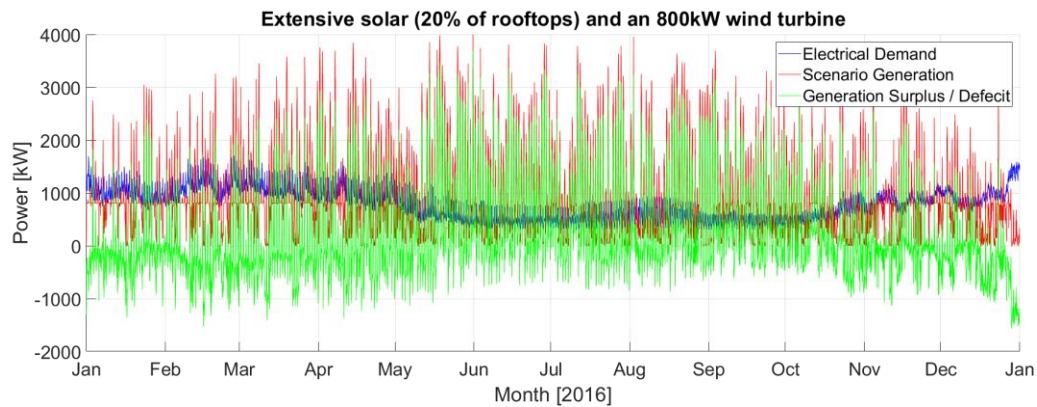


Figure 2.46 Scenario 2: Generation compared with demand for 2016.

Table 2.15 Scenario 2 generation parameters.

Scenario 2	Annual (2016)	Summer (Apr – Sep)	Winter (Jan – Mar, Oct – Dec)
Generation [MWh]	8254.27	4498.03	3756.24
Demand [MWh]	6807.08	2676.61	4130.47
Surplus (+ve) / Deficit (-ve) [MWh]	1447.19	1821.42	-374.23
Number of hours surplus	3926 / 8784	2550 / 4392	1376 / 4392
Number of hours deficit	4858 / 8474	1842 / 4392	3015 / 4392
Largest peak surplus [kW]	3680.66	3680.66	2653.81
Largest peak deficit [kW]	1565.83	1372.67	-1565.83
Usable energy generated (discounting surplus generation) [MWh]	4966.18	2053.80	2912.38

Scenario 3: Extensive solar (20% of rooftops) and one 2MW wind turbine

This scenario is the same as scenario 2 except a 2MW Vestas V90/2MW turbine is installed in place of the 800kW device. There are periods with large surplus generation where the turbine will need to be curtailed or alternative uses of the electricity found. A comparison with demand is shown in Figure 2.47. Total generation is more than double the annual consumption (for 2016), however, there is still a generation deficit 21% of the time, meaning that energy storage or other forms of generation would be required. The parameters are summarised in Table 2.16.



Without any additional storage this scenario would account for 87% of the island's generation requirements. However, this scenario would only be a practical solution if there was a use for the large amount of excess generation, such as an export cable, so that the energy could be used elsewhere.

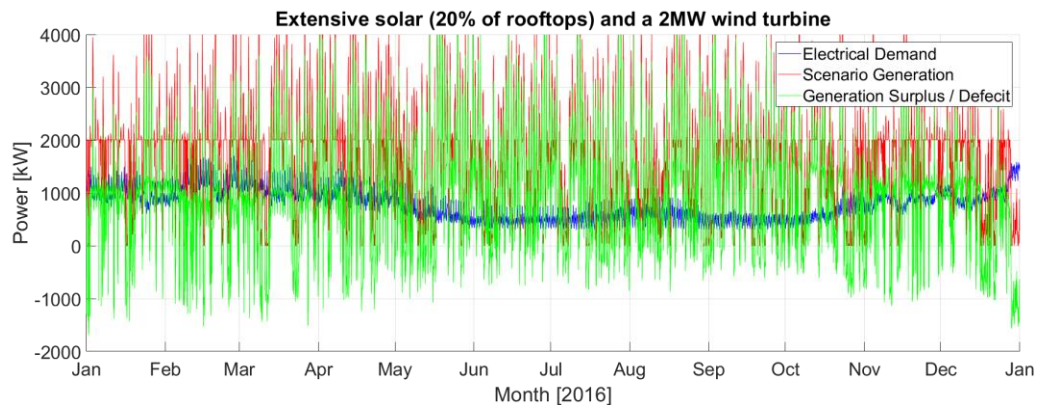


Figure 2.47 Scenario 3: Generation compared with demand for 2016.

Table 2.16 Scenario 3 generation parameters

Scenario 3	Annual (2016)	Summer (Apr – Sep)	Winter (Jan – Mar, Oct – Dec)
Generation [MWh]	14685.50	7275.17	7410.33
Demand [MWh]	6807.08	2676.61	4130.47
Surplus (+ve) / Deficit (-ve) [MWh]	7878.41	4598.56	3279.86
Number of hours surplus	6948 / 8784	3485 / 4392	3463 / 4392
Number of hours deficit	1835 / 8784	907 / 4392	928 / 4392
Largest peak surplus [kW]	4877.46	4877.46	3850.61
Largest peak deficit [kW]	1692.33	1230.33	1692.33
Usable energy generated (discounting surplus generation) [MWh]	5903.60	2376.63	3526.97

Scenario 4: Sabella D10 tidal turbine and planned solar (5 sites)

This scenario examines the generation from the five planned solar installations (as described in scenario 1) and the Sabella D10 turbine. Power production for the Sabella turbine uses tidal flow data derived from a harmonic model and shows close agreement with a numerical simulation outlined in Appendix 2. The combination of tidal and solar gives a variable demand profile with multiple production peaks and troughs every day. The comparison with demand is shown in Figure 2.48; the



total generation is 16% of the annual demand for 2016 and there are a few occasions (approximately 2% of the total time) where there is surplus generation which could be used for energy storage. The parameters are summarised in Table 2.17.

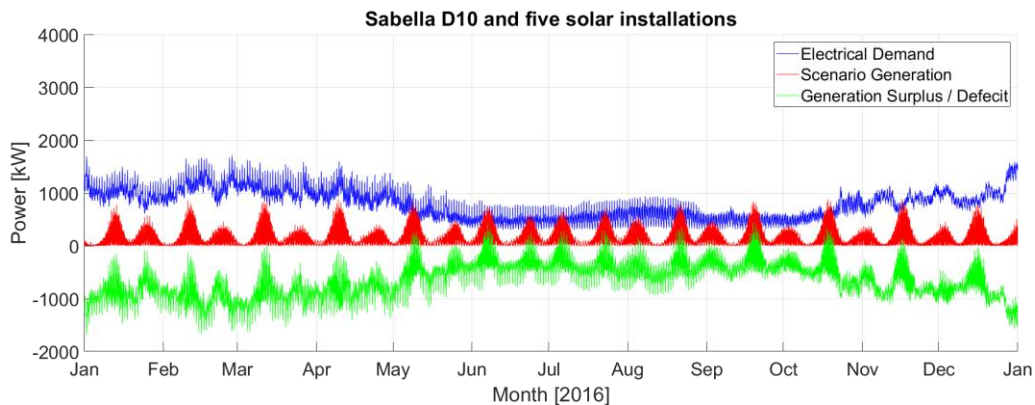


Figure 2.48 Scenario 4: Generation compared with demand for 2016.

Table 2.17 Scenario 4 generation parameters.

Scenario 4	Annual (2016)	Summer (Apr – Sep)	Winter (Jan – Mar, Oct – Dec)
Generation [MWh]	1128.43	597.48	530.69
Demand [MWh]	6807.08	2676.61	4130.47
Surplus (+ve) / Deficit (-ve) [MWh]	-5678.65	-2078.86	-3599.79
Number of hours surplus	171 / 8784	143 / 4392	28 / 4392
Number of hours deficit	8612 / 8784	4249 / 4392	4363 / 4392
Largest peak surplus [kW]	441.19	441.19	326.49
Largest peak deficit [kW]	1692.12	1409.15	1692.12
Usable energy generated (discounting surplus generation) [MWh]	1106.92	579.34	527.59

Scenario 5: Sabella D10 tidal turbine and extensive solar installations (20% of rooftops)

Scenario 5 is the same as scenario 4 but with the solar generation extended to 20% of rooftops. This results in a surplus of electrical generation during the summer months and a deficit in the winter. The seasonal variation is visible in the comparison with demand shown in Figure 2.49. The large surplus at times means it is likely that energy will need to be dumped. The parameters are summarised in Table 2.18.



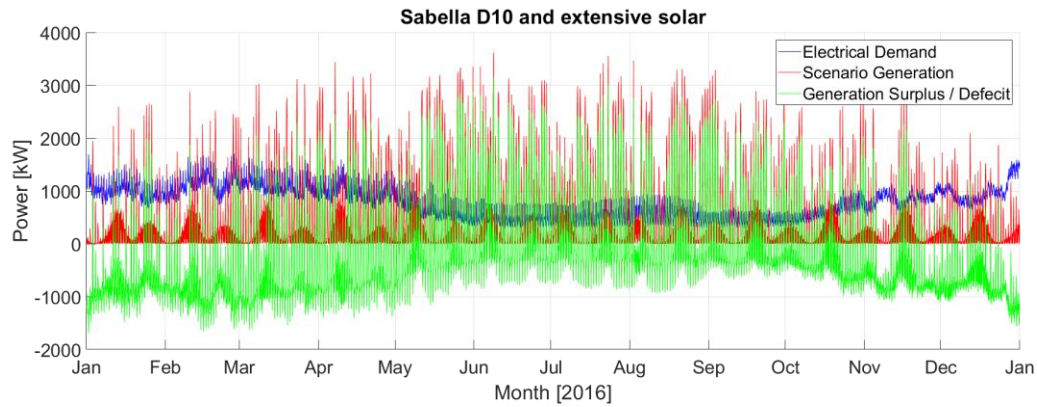


Figure 2.49 Scenario 5: Generation compared with demand for 2016.

Table 2.18 Scenario 5 generation parameters.

Scenario 5	Annual (2016)	Summer (Apr – Sep)	Winter (Jan – Mar, Oct – Dec)
Generation [MWh]	4889.46	3216.00	1673.46
Demand [MWh]	6807.08	2676.61	4130.47
Surplus (+ve) / Deficit (-ve) [MWh]	-1917.62	539.40	-2457.02
Number of hours surplus	2390 / 8784	1735 / 4392	655 / 4392
Number of hours deficit	6393 / 8784	2657 / 4392	3736 / 4392
Largest peak surplus [kW]	3161.24	3161.24	2294.12
Largest peak deficit [kW]	1692.12	1409.15	1692.12
Usable energy generated (discounting surplus generation) [MWh]	2716.29	1491.25	1225.04

Scenario 6: Two Sabella D10 tidal turbines and planned solar installations (5 sites)

This scenario envisages the installation of two Sabella D10 tidal turbines located at the same site. The generation from the two turbines and the five planned solar installations would produce enough energy to meet 27% of the island's electrical demand (31% if surplus energy could be utilised via storage technologies) and would meet the full demand 9.8% of the time. The parameters are summarised in Table 2.19. Figure 2.50 shows the annual comparison with the energy demand.



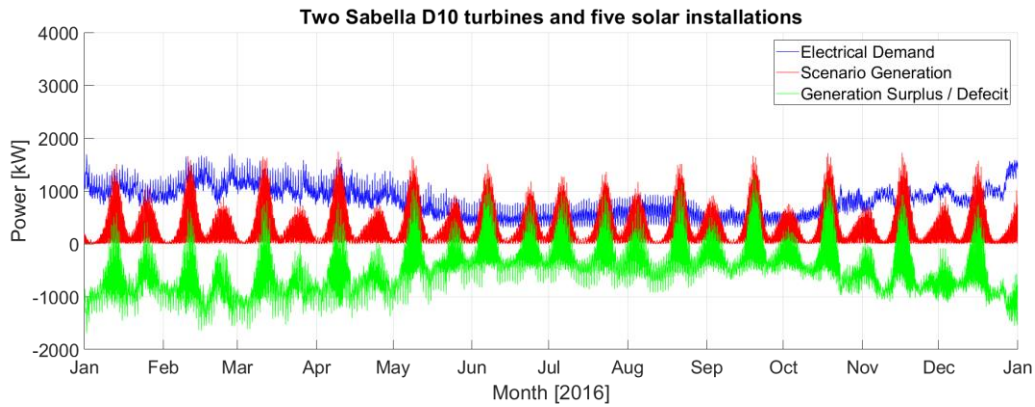


Figure 2.50 Scenario 6: Generation compared with demand for 2016.

Table 2.19 Scenario 6 generation parameters.

Scenario 6	Annual (2016)	Summer (Apr – Sep)	Winter (Jan – Mar, Oct – Dec)
Generation [MWh]	2128.96	1107.00	1201.97
Demand [MWh]	6807.08	2676.61	4130.47
Surplus (+ve) / Deficit (-ve) [MWh]	-4678.12	-1569.62	-3108.50
Number of hours surplus	868 / 8784	624 / 4392	244 / 4392
Number of hours deficit	7915 / 8784	3768 / 4392	4147 / 4392
Largest peak surplus [kW]	1273.55	1273.55	1147.48
Largest peak deficit [kW]	1691.92	1408.98	1691.92
Usable energy generated (discounting surplus generation) [MWh]	1864.48	916.97	947.51

Scenario 7: Sabella D10 tidal turbine, extensive solar installations (20% of rooftops) and an 800kW wind turbine

The final scenario assesses a combination of solar, wind and tidal technologies. In this scenario, the island's demand is completely satisfied 54% of the time (66% of the time in summer), and this could be improved with the use of energy storage. The parameters are summarised in Table 2.20 and the comparison with demand presented in Figure 2.51. The combination of multiple technologies gives the greatest likelihood that there will be some renewable generation at any specific time. This combination, along with an energy storage solution and smart changes to energy use behaviour, could lead to a practical low carbon solution for isolated communities.



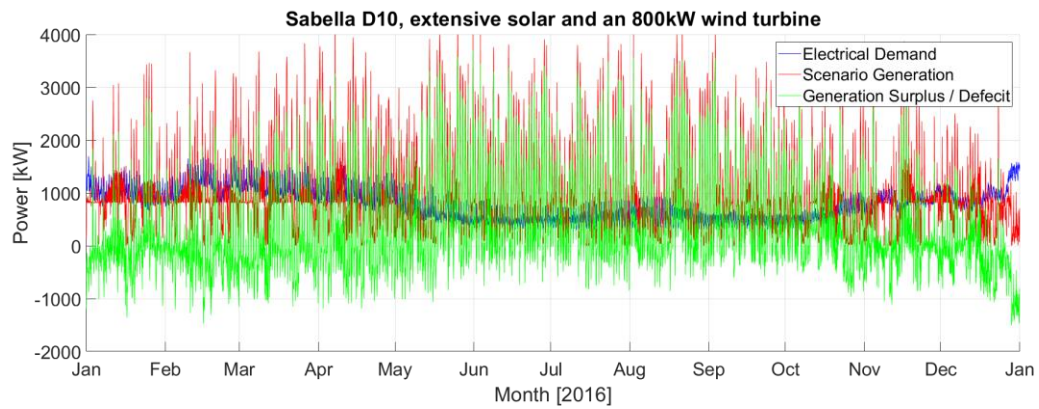


Figure 2.51 Scenario 7: Generation compared with demand for 2016.

Table 2.20 Scenario 7 generation parameters.

Scenario 7	Annual (2016)	Summer (Apr – Sep)	Winter (Jan – Mar, Oct – Dec)
Generation [MWh]	9254.80	5007.27	42447.53
Demand [MWh]	6807.08	2676.61	4130.47
Surplus (+ve) / Deficit (-ve) [MWh]	2447.72	2330.67	117.05
Number of hours surplus	4725 / 8784	2896 / 4392	1829 / 4392
Number of hours deficit	4058 / 8784	1496 / 4392	2562 / 4392
Largest peak surplus [kW]	3695.95	3695.95	3076.00
Largest peak deficit [kW]	1507.07	1193.39	1507.07
Usable energy generated (discounting surplus generation) [MWh]	5406.23	2232.64	3173.59



3 University of East Anglia Campus Energy Assessment

3.1 Site Overview

The University of East Anglia is a campus-based university located close to Norwich in Norfolk, in the East of England (Figure 3.1). The site covers approximately 330 hectares and consists of teaching space, laboratories, offices, retail shops, catering outlets, a sports centre and student residences, shown in an aerial photograph in Figure 3.2. The campus was constructed in 1963 and has since been expanded several times. Some of the original buildings are 'grade II listed' as having cultural significance. The site includes much green space including woodland and a lake.

There are approximately 14,500 undergraduate students and 4,500 postgraduates and staff using the campus daily throughout term time; the campus has 4,500 resident students, mostly first-year undergraduates. Outside of term time the campus continues to be used by post-graduates and staff and also plays host to conferences and events.



Figure 3.1 Map showing the location of the UEA site in the UK. (Source: Open Street Map)





Figure 3.2 Aerial photography of the UEA campus. (Source: Google Maps)

3.2 Energy Demand Assessment

The campus has a centrally controlled energy management system consisting of combined heat and power (CHP) units, gas and oil boilers, solar PV and a national grid connection. Electricity is generated or imported onto the campus and then distributed to the many buildings. A district heating system supplies the majority of the buildings with heat produced from gas boilers and the thermal output of CHP units.

In the year August 2015 – July 2016 the campus consumed 34,351MWh of electricity, 36,520MWh of heat and 23,041MWh of losses and other uses. This was supplied in the form of 18,659MWh of electricity imported from the national grid and 75,253MWh of imported gas used in boilers and CHP units. Solar PV provided just 102MWh of electricity, accounting for less than 1% of electricity use.

In 2017 an extensive upgrade was made to the campus energy systems with the installation of new CHP units and gas boilers. Following the upgrade, the campus systems consist of:

- Three CHP units:



- Units 1 and 2 produce 2MW of electricity and 1.8MW of heat, each with 40% electrical efficiency and 36% thermal efficiency
- Unit 3 produces 1.7MW of electricity and 2.3MW of heat with 33% electrical and 45% thermal efficiency
- Three 6MW gas boilers, each 91% thermally efficient
- One 4MW gas boiler kept as backup, with 80% efficiency
- 280kW_p of solar PV
- A 1MW biomass boiler, not currently in use
- One oil boiler used for back-up only.

The energy use for 2015-16 is shown in a Sankey diagram in Figure 3.3; note that this is before the systems upgrade.

Heat provided from the district heating system is used to heat teaching spaces, offices, laboratories and student residences. A thermal storage tank is included in the system. This helps in ensuring that the output from the system is fully utilised by storing heat when electrical demand is high and releasing heat when electrical demand is low. Currently the end users have no control over the temperatures in rooms although improved control systems have been discussed for the future.

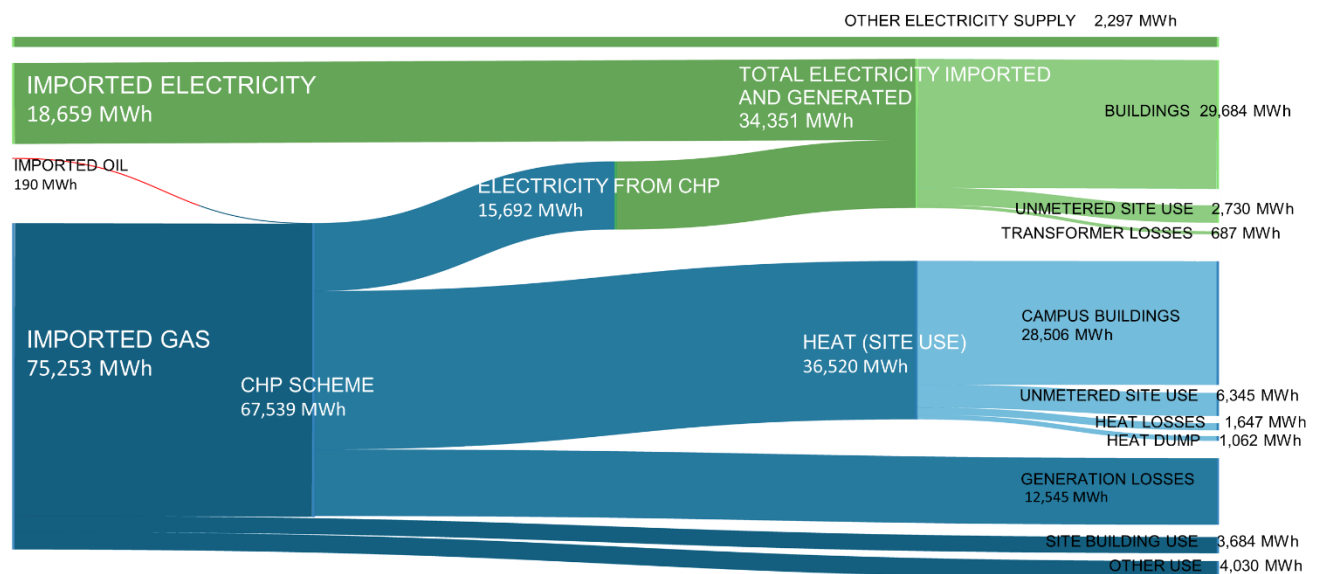


Figure 3.3 Sankey diagram showing energy production and use in 2015-16.

3.3 Local Network Conditions

Details of the electricity and heating networks were not available to the ICE project for inclusion in this report. Buildings on campus are all connected to the campus network with a single national grid connection managed for the whole system. Energy on campus is controlled from a centralised building management system (BMS). Generation and import of electricity are monitored and controlled from a centralised computer system with the aim to maximise the use of the more efficient CHP units. The district heating system has a thermal storage capacity (large insulated hot water tanks) so that if, to meet electrical demand, output from the CHP units produces more heat than currently required, it can be stored in the thermal buffer to be used at a later time.



3.4 Resource Assessment: Solar

There is approximately 280kW_p of rooftop solar PV installed on the campus and there are planned developments to expand this to 1MW by 2020. A list of the buildings with installed PV systems is shown in Table 3.1.

Table 3.1 Description of PV installations on the UEA campus.

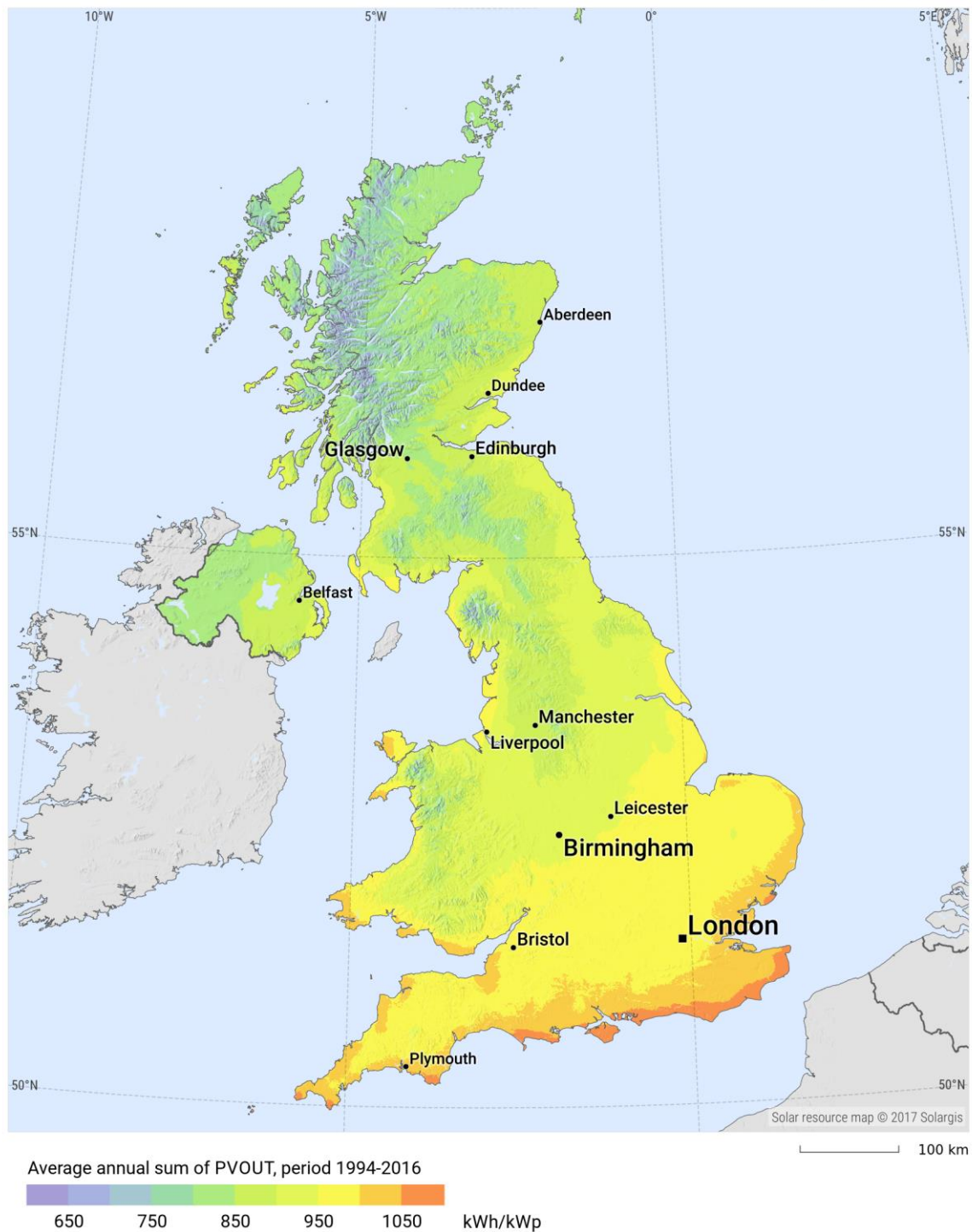
Building Name	Installed Capacity [kW _p]	Electricity Supplied [MWh]	
		Aug 15-Jul-16	Aug 16-Jul 17
Zicer	34	11.899	19.171
Julian	19.17	17.608	17.870
Chrome Court	20.7	17.297	15.940
Enterprise Centre	48	45.040	46.370
Barton (installed Feb 2017)	18.81	-	10.505
Hickling (installed Feb 2017)	21.66	-	12.003
Bob Champion	17.75	10.753	16.912
INTO (not recorded)	99.58	Not recorded	
Total (not including INTO building)	280	102.597	138.771

3.4.1 Resource Constraints

The PVGIS model describes the site as having a solar resource of 954 kW/m²/year DNI and 1071kWh/year GHI (Huld, et. al, 2012), shown in Figure 3.4, which due to the high latitude of the site is extremely seasonal. The largest resource is in the summer months where the longer days and higher intensity provide a larger level of irradiation. The monthly radiation figures are shown in Table 3.2 and can be seen graphically in Figure 3.5. The daily variation in the mean monthly radiation is presented in Figure 3.6. The optimum angle of inclination for solar panels is 39° at the site.



PHOTOVOLTAIC POWER POTENTIAL UNITED KINGDOM

SOLARGIS


This map is licensed by Solargis under the Creative Commons Attribution license (CC BY-SA 4.0). You are encouraged to use content of the map to benefit yourself and others in creative ways. For more information, please visit <http://solargis.com/download>.

Figure 3.4 Average annual GHI for the UK, provided by SolarGIS (SolarGIS, 2018)



BRETAGNE
DÉVELOPPEMENT
INNOVATION

SOY
SOLAR
ENERGY

TECHNOLOGIE
ENVIRONNEMENTALE

TECHNOLOGIE
ENVIRONNEMENTALE

TECHNOLOGIE
ENVIRONNEMENTALE

EXTTER

PLYMOUTH
UNIVERSITY

UEA

marine

marine

Table 3.2 Solar irradiance for the UEA campus

Month	DNI [kWh/m ²]	GHI [kWh/m ²]	G(39) [kWh/m ²]
Jan	33.48	21.73	40.92
Feb	46.33	38.70	61.30
Mar	76.88	82.15	108.81
Apr	119.1	127.5	147.6
May	122.76	155.93	159.03
Jun	111.6	157.8	152.4
Jul	110.36	158.1	156.55
Aug	103.85	130.2	141.67
Sep	88.2	95.4	120.3
Oct	62.93	56.73	84.63
Nov	43.8	28.38	52.8
Dec	34.72	18.724	39.99
Total	954	1071.3	1266

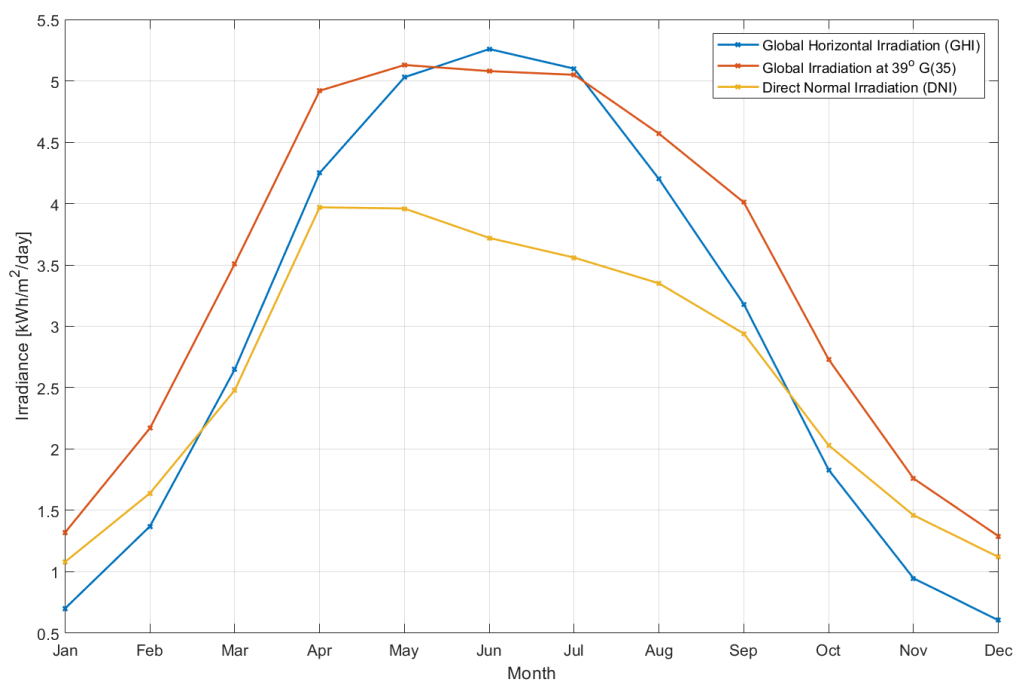


Figure 3.5 Monthly solar radiation on the UEA campus



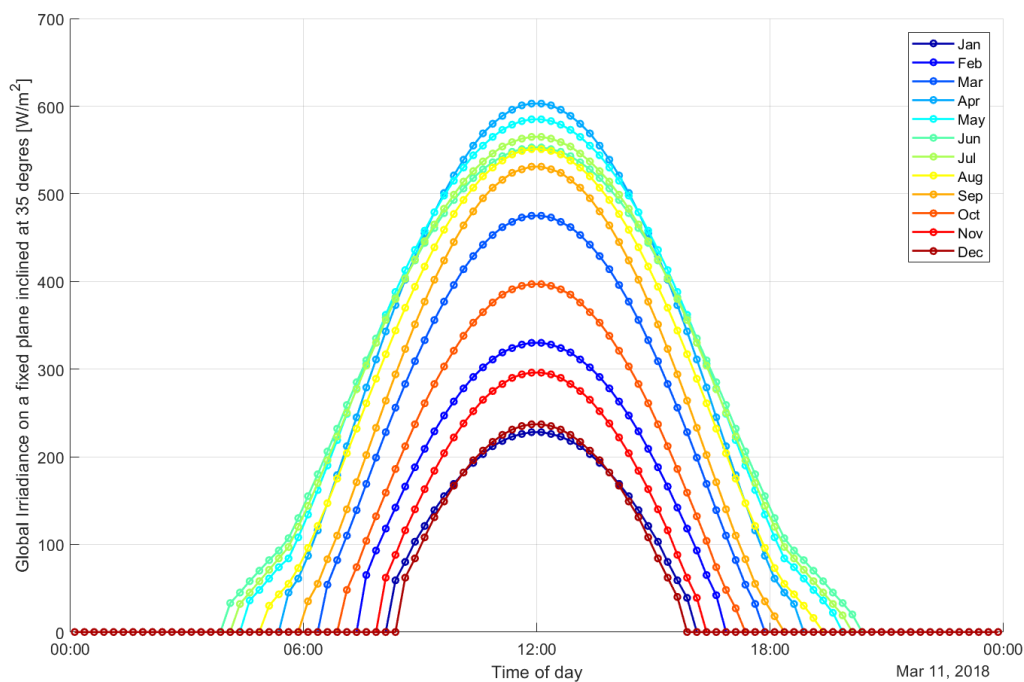


Figure 3.6 Mean solar radiation throughout the day for each month of the year at UEA.

3.4.2 Technical Constraints

Solar PV panels will need to be connected to the electrical systems of the building on which they are installed. As the campus has a centrally managed energy system any PV installations will need to be connected to that network. In order for the energy data to be collected and monitored the system will need to be connected to the campus building management system.

3.4.3 Environmental, Social and Political Constraints

Solar PV installations of up to 1MW_p on commercial and residential rooftops in England are generally considered 'permitted developments', not requiring planning permission. Confirmation of this status can be confirmed with the local planning authority (Planning Portal, 2018). While there are constraints on some campus buildings, which are 'listed' as having particular heritage importance, there are ample rooftop locations to at least fulfil the campus plans for 1MW_p installed solar PV capacity by 2020.

Ground-mounted solar PV is possible on the UEA campus, subject to the local spatial planning process. While the first commercial ground-mounted solar PV installation on a site can be treated as 'permitted development', the suburban location of the campus, with many close neighbours and the likely challenges of overcoming local resistance to such plans mean that rooftop solar should be considered in the first instance.

3.4.3.1 Site Identification

There is sufficient roof-space to accommodate an extensive expansion of campus solar power. The campus management have plans to install a further 720kW_p of solar PV, taking the total installed capacity to 1MW. This can be achieved by utilising the available roof space on the existing buildings. There are four buildings with grade-II listed status (Norfolk Terrace, Suffolk Terrace, The Teaching Wall and the library) for which any solar developments would likely be rejected. The campus buildings, with



existing solar PV and potential for installation of additional panels, can be seen on a GIS map in Figure 3.7.



Figure 3.7 GIS of the UEA campus showing buildings with existing solar installations (yellow), buildings with the potential for solar installations (blue) and listed buildings (grey).

3.4.4 Power Production

An estimation of the power potential of an expanded solar system suggests that if the planned expansion of solar power to 1MW is undertaken then the campus would receive 1278.3MWh of electrical energy per year, equal to approximately 3.7% of the 2015-16 total electricity consumption for the campus, or 6.7% of imported electricity.



3.5 Resource Assessment: Wind

3.5.1 Methodology

For this study modelled and measured wind speed data are used to estimate the resource that would be available to be exploited by one or more wind turbines at or near the UEA campus.

As for the Ushant study (section 2.5) data was acquired from the Global Wind Atlas and from the NOAA database.

Power production from a wind turbine was calculated by applying the NOAA data to the power curve for a selected turbine. It was then possible to match the times of each wind speed to the generation curve of the turbine and the output power shown.

The measured resource data are taken from Norwich Airport, located 5km from the campus. Modelled data are not available at a high enough resolution to identify any variation between the campus and the airport, and both sites are at similar altitude (approximately 35m above sea level). The data from the airport are therefore used without adjustment for these calculations.

3.5.2 Resource Constraints

The Global Wind Atlas (2017) states that there is an average 407W/m^2 of wind power at 100m above sea-level. Over the 10 years from 2007-2017 the NOAA measured data show an average wind speed for Norwich airport of 4.3ms^{-1} and a maximum sustained speed of 18ms^{-1} . As with the Ushant study the wind speeds were analysed and scaled up. As the campus is in a more build up area there would be a higher surface roughness. A constant of $z_0=0.1$ was used in scaling the log law. Average monthly values are shown in Figure 3.8. The available data are constrained to hourly averages of wind speed so maximum gust speeds are not available.

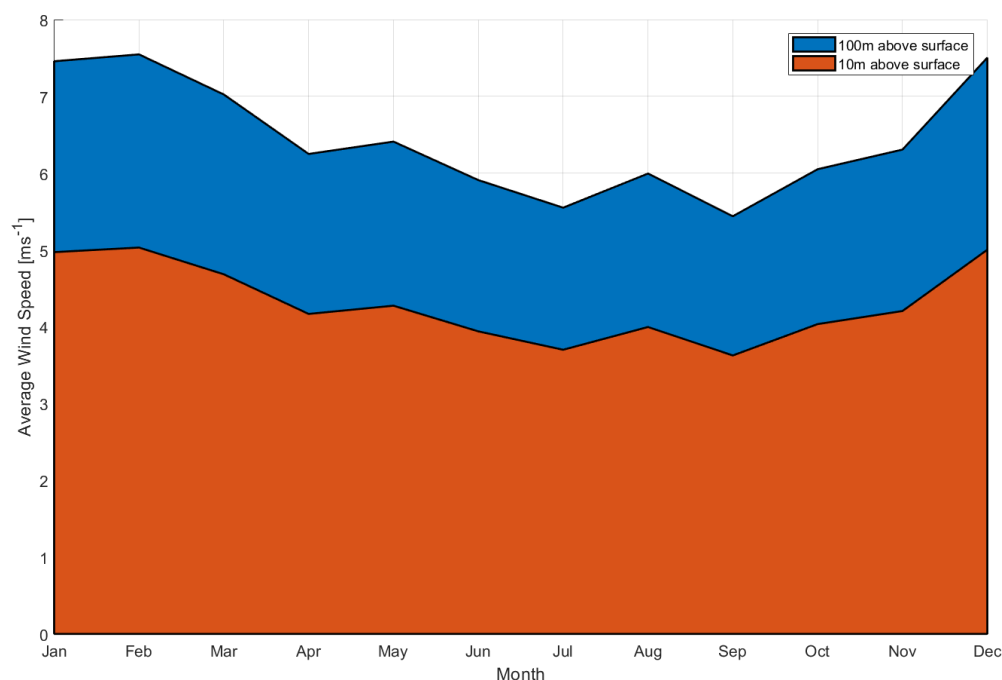


Figure 3.8 Monthly average wind speed.



The data suggest a significant intra-day variation in the wind speed. The wind speeds increase to a peak in the early afternoon then dropping on average by 65% in the late evening and overnight (shown in Figure 3.9). This pattern appears consistently in the Norwich Airport NOAA data, however, it should be confirmed whether this is still the case at the UEA site with a measurement campaign, if any wind development were proposed. The distribution of wind speeds at Norwich Airport is shown in Figure 3.10.

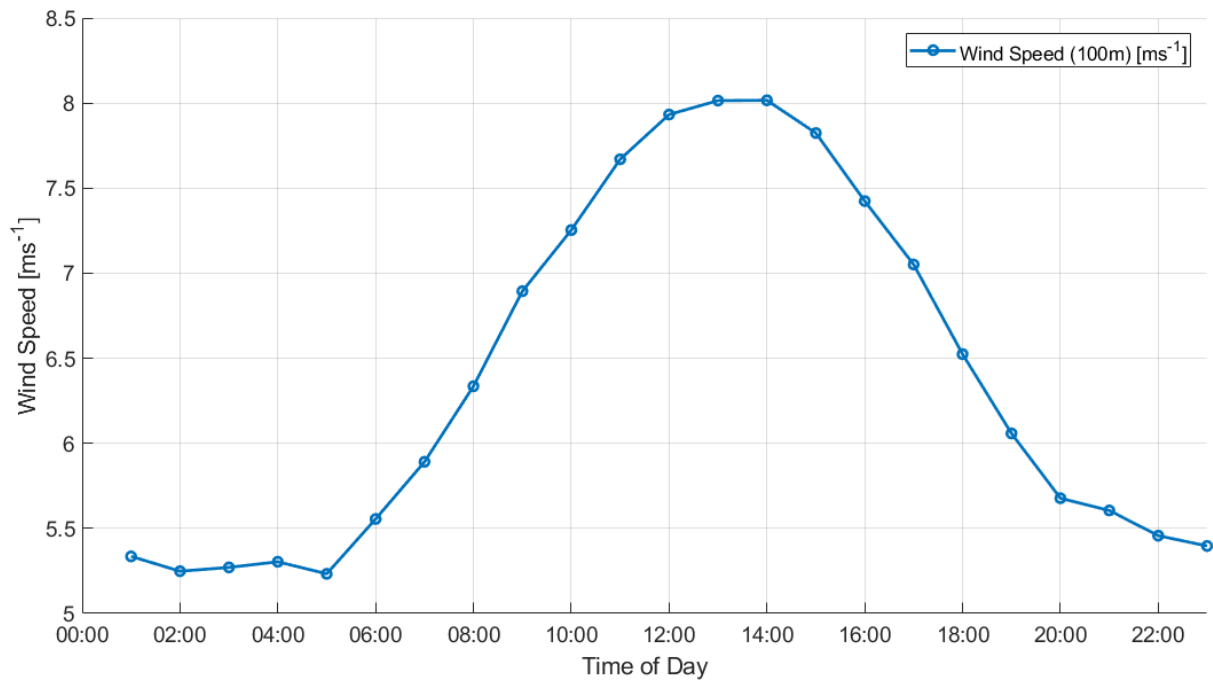


Figure 3.9 Daily variation in wind speed at the campus.

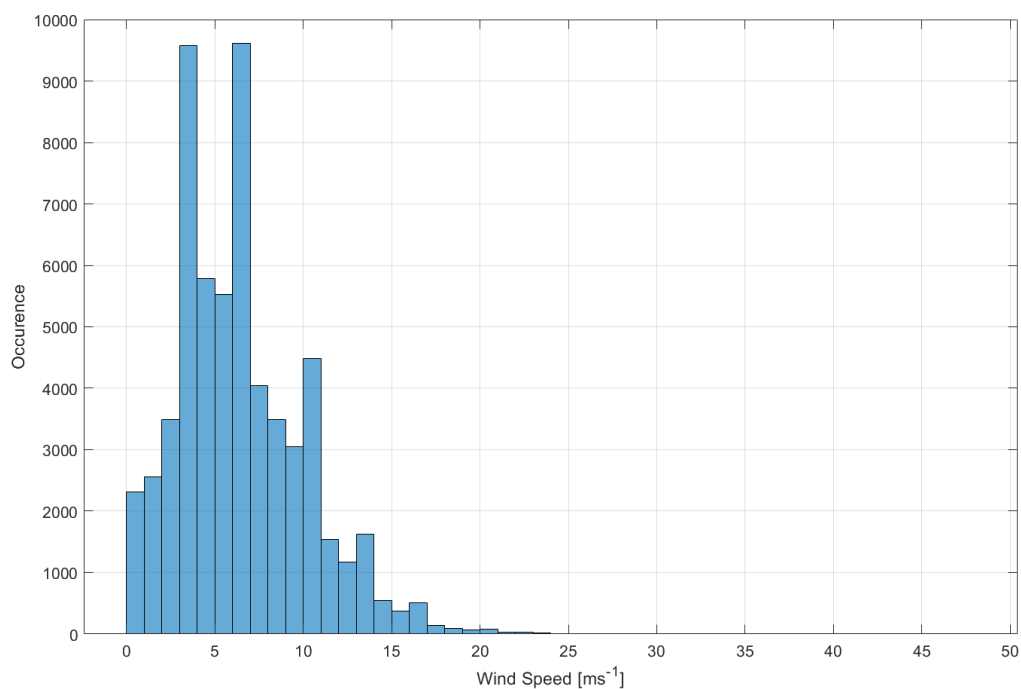


Figure 3.10 Distribution of wind speeds at Norwich Airport (100m).



3.5.3 Technical Constraints

Wind turbines could be integrated into the campus energy network and BMS, and the electrical energy generated could then be used on campus. A connection from the turbine(s) to the campus energy centre would be required. There is good access to the site for construction equipment and materials. There is also plenty of green space with sufficient distance from buildings and roads where turbines could technically be installed, although planning consent is unlikely.

3.5.4 Environmental, social and Political Constraints

Current UK regulations for onshore wind development make it practically impossible to develop a substantial onshore wind project on a site such as the UEA campus. While in some circumstances very small turbines can be installed without recourse to the planning system, the limited generation potential and the difficulty of meeting the planning requirements on the UEA campus, parts of which are a site of special scientific interest (SSI), mean that there is very little appetite or likelihood of onshore wind development.

Campus users and local residents consider the UEA site to have an aesthetically pleasing appearance and considerable effort has been made by the campus management to maintain the attractive landscape. There are no plans for wind turbines and it is suggested that any proposals would be very heavily opposed by the community (Richard Bettle, UEA energy staff, *personal correspondence*).

3.5.5 Site Identification

The planning and social restrictions mean that it is not possible to select a site for a potential turbine location.

3.5.6 Power Production

Power generation calculations for three example turbines were carried out using the NOAA measured wind data for 2016 from Norwich Airport. A 2MW Vestas V90/2MW, an 800kW Enercon E53-800 and a 300kW Enercon E33-300 were used in the calculations as for the Ushant study; the power curves can be seen in the earlier Figure 2.25. Results are presented in Table 3.3

Table 3.3 Output values for UEA wind generation examples.

Turbine	Annual Generation	Summer Generation	Winter Generation	Proportion
Vestas V90/2MW	5.10GWh	2.34GWh	2.75GWh	45.9% / 54.1%
Enercon E53-800	2.03GWh	0.93GWh	1.10GWh	45.9% / 54.4%
Enercon E33-300	0.71GWh	0.33GWh	0.39GWh	46.4% / 53.6%

The electrical demand for 2015-2016 was 34.35GWh, of which 18.66GWh was imported from the national grid. The largest example turbine (Vestas V90/2MW) could replace up to 27.3% of the imported electrical energy. The peak and minimum loads for the campus were not available for this report so it is not known whether there are times where the wind energy would generate more than the campus demand and would have to be stored or curtailed. The times of generation throughout 2016 are shown in Figure 3.11.



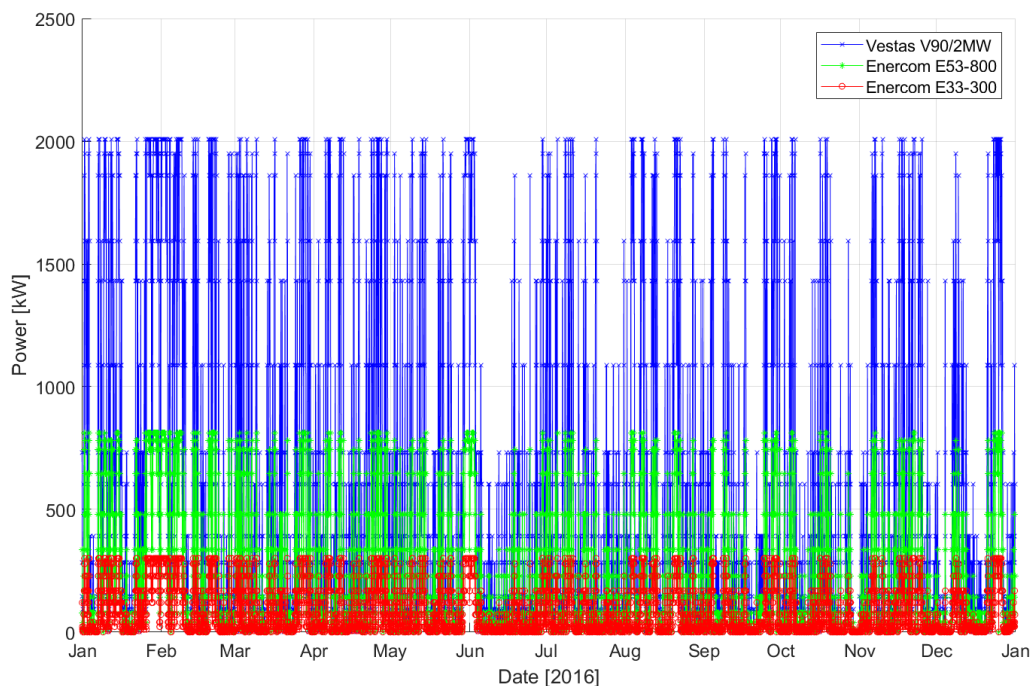


Figure 3.11 Time series of generation for UEA wind turbine examples.

3.6 Supply of other generation technologies

3.6.1 Biomass

The campus has a 1MW woodchip biomass generator. This unit is currently inactive however if it (or other biomass generation) were to be included, then the amount of electricity imported from the grid could be further reduced.

3.7 Demand side technology

The ICE project is working to provide energy saving incentives for UEA resident students. One method under development is the release of a smartphone app to encourage energy use at times when the electricity and heat are produced from the campus CHP units. The aim would be to reduce the amount of energy imported or generated from high carbon sources and to get maximum utilisation of the more efficient CHP units. For example, the app would encourage the student to have a shower at a time when there was generation capacity in the CHP units and discourage them from showering during peak times when electricity is imported from the national grid.

3.8 Scenarios for energy generation

Two different combinations of solar and wind generation were examined. As there are no demand profiles available for this report, the generation totals are simply noted.

Scenario 1: 1MW solar with an 800kW wind turbine

The first scenario assesses the electricity generated from 1MW of solar PV installations and a single Enercon E53-800 800kW wind turbine. Measured hourly solar data are not available for specific years so the solar calculations are based on the hourly time series for a 'typical' year, using PVsyst. The wind turbine power calculations use the measured NOAA wind speed data scaled up to the hub height for



2016. The generation data are summarised in Table 3.4 and the time series of generation for 2016 is seen in Figure 3.12.

If this scenario were to be implemented at the UEA campus then there would be a reduction in the amount of energy required to be imported from the national grid of approximately 18%. As there are occasions where both the solar and wind technologies are producing zero output (when there is no wind or sunlight) there will still need to be sufficient grid capacity to supply the entire peak load.

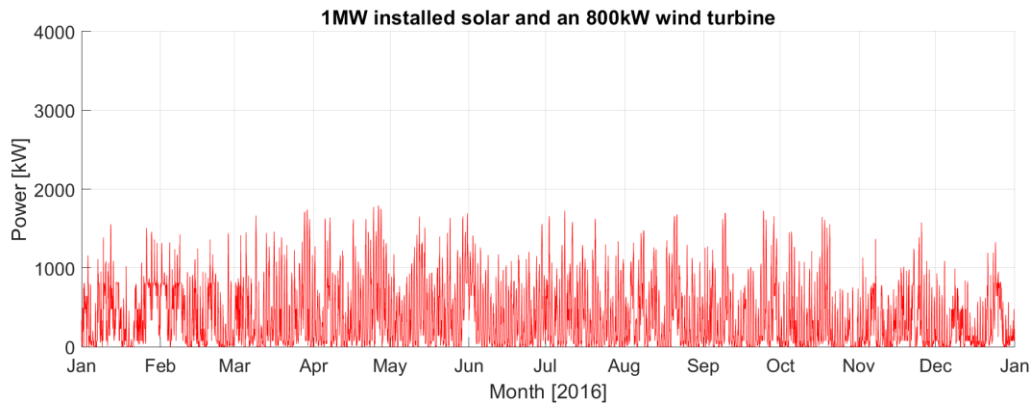


Figure 3.12 Scenario 1 generation time series (2016).

Table 3.4 Scenario 1 generation parameters.

Scenario 1	Annual (2016)	Summer (Apr – Sep)	Winter (Jan – Mar, Oct – Dec)
Generation [MWh]	3308.32	1793.51	1514.81

Scenario 2: 2MW solar with a 2MW wind turbine

Scenario 2 investigates the energy generated from expanded solar PV installations (2MW_p) and a larger 2MW wind turbine. This scenario would provide 7652.12MWh of electricity a year which would reduce the amount imported from the grid by 41%. The parameters are shown in Table 3.5 and the time series of generation is shown in Figure 3.13.

Table 3.5 Scenario 2 generation parameters.

Scenario 2	Annual (2016)	Summer (Apr – Sep)	Winter (Jan – Mar, Oct – Dec)
Generation [MWh]	7652.12	4061.27	3590.85



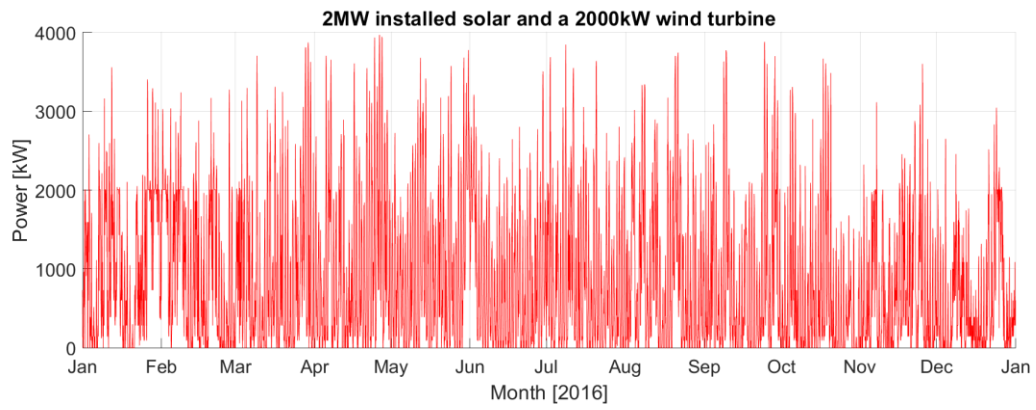


Figure 3.13 Scenario 2 generation time series (2016).



4 Conclusions

This report has analysed the energy requirements of the island of Ushant and the UEA and provided resource calculations for three renewable generation technologies.

An assessment of the energy demand was undertaken for Ushant, and the annual, seasonal and intra-day variability were examined and compared to the generation from each technology. For UEA the total annual generation was presented for 2015-16 and a breakdown of energy use shown.

The findings for each generation technology can be summarised as follows:

Solar

An examination of the solar resource shows considerable potential for expanded solar generation on both the island of Ushant and the UEA campus. For Ushant, solar radiation is much greater in the summer months whereas the island's energy demand is greatest in the winter. This limitation means that other sources of generation will always be required even if an extensive expansion of PV was applied. For UEA, there is also a large seasonal disparity of generation and although data is not available it is likely that demand will similarly be higher in the winter months.

Wind

On Ushant, wind energy generation is shown to be sufficient to achieve the 70% (2020) and 100% renewable targets if combined with battery storage and further solar and/or tidal generation. Planning consent and environmental and/or social issues will need to be overcome before a wind energy project can be taken forward. For UEA there are considerable barriers for consent to build wind turbines and no appetite for such a development.

Tidal

This study has explored the tidal characteristics at the region around the Ushant Island with the development of a numerical model (Delft3D-FLOW). The model output for both tidal level and tidal current at the sites near Ushant agree well with observed and predicted values. Technical, environmental, social and political constraints are all considered, together with the tidal characteristics around Ushant obtained from the numerical model, to identify the proper potential sites for tidal current energy absorption. It was found that the sites at the Fromveur Passage are well suited for tidal current energy exploitation. Tidal harmonic analysis was carried out on the tidal range and currents at the sites. This allowed for the prediction of current flow over any desired period. Additionally, potential power production by Sabella D10 at the preferred site was evaluated based on the numerical results.

This report shows that a combination of generation technologies can play a key role in creating a low carbon energy system. Along with storage solutions, energy reduction schemes and smart behaviour, the ICE project aims to provide a transferable methodology for isolated communities. ICE report T1.2 will explore the options for energy storage and the reliability of the electrical networks to further determine if the renewable technologies presented in this report are feasible for the sites.



The work in this report will be further integrated into the ICE methodology with the publication of ICE report T2.1 where a generalised methodology for low carbon smart solutions are discussed for isolated communities.



References

- Agence des aires marines protégées, 2015. *Marine Nature Parks*. Agence des aires marines protégées, Brest, France.
- Ashlock, J.C. & Schaefer, V., 2011. *Foundations for Wind Turbines*. [online] Available at: <http://home.eng.iastate.edu/~jdm/engr340-2011/ENGR%20340%20-%20Foundations%20%20-%20Ashlock%20-%20Schaefer.pdf> [Accessed 2/5/18].
- BBC, 2015. *Heat pumps extract warmth from ice cold water*. [online] Available at: <http://www.bbc.co.uk/news/business-31506073> [Accessed 2/5/18].
- Berrisford, P., Dee, D., Poli, P., Brugge, R., Fielding, K., Fuentes, M., Kallberg, P., Kobayashi, S., Uppala, S. and Simmons, A., 2011. *The ERA-Interim archive Version 2.0*, ERA Report Series 1, ECMWF, Reading, UK.
- Brower, M., 2012. *Wind resource assessment: a practical guide to developing a wind project*. John Wiley & Sons, Hoboken, New Jersey.
- Carballo, R., Iglesias, G. & Castro, A., 2009. Numerical model evaluation of tidal stream energy resources in the Ría de Muros (NW Spain). *Renewable Energy*, 34, pp1517-1524.
- CORDIS (Community Research and Development Information Service), 1984. *Wind Turbine for Local Supply of Ouessant Island*. European Commission, Project ID WE./00315/84
- Coriolis Cotier, 2018. Coastal ocean observing system. [online] Available at: <http://data.coriolis-cotier.org/> [Accessed 10/5/18].
- Dee, D. P., Uppala, S. M., Simmons, A. J., Berrisford, P. , Poli, P. , Kobayashi, S. , Andrae, U. , Balmaseda, M. A., Balsamo, G. , Bauer, P. , Bechtold, P. , Beljaars, A. C., van de Berg, L. , Bidlot, J. , Bormann, N. , Delsol, C. , Dragani, R. , Fuentes, M. , Geer, A. J., Haimberger, L. , Healy, S. B., Hersbach, H. , Hólm, E. V., Isaksen, I. , Kållberg, P. , Köhler, M. , Matricardi, M. , McNally, A. P., Monge-Sanz, B. M., Morcrette, J. , Park, B. , Peubey, C. , de Rosnay, P. , Tavolato, C. , Thépaut, J. and Vitart, F. (2011), The ERA-Interim reanalysis: configuration and performance of the data assimilation system. *Q.J.R. Meteorol. Soc.*, 137: 553-597. doi:10.1002/qj.828
- Department for Transport, 2013. *The Strategic Road Network and the Delivery of Sustainable Development*. Department for Transport, London, UK.
- Drew, B., Plummer, A.R., Sahinkaya, M.N., 2009. A review of wave energy converter technology. *Proceedings of the Institution of Mechanical Engineers, Part A: Journal of Power and Energy*, 223(8), pp887-902.
- DTU, 2017. *Global Wind Atlas 2.0*, Technical University of Denmark (DTU) [online] Available at: <https://globalwindatlas.info>.
- *“Global Wind Atlas 2.0, a free, web-based application developed, owned and operated by the Technical University of Denmark (DTU) in partnership with the World Bank Group, utilizing data provided by Vortex, with funding provided by the Energy Sector Management Assistance Program (ESMAP). For additional information: <https://globalwindatlas.info>”
- EDF, 2016. *Open Data de EDF sur les îles du Ponant*. [online] Available at: <https://opendata-iles-ponant.edf.fr> [Accessed 12/03/2018].
- Egbert, G.D., Bennett, A.F. & Foreman, M.G.G., 1994. Topex/Poseidon tides estimated using a global inverse model. *Journal of Geophysical Research*, 99, pp24821-24852.
- European Environment Agency, 2016. *Heating and cooling degree days*. EEA, Copenhagen, Denmark.
- European Commission, 2014. *Directive establishing a framework for maritime spatial planning*. European Commission, 2014/89/EU.



Fitch-Roy, O. & Connor, P., 2018. *ICE report T1.1.2 Policy Issues: An overview of the renewable energy policy and regulatory considerations in Ouessant and the UEA campus*. ICE Project report, Penryn, UK.

Fournisseurs Electricite, 2018. *Puissance compteur EDF*. [online] Available at: <https://www.fournisseurs-electricite.com> [Accessed 2/5/18].

Global Wind Atlas, 2017. *Global Wind Atlas*. [online] Available at: <https://globalwindatlas.info/> [Accessed 25/1/18].

Google, 2018. "Google Maps" [online], Available at: maps.google.com

Goth, Jamie. 2015, "How to choose the correct heat pump". Energy Institute: CPD Fundamentals. 13.[online] Available at: <https://www.energyinst.org/filegrab/?ref=3774&f=EiBI+Series+13+-+Module+1>

Green Car Congress, 2016. *Ricardo and Recycling Technologies to characterize Plaxx plastic-waste-derived-fuel for marine applications*. [online] Available at: <http://www.greencarcongress.com/2016/07/20160705-plaxx.html> [Accessed 2/5/18].

Guillou, N. & Chapalain, G., 2017. Assessing the impact of tidal stream energy extraction on the Lagrangian circulation. *Applied Energy*, 203, pp321-332.

Guillou, N., & Thiébot, J., 2016. The impact of seabed rock roughness on tidal stream power extraction. *Energy*, 112, pp762-773.

Hardwick, J., Smith, H. C. M., Fitch-Roy, O., Connor, P. M. & Sundaram, S., 2018. *ICE report T1.1.1: An overview of renewable energy supply potential*. ICE Project Report, Penryn, UK.

Huld, T., Muller, R. & Gambardella, A., 2012. A new solar radiation database for estimating PV performance in Europe and Africa. *Solar Energy*, 86, pp1803-1815.

Iglesias, G., Sánchez, M., Carballo, R. & Fernandez, H., 2012. The TSE index- A new tool for selecting tidal stream sites in depth-limited regions. *Renewable Energy*, 48, pp350-357.

IGN, 2017, *Geoportail*. Institut National de L'Information Geographique et Forestiere. [online] Available at: <https://www.geoportail.gouv.fr/carte>

Îles du Ponant, Sept 2016. *Revue De Presse: Les Îles du Finistere Lancement Operationnel de la Transition Energetique*. France

Îles du Ponant, 2017. *Les Touristes et Excursionnistes sur L'Ile D'Ouessant*. France

Intertec, 2015. *CELTIC interconnector - Marine consultancy and engineering services. Route investigation report*. [online] Available at: <http://www.eirgridnortheastprojects.ie/site-files/library/EirGrid/Celtic-Interconnector-Marine-Route-Investigation.pdf> [Accessed 2/5/18].

In Sun We Trust, 2018, *Panneaux photovoltaïques : LE guide ultime (2018)*, [online] Available at: <https://www.insunwetrust.solar/blog/le-solaire-et-vous/panneaux-photovoltaïques-guide-ultime-2017/>

IUCN, 2017. Iroise, the jewel of France's west coast. [online] Available at: <https://www.iucn.org/news/protected-areas/201706/iroise-jewel-frances-west-coast> [Accessed 17/5/18].

Legrand, C., 2009. *Assessment of Tidal Energy Resource*. BSI, London, UK.

Matt S. Mitchell & Jeffrey D. Spitler. (2013). "Open-loop direct surface water cooling and surface water heat pump systems—A review", *HVAC&R Research*, 19:2, 125-140, DOI:10.1080/10789669.2012.747374



Mermoud, A. & Wittmer, B., 2014. *PVsyst User's Manual*. [online] Available at: http://www.PVsyst.com/images/pdf/PVsyst_Tutorials.pdf [Accessed 19/12/17].

NOAA, 2018. "National Oceanic and Atmospheric Administration: National Centres for Environmental Information". [online] Accessed at: <https://www.ncdc.noaa.gov/data-access/land-based-station-data>

OpenStreetMap, 2018. "Open Street Map" [online]. Available at: www.openstreetmap.org

Paboeuf, S., Sun, P.Y.K., Macadré, L.-M. & Malgorn, G., 2016. Power Performance Assessment of the Tidal Turbine Sabella D10 Following IEC62600-200. *Proc. 35th International Conference on Ocean, Offshore and Arctic Engineering*, American Society of Mechanical Engineers, Busan, South Korea, June 19–24, 2016.

Pawlowicz, R., Beardsley, B. & Lentz, S., 2002. Classical tidal harmonic analysis including error estimates in MATLAB using T_TIDE. *Computers and Geosciences*, 28(8), pp929-937.

Planning Portal, 2018. *Permitted Development Rights*". [online] Available at: https://www.planningportal.co.uk/info/200187/your_responsibilities/37/planning_permission/2

Pleijel, C., 2015. Energy audit on Ouessant. Report supported by Intelligent Energy Europe. 1-17.

PV Financing, 2017. *PV Financing* [online] Available at: <http://www.pv-financing.eu/>

SHOM, 2018. *MNT Bathymétrie de façade Atlantique*. [online] Available at: <http://diffusion.shom.fr/pro/environnement/bathymetrie/mnt-facade-atl-homonim.html> [Accessed 9/5/18].

Sogreah Consultants, 2009. *Etude de faisabilité d'une operation de maitrise de l'énergie et de developpement des energies renouvelables sur les îles de Molene at Ouessant*. Sogreah, Lyon, France.

SolarGIS. 2018. *Solar Resource Maps*. [online] Available at: <https://solargis.com> [Accessed 2/5/18].

Subsea World News, 2015. *Bourbon in SABELLA's D10 Subsea Cable Project*. [online] Available at: <https://subseaworldnews.com/2015/06/25/watch-bourbon-in-sabellas-d10-subsea-cable-project/> [Accessed 17/5/18].

Tawil, T.E., Charpentier, J.F. & Benbouzid, M., 2018. Sizing and rough optimization of a hybrid renewable-based farm in a stand-alone marine context. *Renewable Energy*, 115, pp1134-1143.



Appendix 1: PVsyst reports



Appendix 2: Tidal harmonic analysis

A2.1 Harmonic analysis overview

The tidal range and currents at a site can be predicted for any period of time using the finite number of harmonic constituents specific to the site. Each sinusoidal constituent at a particular location has a defined frequency, amplitude and phase, which can be determined through the mathematical analysis of directly measured tidal range and/or velocity data. The harmonic constituents may then be used to predict the tidal range and/or current velocities at the site over any given period.

A harmonic analysis toolbox written in MATLAB, T-Tide (Pawlowicz et al., 2002), is used in this study to perform the harmonic analysis. Numerical data for the tidal level at the location of the Sabella turbine for the period 01/08/2017 to 01/10/2017 with an interval of 10 mins are used as input for the harmonic analysis in order to generate 35 standard tidal constituents.

A2.2 Tidal level

Table A2.1 presents the 35 tidal constituents derived from harmonic analysis of the tidal level at point A, shown in Figure A2.1.

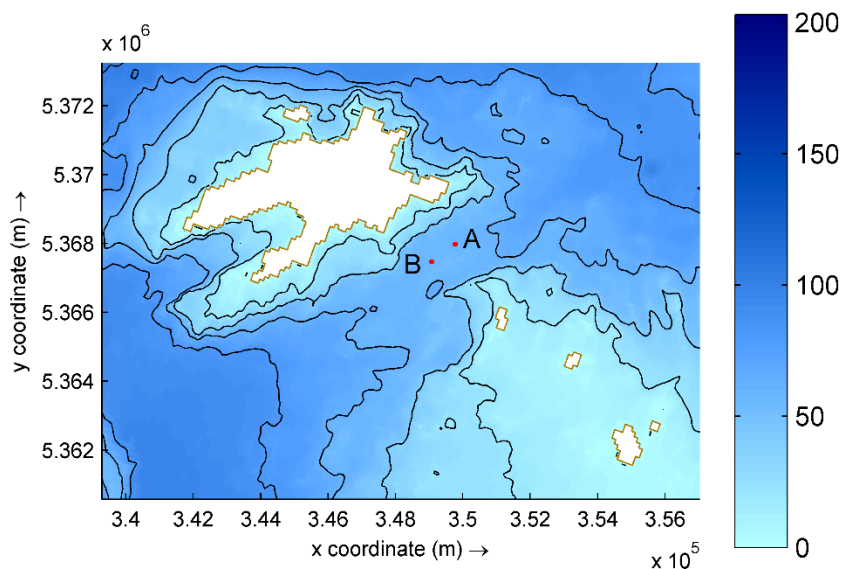


Figure A2.1 Map of the Fromveur Strait, showing the location of point A used for the harmonic analysis.



Table A2.1 Tidal constituents of the tidal level at point A, with asterisks showing the constituents used in predictions.

Constituent	Frequency (°/h)	Amplitude (m)	Phase (°)
*MM	0.001512	0.0296	196.08
*MSF	0.002822	0.0500	234.17
ALP1	0.034397	0.0024	235.48
2Q1	0.035706	0.0011	265.44
*Q1	0.037219	0.0190	281.36
*O1	0.038731	0.0634	328.39
NO1	0.040269	0.0076	177.14
*K1	0.041781	0.0638	87.97
J1	0.043293	0.0013	305.94
OO1	0.044831	0.0021	149.61
UPS1	0.046343	0.0030	306.03
EPS2	0.076177	0.0034	187.98
MU2	0.07769	0.0054	323.39
*N2	0.078999	0.4362	97.51
*M2	0.080511	2.1375	116.77
L2	0.082024	0.0196	344.89
*S2	0.083333	0.8814	164.37
ETA2	0.085074	0.0035	154.77
MO3	0.119242	0.0013	219.46
M3	0.120767	0.0005	191.42
MK3	0.122292	0.0014	145.08
SK3	0.125114	0.0004	51.64
*MN4	0.159511	0.0524	222.02
*M4	0.161023	0.0658	224.94
SN4	0.162333	0.0103	315.93
*MS4	0.163845	0.0895	298.45
S4	0.166667	0.0111	25.59
2MK5	0.202804	0.0007	248.11
2SK5	0.208447	0.0009	326.08
*2MN6	0.240022	0.0231	283.41
*M6	0.241534	0.0173	293.53
*2MS6	0.244356	0.0306	17.13
*2SM6	0.247178	0.0100	96.11
3MK7	0.283315	0.0003	20.96
*M8	0.322046	0.0037	196.14

Sixteen tidal constituents, marked with asterisks Table A2.1, were used to predict tidal levels. Figure A2.2 shows the time series of predicted tidal heights (shown as points) and computed tidal heights (line) at Point A in August-September 2017. A good agreement between the predicted and computed results is obtained.



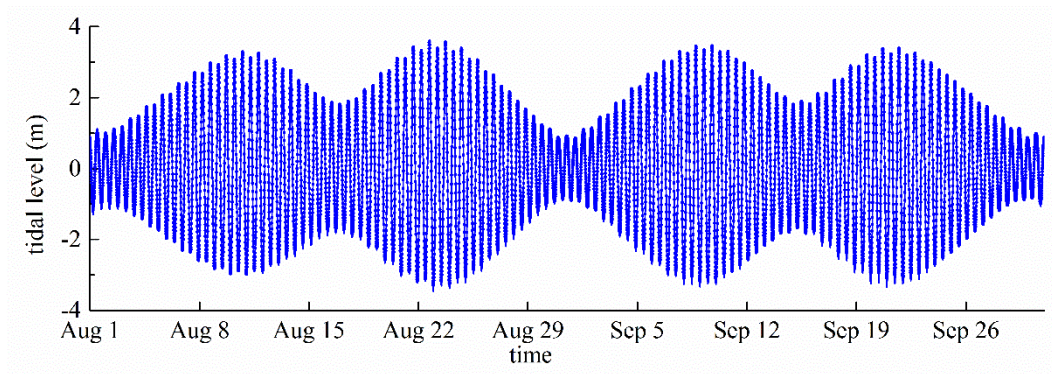


Figure A2.2 Predicted (points) and computed (line) time series of the tidal level at Point A in August-September 2017

A2.3 Tidal current

Table A2.2 presents the 35 tidal constituents for tidal velocities derived from the harmonic analysis of the tidal current at point A. For the velocity constituents, each constituent comprises location-specific information relating to the ellipse traced by the tip of the velocity vector: the lengths of the semi-major and semi-minor axis, the inclination of the northern semi-major axis anti-clockwise from east, and the frequency and phase.

Sixteen tidal constituents, marked with asterisks in Table A2.2, were used to predict the tidal velocities. Figure A2.3 shows the predicted (points) and computed (line) time series of the x and y components of the tidal current at point A in August-September 2017. A good agreement between the predicted and computed results is obtained.

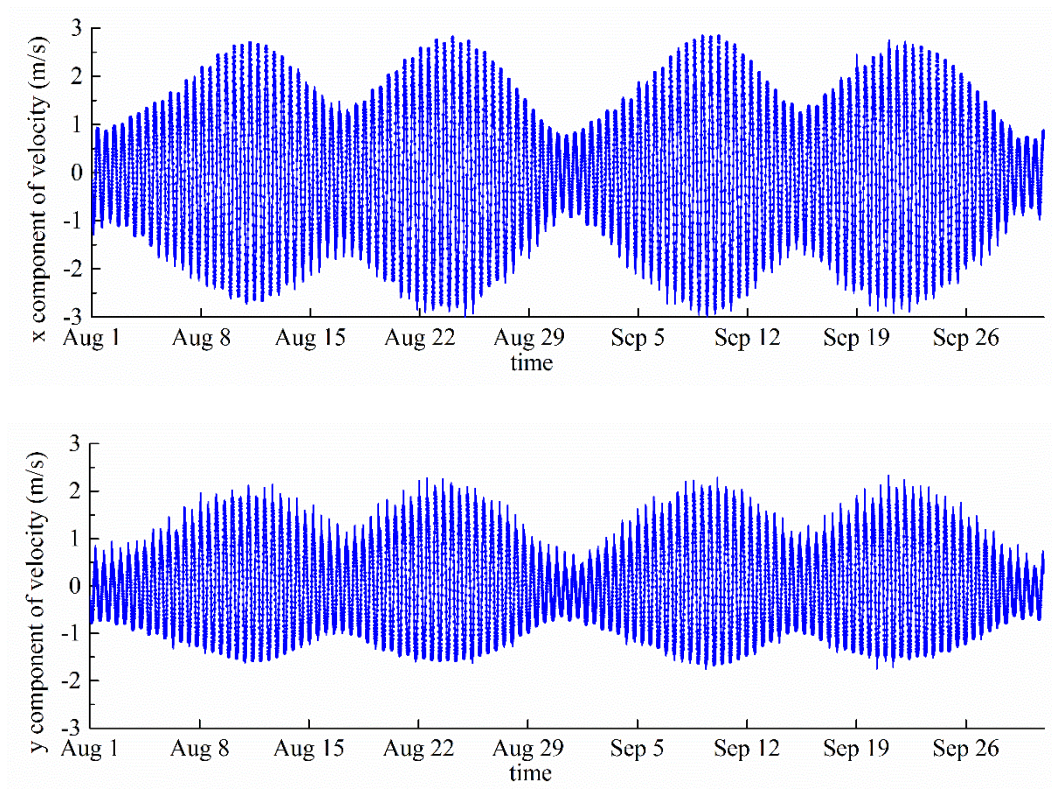


Figure A2.3 Predicted (points) and computed (line) time series of the tidal current at Point A in August-September 2017.



Table A2.2 Tidal constituents of the tidal velocities at point A, with asterisks showing the constituents used in predictions.

Constituent	Frequency (°/h)	Semi-major axis (m/s)	Semi-minor axis (m/s)	Inclination (°)	Phase (°)
*MM	0.001512	0.044	-0.003	114.11	21.88
*MSF	0.002822	0.085	0.007	87.80	48.66
*ALP1	0.034397	0.019	-0.004	51.35	252.88
2Q1	0.035706	0.005	0.003	41.64	47.19
Q1	0.037219	0.008	0.006	29.08	158.49
*O1	0.038731	0.026	-0.004	44.15	159.44
NO1	0.040269	0.021	-0.002	64.66	293.75
*K1	0.041781	0.040	-0.005	36.89	291.13
J1	0.043293	0.009	-0.004	33.78	212.66
*OO1	0.044831	0.040	0.013	50.09	123.08
*UPS1	0.046343	0.023	0.001	24.44	340.30
EPS2	0.076177	0.034	0.002	19.03	219.47
*MU2	0.07769	0.196	-0.011	25.74	245.45
*N2	0.078999	0.412	-0.004	33.28	19.23
*M2	0.080511	2.087	-0.055	34.00	49.19
L2	0.082024	0.025	-0.001	40.70	197.00
*S2	0.083333	0.989	-0.002	33.09	95.66
ETA2	0.085074	0.015	-0.006	22.40	312.93
*MO3	0.119242	0.019	0.003	30.03	184.83
M3	0.120767	0.009	0.002	171.55	54.19
*MK3	0.122292	0.016	0.001	26.15	229.08
SK3	0.125114	0.008	0.001	60.17	230.04
*MN4	0.159511	0.055	0.011	26.08	319.09
*M4	0.161023	0.171	0.043	26.43	354.95
*SN4	0.162333	0.023	-0.002	7.77	343.06
*MS4	0.163845	0.111	0.021	13.48	29.63
*S4	0.166667	0.033	-0.002	25.63	56.44
2MK5	0.202804	0.015	0.000	70.24	329.17
2SK5	0.208447	0.009	-0.001	8.10	329.29
*2MN6	0.240022	0.047	-0.008	43.00	1.32
*M6	0.241534	0.077	-0.008	41.31	23.81
*2MS6	0.244356	0.099	-0.024	38.61	82.40
*2SM6	0.247178	0.040	-0.012	43.38	107.52
3MK7	0.283315	0.010	0.000	119.73	114.72
M8	0.322046	0.007	0.005	2.97	331.33



Appendix 3: Tidal resource modelling study

A3.1 Hydrodynamic model overview

A numerical model of the hydrodynamics of Ushant was implemented and validated based on field data. The model, Delft3D-FLOW, developed by Delft Hydraulics, is a finite-difference code solving the baroclinic Navier-Stokes and transport equations. It can be used as a 3D model, or as a 2DH (vertically averaged) model, as used in previous assessments of the tidal resource (e.g. Carballo et al., 2009; Iglesias et al., 2012) and in the present work. The depth-mean equations then read:

$$\frac{\partial \zeta}{\partial t} + \frac{\partial [(d + \zeta)U]}{\partial x} + \frac{\partial [(d + \zeta)V]}{\partial y} = Q, \quad (\text{A3-1})$$

$$\left. \begin{aligned} \frac{\partial U}{\partial t} + U \frac{\partial U}{\partial x} + V \frac{\partial U}{\partial y} - fV &= -g \frac{\partial \zeta}{\partial x} - \frac{g}{\rho_0} \int_{-d}^{\zeta} \frac{\partial \rho'}{\partial x} dz + \frac{\tau_{sx} - \tau_{bx}}{\rho_0 (d + \zeta)} + \nu_h \nabla^2 U \\ \frac{\partial V}{\partial t} + U \frac{\partial V}{\partial x} + V \frac{\partial V}{\partial y} + fU &= -g \frac{\partial \zeta}{\partial y} - \frac{g}{\rho_0} \int_{-d}^{\zeta} \frac{\partial \rho'}{\partial y} dz + \frac{\tau_{sy} - \tau_{by}}{\rho_0 (d + \zeta)} + \nu_h \nabla^2 V \end{aligned} \right\}, \quad (\text{A3-2})$$

$$\frac{\partial (\zeta + d)c}{\partial t} + \frac{\partial [(\zeta + d)Uc]}{\partial x} + \frac{\partial [(\zeta + d)Vc]}{\partial y} = D_h \nabla^2 c - \lambda_d (d + \zeta)c + R, \quad (\text{A3-3})$$

where d is the local water depth relative to a reference plane; U and V stand for the vertically integrated velocity components in the x and y directions, respectively; Q represents the intensity of mass sources per unit area; f is the Coriolis parameter, ν_h is the kinematic horizontal eddy viscosity, ρ_0 is the reference density, ρ' is the anomaly density, τ_{sx} and τ_{sy} are the components of the wind stress acting on the sea surface, and τ_{bx} and τ_{by} are the shear stress components at the bottom. Finally, in the transport equation (Eq. A2-3), c stands for salinity or temperature, D_h is the horizontal eddy diffusivity, λ_d represents the first order decay process and R is the source term per unit area. Eqs. A3-1 and A3-2 express the conservation of mass and momentum; Eq. A3-3 is the transport equation, which is solved both for salinity and temperature.

For the spatial discretisation the model uses the Arakawa-C approach, a staggered grid in which water levels (ζ) are computed at grid cell centres, whereas flow velocity components (U and V) are defined at the mid-points of the grid cell faces to which they are perpendicular. The water depth values at the water level points are taken as the maximum of the water depths at the four nearest grid nodes; the water depths at the velocity points are computed as the mean of the water depths at the endpoints of the corresponding cell face.

A3.2 Grids

The area covered by the model should be sufficient to include all important hydrodynamic effects, and be such that calibration and validation of tidal range and/or currents is possible.

In order to obtain high-resolution results at the location of interest without too large a cost in computation time, the model was implemented in the so-called nested mode, with two computational grids as shown in Figure A3.1: a coarser grid, covering a large area of about $1.4 \times 10^5 \text{ km}^2$, and a finer (nested) grid for the area around the Ushant and the coastal area nearby.



The coarse grid has 43917 cells of variable size, from 3220×3200 m at the ocean boundary to 800×800 m close to Ushant island. The finer (nested) grid (see Figure A3.1) has 139714 cells of variable size, from 480×480 m at the ocean boundary to 120×120 m close to Ushant island and the coastal area nearby.

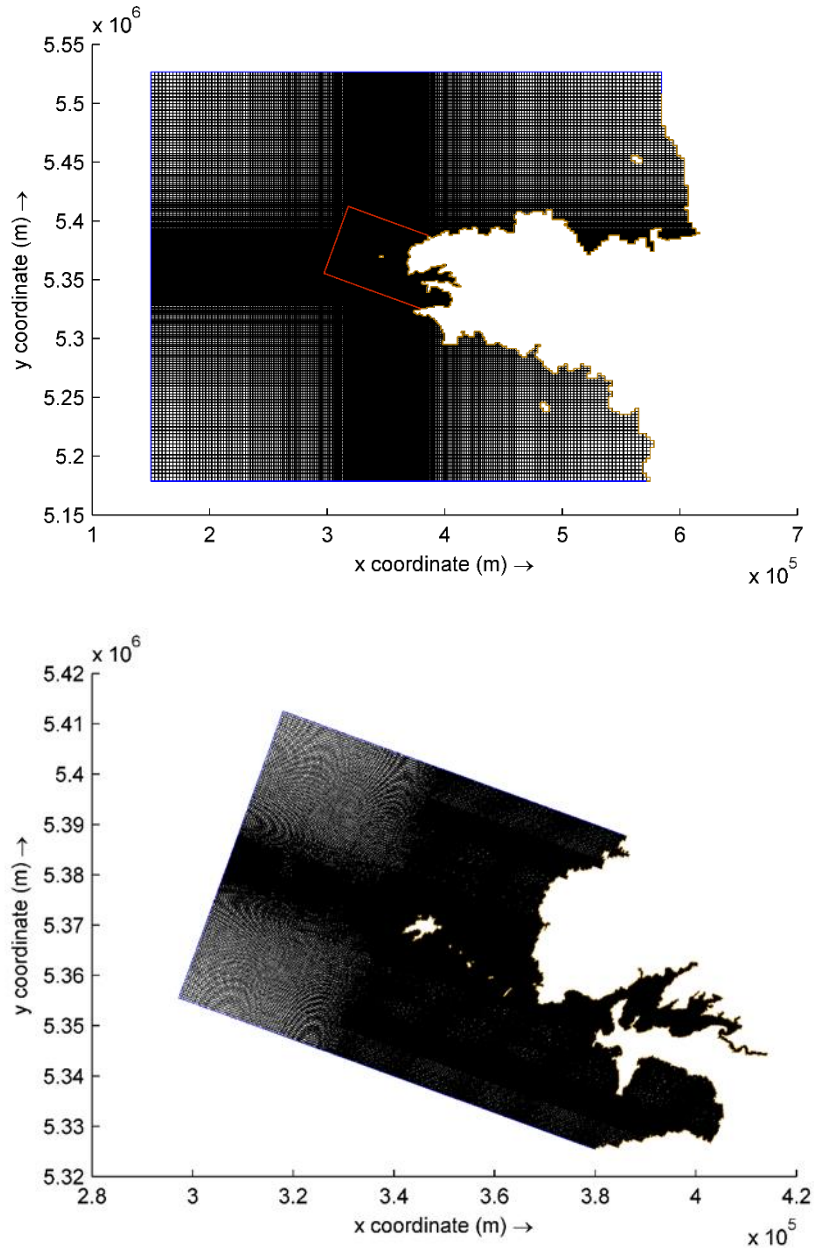


Figure A3.1 Coarse and fine (nested) grids for the Delft3D FLOW model.



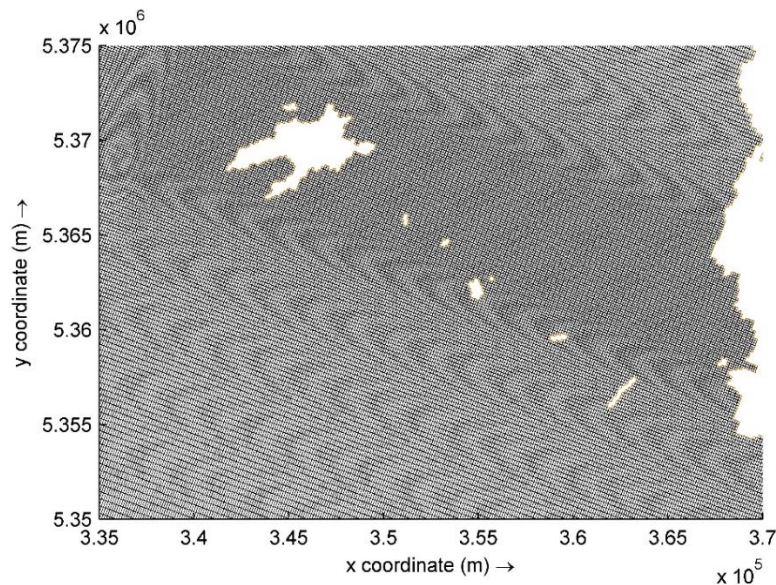


Figure A3.2 Fine (nested) grids for the Delft3D FLOW model.

A3.3 Boundary conditions

To use the required grid resolution in the area of interest (the area around Ushant), nested grids are used, i.e., the nesting of the fine model in the coarse model.

Open boundary conditions

Open boundary conditions, i.e. the water levels used to drive the ocean boundary of the model domain, are specified at a limited number of boundary points. Linear interpolation is used to generate the boundary conditions at the intermediate points along the boundary. For the coarse model, water levels used to drive ocean boundary of the model domain are specified in terms of amplitudes and phases for the astronomic components by using the global ocean tidal model TPXO 7.2 (Egbert et al., 1994). The hydrodynamic boundary conditions of the fine model are generated by the coarse model. In principle, the nested boundary conditions are generated by bi-linear interpolation of computational results at monitoring stations of the overall model.

Closed boundary conditions

A closed boundary is situated at the transition between land and water. At a closed boundary, two boundary conditions have to be prescribed. One boundary condition relates to the flow normal to the boundary and the second to the shear-stress along the boundary. In this model, for flow normal to the boundary, the velocities normal to the closed boundary are set to zero. For the shear stress along the boundary, the zero tangential shear-stress (free slip) condition is adopted.

Fresh water inflow locations and data used

In the coastal region considered in the numerical model, the largest river is the Elorn, with a source in the Arrée Mountains, at the foot of the Tuchen Kador at 300m altitude. After a 42 km course to Landerneau, it widens into a large estuary, which then opens into the harbour of Brest at the Plougastel bridge. Its modest surface watershed (approximately 300 km²) consists of crystalline, metamorphic, shale and sandstone rocks, alternating impervious zones and permeable granite arena zones. It is subject to an oceanic climate. This gives it a fairly regular annual flow, the low water being further supported by the Drennec reservoir lake. The average flow rate of the Elorn is only 5.5 m³s⁻¹, too small to affect hydrodynamics in the model, thus fresh water inflow is ignored in the simulation.



Bottom friction parameterisation

The bed shear-stress due to flow alone may be computed using various formulations including Chézy, Manning or White Colebrook. In this numerical simulation, the roughness formula of Manning is adopted to induce the influence of bottom roughness/friction.

For high resolution models where much of the details of the flow are resolved by the grid, with grid sizes of tens of metres or less, the values for the eddy viscosity and the eddy diffusivity are typically in the range of 1 to 10 m²s⁻¹. For large (tidal) areas with a coarse grid, i.e. grid sizes of hundreds of metres or more, the coefficients typically range from 10 to 100 m²s⁻¹. In the coarse and fine models used in this study, the horizontal eddy viscosity is set to 20 m²s⁻¹ and 10 m²s⁻¹, respectively.

Other parameters

Other parameters used in the simulation include the constants for acceleration due to gravity, $g = 9.81 \text{ ms}^{-2}$, and water density, $\rho = 1025 \text{ kgm}^{-3}$. Other parameters, such as wind stress, salinity and temperature, are believed to have an extremely small influence on the hydrodynamics and are not considered in the numerical simulation.

A3.4 Initial conditions

Uniform initial conditions for water level are used in the hydrodynamic model. A large discrepancy between the initial condition and the boundary conditions at the simulation start time can result in short wave disturbances that propagate into the model area. The time to reduce these short wave disturbances by internal dissipation such as bottom friction might be quite large, for example one or more tidal cycles. The effects of a discrepancy between the initial condition and the boundary conditions at the start time of the simulation can be substantially reduced by applying a transition period from the initial condition to the actual boundary conditions. Here, at least 7 days is added to the simulation time prior to the initial period of interest to reduce these short wave disturbances.

A3.5 Calibration and validation

The port of Brest, located at 4.4951°W, 48.3829°N, lies within the finer (nested) grid region, with observational data of sea level available from the coastal ocean observing system Coriolis Cotier (2018). The sea level at Brest can be easily modified into tidal level by subtracting 4.041 m.

There are also three IHO (International Hydrographic Organisation) tidal gauge stations located in the finer (nested) grid region, located at Ushant, Le Conquet and Douarnenez, where the tidal data are recorded and can be used for tidal predictions. These four tidal gauge stations are plotted in Figure A3.3.



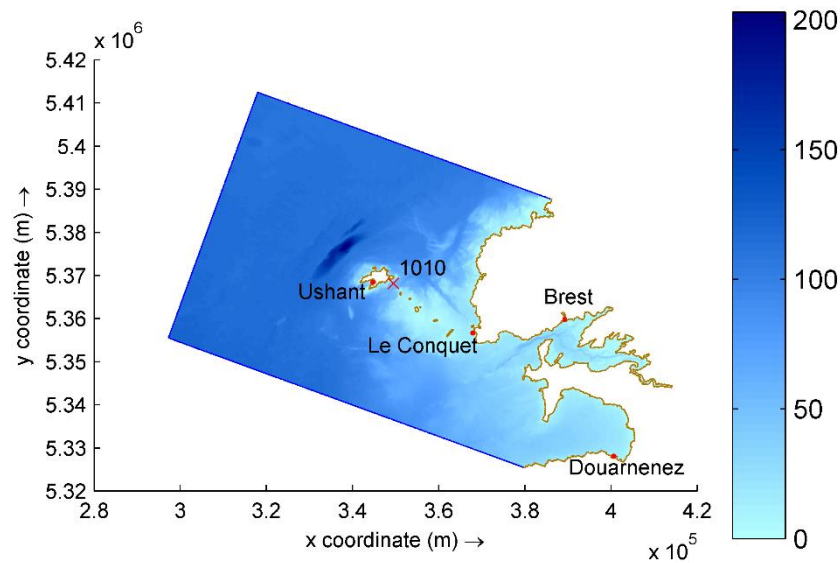


Figure A3.3 Location of the tidal observation points.

Figure A3.4 presents the time series of the predicted/observed tidal range values (shown as points) and modelled tidal range (solid line) at the different tidal gauges in August 2017. Note that seven more days prior to this period was added in the numerical simulation to reduce the short wave disturbances induced by the initial conditions. It can be seen from Figure A3.4 that seven days is sufficiently long to stabilise the hydrodynamic model. In the following cases, at least seven days prior to the period of interest are included in the numerical simulations, although the results during this transition period are not presented.



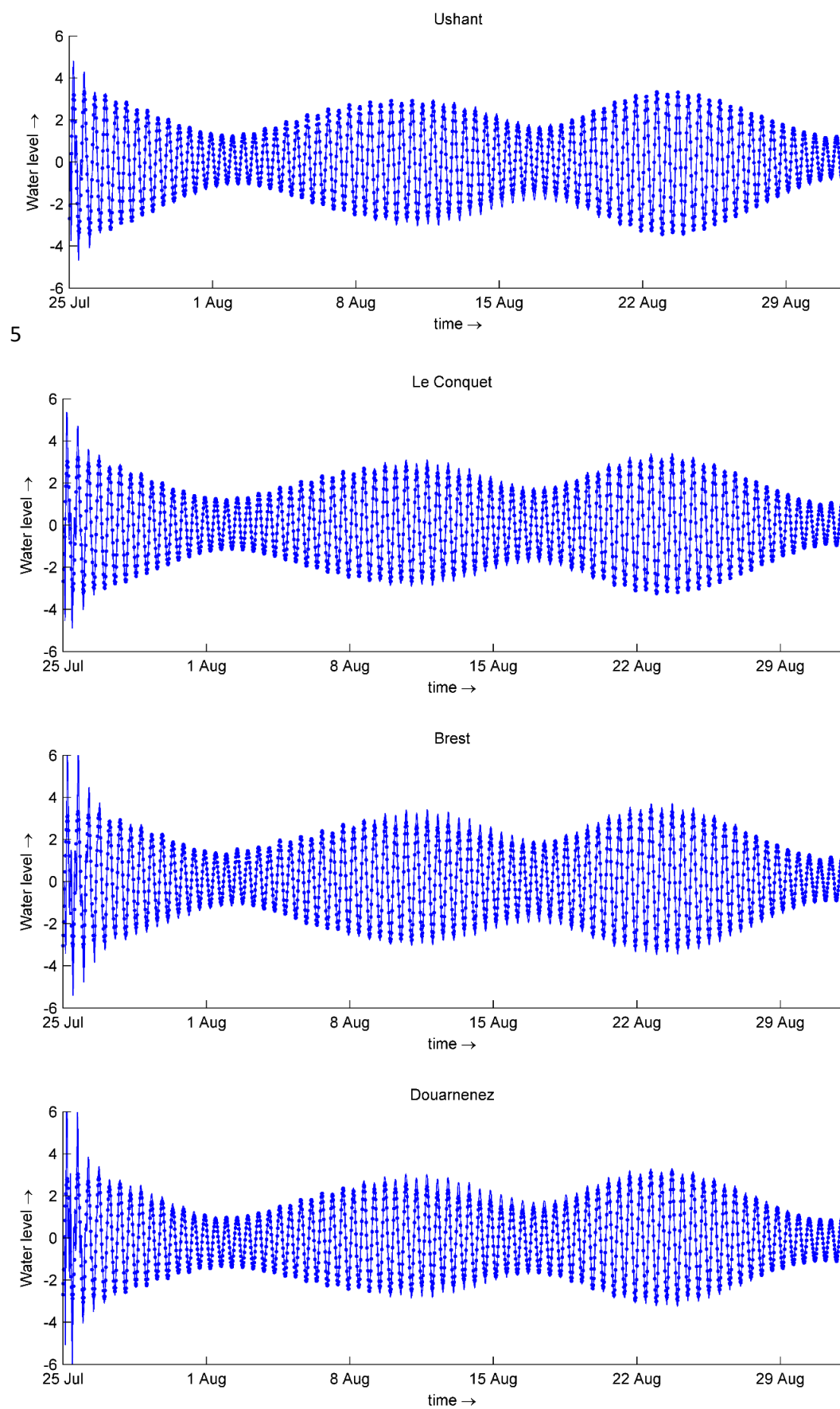


Figure A3.4 Predicted/observed (points) and computed (line) time series of the tidal range at different observation points in August 2017.



As discussed previously, the current 10 m above the seabed at point #1010 was recorded in March-April 1993. Since the numerical model used in this study is a depth averaged 2-D model, there is no information on the velocity profile at the site available from the numerical simulation. However, values 10 m above the bed can be computed from modelled depth averaged velocities, assuming a vertical logarithmic profile in the water column. Here, the 1/10th law is used to describe the velocity reduction with depth as shown in Figure A3.5, where V_0 is the speed at the surface (ms^{-1}), z is the distance above the seabed (m), d is the depth (m) and V is the corresponding speed at the distance z above the seabed.

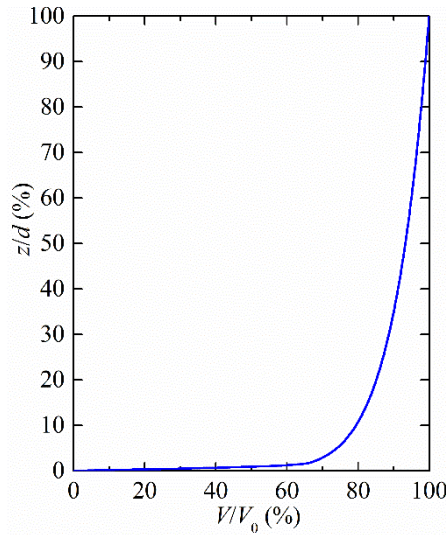


Figure A3.5 Tidal current profile.

According to the 1/10th law, V at the distance z above the seabed can be written as:

$$V = V_0 \left(\frac{z}{d} \right)^{1/10}. \quad (\text{A2-4})$$

The averaged velocity can be then expressed as:

$$\bar{V} = \frac{1}{d} \int_0^d V_0 \left(\frac{z}{d} \right)^{1/10} dz = \frac{10V_0}{11} \quad (\text{A2-5})$$

Hence the current velocity at 10 m above the bed can be extrapolated from predicted depth averaged velocities as follows:

$$V_{10\text{m}} = V_0 \left(\frac{10}{d} \right)^{1/10} = \frac{11}{10} \bar{V} \left(\frac{10}{d} \right)^{1/10} \quad (\text{A2-6})$$

Figure A3.6 presents time series of the amplitude and direction (using the directional convention measuring anticlockwise from East) of the current 10 m above the seabed at point #1010 in March-April 1993, showing measured data as points and modelled as a solid line.



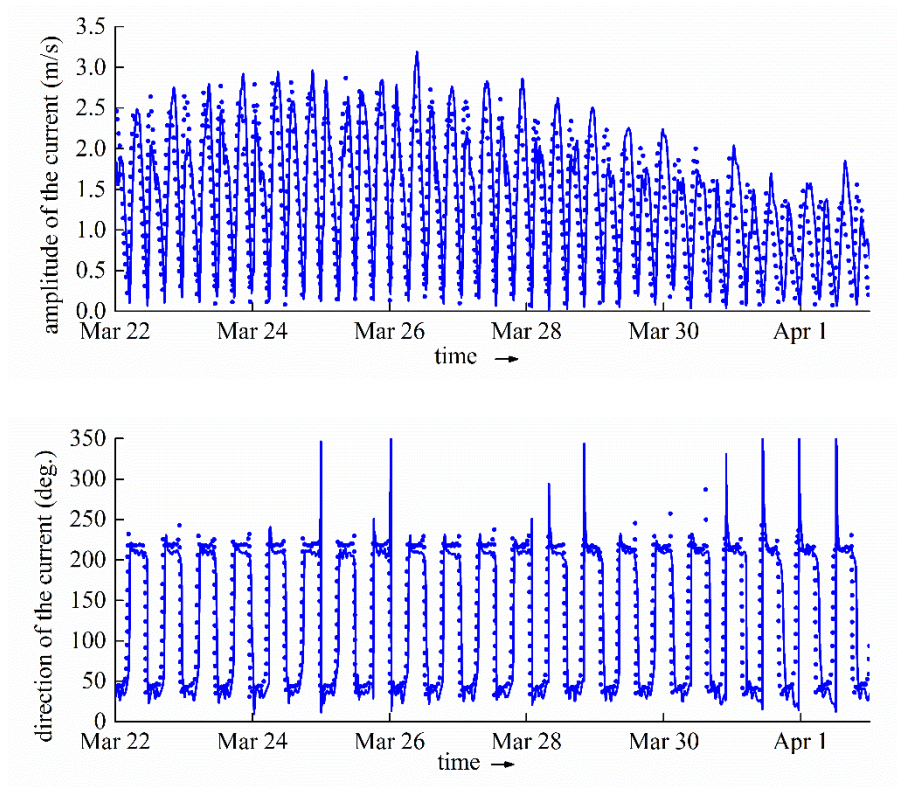


Figure A3.6 Measured (points) and computed (line) time series of the amplitude and direction (anticlockwise convention from the East) of the current 10 m above the seabed at point #1010 in March-April 1993.

The computed results of both tidal levels at the four tidal gauge stations and the current at #1010 show good agreements with predicted/observed data, indicating that the present hydrodynamic model performs well in evaluating tidal hydrodynamics around Ushant.



Appendix 4: Tidal turbine power production calculations

A4.1 Weighted tidal velocities

The first step in the prediction of tidal turbine power production is the calculation of the weighted tidal velocities. As illustrated in Figure A4.1, the current velocity $U_{j,k}$ must be found for each vertical section of the water column, either through measurement with an ADCP or 3D modelling. It can be assumed that the current velocity at location k should be weighted by the corresponding area A_k and further integrated across the projected capture area (Paboeuf et al., 2016). This is mathematically translated by Eq. (A4-1):

$$U_j = \left[\frac{1}{A} \sum_{k=1}^N (U_{j,k}^3 A_k) \right]^{1/3} \quad (\text{A4-1})$$

where j is the index number of the time instant at which the measurement is performed; k is the index number of the current profiler measurement/prediction position across the projected capture area; N is the total number of current profiler positions across the projected capture area; A is the project capture area of the rotor in m^2 ; A_k is the area corresponding to the current profiler measurement position k across the projected area in m^2 ; $U_{j,k}$ is the effective current velocity (perpendicular to the rotor plan) profiler at location k .

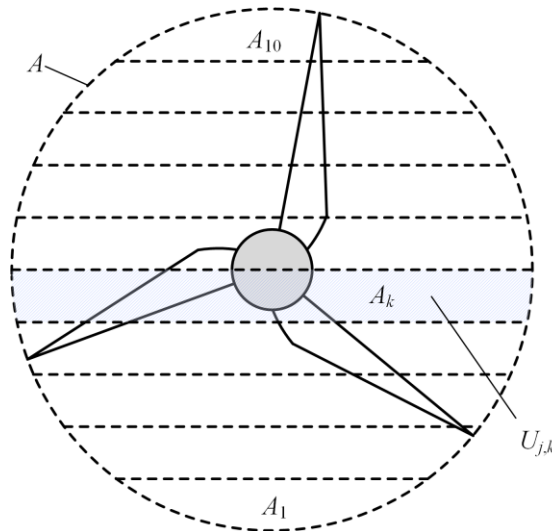


Figure A4.1 Projected turbine area used for current velocity measurements.

The weighted tidal velocities at the site of the Sabella D10 are plotted in Figure A4.2, in which $U_j > 0$ represents the flood current, whereas $U_j < 0$ represents the ebb current.



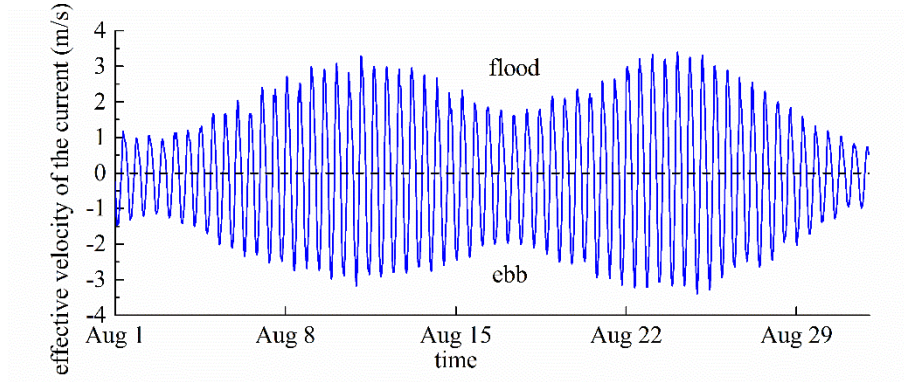


Figure A4.2 Time series of the weighted tidal velocities.

A3.2 Power density

The average power density (APD) available across the surface considered can be calculated directly from the hydrodynamic model, expressed as (Legrand et al, 2013):

$$APD = \frac{1}{2} \rho \bar{U}^3 = 3.167 \text{ kW/m}^2, \quad (\text{A4-2})$$

where U is the root mean cubed velocity written as:

$$\bar{U} = \left[\frac{1}{L} \sum_{j=1}^L |U_j^3| \right]^{1/3} = 1.835 \text{ m/s}, \quad (\text{A4-3})$$

in which j is the index of the 10 min increments, U_j is the weighted tidal velocity obtained from Eq. (A4-1) and L is the total number of time intervals.

A3.3 Annual electrical power

Velocity distribution

A velocity distribution for the tidal current velocity can be produced from a histogram of results from the harmonic analysis, at 10 min intervals, with 0.1 ms^{-1} bin size. The percentage of time, $f(U_i)$, that the velocity occurs within each bin is then computed. The velocity distribution curve for the Sabella site is shown in Figure A4.3.

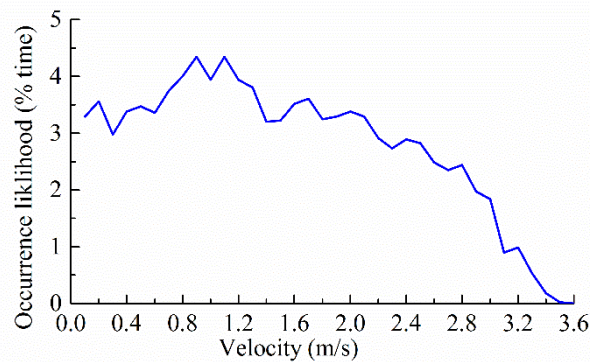


Figure A4.3 Velocity distribution curve for the Sabella site.



Electrical power per bin

The rotor efficiency can be assumed to rise from 38% at cut-in speed to reach 45% at the rated velocity. For the Sabella D10, the production cut-in speed is 0.4ms^{-1} and the cut-out speed is 4.0ms^{-1} (Paboeuf et al., 2016). Table A4.1 shows the calculation of the electrical power per bin, $P(U_i)$ for the Sabella D10 site. In the example, the rotor diameter is 10m, so the swept area A , is 78.54m^2 .

Table A4.1 Electrical power per bin.

Average bin velocity	Available power	Rotor efficiency	Electrical power per bin
U_i	$P_{av,i}=0.5\rho AU_i^3$	η_R	$P(U_i)=P_{av,i} \eta_R$
ms^{-1}	kW	%	kW
0.05	0.01	0.00	0.00
0.15	0.14	0.00	0.00
0.25	0.63	0.00	0.00
0.35	1.73	0.00	0.00
0.45	3.67	38.10	1.40
0.55	6.70	38.29	2.56
0.65	11.05	38.49	4.25
0.75	16.98	38.68	6.57
0.85	24.72	38.88	9.61
0.95	34.51	39.07	13.48
1.05	46.60	39.26	18.30
1.15	61.22	39.46	24.16
1.25	78.62	39.65	31.17
1.35	99.03	39.85	39.46
1.45	122.71	40.04	49.14
1.55	149.89	40.24	60.31
1.65	180.82	40.43	73.10
1.75	215.72	40.63	87.64
1.85	254.86	40.82	104.03
1.95	298.46	41.01	122.41
2.05	346.77	41.21	142.90
2.15	400.04	41.40	165.63
2.25	458.49	41.60	190.72
2.35	522.38	41.79	218.31
2.45	591.95	41.99	248.54
2.55	667.43	42.18	281.52
2.65	749.07	42.38	317.42
2.75	837.11	42.57	356.35
2.85	931.79	42.76	398.47
2.95	1033.36	42.96	443.91
3.05	1142.05	43.15	492.82
3.15	1258.10	43.35	545.35
3.25	1381.76	43.54	601.64
3.35	1513.28	43.74	661.85
3.45	1652.88	43.93	726.12



Figure A4.4 presents the electrical power curve for the Sabella D10. All the average bin velocities are less than the rated velocity of 4.0ms^{-1} , therefore the electrical power does not reach the constant rated power at any point.

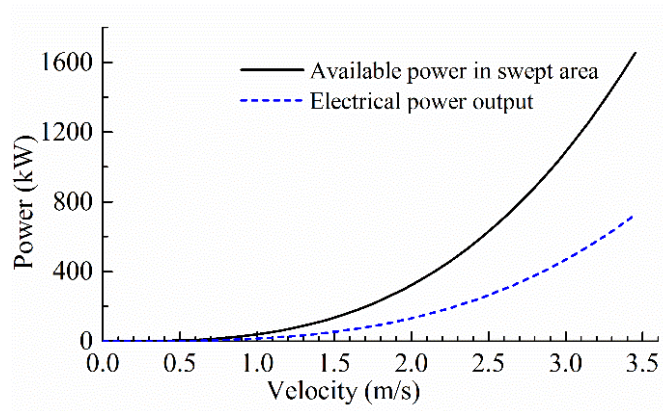


Figure A4.4 Electrical power curve for the Sabella D10..

Mean annual electrical power

The mean annual electrical power (P_{mean}) can be obtained by combining the velocity distribution $f(U_i)$ as shown in Figure A4.3 with the average absorbed power for each velocity bin $P(U_i)$ calculated as described in Table A4.1, using the following equation (Legrand et al, 2013):

$$P_{mean} = \sum_{i=1}^{N_B} (P(U_i) f(U_i)) = 104.055 \text{ kW} \quad (\text{A4-4})$$

Table A4.2 presents the results of calculating P_{mean} .



Table A4.2 Mean electrical power calculation.

Average bin velocity	Velocity occurrence likelihood	Electrical power per bin	Mean annual electrical power per bin
U_i	$f(U_i)$	$P(U_i)$	$f(U_i) P(U_i)$
ms^{-1}	%	kW	kW
0.05	3.29	0.00	0.00
0.15	3.56	0.00	0.00
0.25	2.98	0.00	0.00
0.35	3.38	0.00	0.00
0.45	3.47	1.40	0.05
0.55	3.36	2.56	0.09
0.65	3.74	4.25	0.16
0.75	4.01	6.57	0.26
0.85	4.34	9.61	0.42
0.95	3.94	13.48	0.53
1.05	4.34	18.30	0.79
1.15	3.94	24.16	0.95
1.25	3.81	31.17	1.19
1.35	3.20	39.46	1.26
1.45	3.23	49.14	1.58
1.55	3.52	60.31	2.12
1.65	3.61	73.10	2.64
1.75	3.25	87.64	2.85
1.85	3.29	104.03	3.43
1.95	3.38	122.41	4.14
2.05	3.29	142.90	4.70
2.15	2.91	165.63	4.82
2.25	2.73	190.72	5.21
2.35	2.89	218.31	6.31
2.45	2.82	248.54	7.01
2.55	2.49	281.52	7.00
2.65	2.35	317.42	7.46
2.75	2.44	356.35	8.70
2.85	1.97	398.47	7.85
2.95	1.84	443.91	8.15
3.05	0.90	492.82	4.41
3.15	0.99	545.35	5.37
3.25	0.54	601.64	3.23
3.35	0.18	661.85	1.19
3.45	0.02	726.12	0.16
Mean annual electrical power, P_{mean}			104.05



Annual energy production

For each tidal current energy converter, the annual energy production (*AEP*) is obtained by multiplying P_{mean} by the available hours per year:

$$AEP = 8760 A_v P_{mean} \text{ (kWh)} \quad (A4-5)$$

where A_v is the ratio of the total number of hours during a certain period excluding the number of hours that the tidal current energy converters could not be operated (owing to maintenance or fault conditions), to the total number of hours in the period, expressed as a percentage. If $A_v=80\%$, the annual energy production (*AEP*) would be 729.2MWh.

